# Energy rating of bifacial photovoltaic modules

Giorgos Pilis

TU Delft

# Energy rating of bifacial photovoltaic modules

**Master thesis report**

by

Giorgos Pilis

to obtain the degree of

**Master of Science**
in Sustainable Energy Technology

at the Delft University of Technology,
to be defended publicly on Wednesday July 14, 2021 at 14:00 PM

| | | |
|---|---|---|
| Student number: | 5057205 | |
| Supervisor: | Dr. Rudi Santbergen | |
| Daily supervisor: | Dr. Malte Ruben Vogt | |
| Project duration: | November 2020 - July 2021 | |
| Thesis committee: | Dr.Olindo Isabella | Associate Prof. Head of the PVMD group |
| | Dr. Rudi Santbergen | Assistant Prof. PVMD group |
| | Dr. Ricardo Guerra Marroquim | Assistant Prof. CGV group |
| | Dr. Malte Reuben Vogt | Post Doc, PVMD group |

*This thesis is confidential and cannot be made public until December 31, 2021.*



TU Delft

# Abstract

Climate change and global warming effect is currently one of the main threats that humanity is facing. The significant increase of greenhouse gas emissions since industrialization has contributed to the global warming and therefore, the use of sustainable energy sources with zero greenhouse gas emissions has emerged as an urgent priority. Photovoltaic modules have become one of the world's leading methods of generating electricity using solar energy. The share of solar PV electricity generation has significantly increased in the last decade and is expected to keep rising in the following years. However, the land area cost required for the development of photovoltaic solar systems is very high and it is therefore of foremost importance to increase the energy yield per unit area of PV modules. This is achieved using bifacial PV modules which make use of the irradiance incident on both sides of the module leading to higher energy generation. This, combined with the prediction that bifacial modules will dominate the market in less than 6 years, a parameter used for the evaluation of PV modules performance in different climates needs to be defined namely "energy rating".

Energy ratings have been developed only for monofacial modules as described in IEC-61853 standard and this work focuses on the extension of this standard to bifacial modules. For the calculation of the energy rating the energy yield and the irradiance incidence on both faces of the module have to be obtained. For this reason, an irradiance model is developed in MATLAB to calculate the irradiance on the rear side of the module using the data given in the standard IEC-61853. Note that the front side irradiance is available in the existing data and as a result no further calculations for the front side of the module are required. The irradiance on the rear side of the module is obtained using 2D view factors taking into consideration the shading of the ground which can substantially affect the results. Also, the effect of the elevation of the module from the ground surface is examined and found that at sufficient height ($\geq 1m$) the impact of ground clearance on the rear side irradiance is minimized. Finally, the ground reflected irradiance is obtained using the spectral reflectivity of different ground materials where it is shown that the use of improper albedo values can lead to inaccurate results.

The next step is the calculation of the energy yield of the bifacial module. For this, a similar methodology used to obtain the energy yield of monofacial modules in the standard IEC-61853 is used. More specifically, the incident irradiance on the rear side of the module is corrected for the angle of incidence and spectrum effects to generate similar conditions as in the STC. Additionally, the operating module temperature is obtained and using the total irradiance on the front and the rear side of the module the energy yield is calculated. Finally, the energy rating of bifacial modules is determined using two different approaches. In the first approach, CSER of bifacial modules is obtained using the energy yield and the total irradiance on bifacial modules. This approach results in lower energy rating than unity but needs re-scaling of the monofacial module energy rating compared to the standard. The second approach use the energy generated from both sides of the module but only the irradiation on the front side of the module is taken into account leading to CSER values higher than one, while the energy rating of monofacial modules as obtained in the standard is used. In both approaches the energy rating of bifacial modules found to be up to 17% higher than that of monofacial depending on the bifaciality of the module and the climate conditions.

The developed model is validated using real outdoor measurements for a system located in Weurt, Eastern Netherlands. First, the in-plane irradiance on both sides of the module is obtained from the model and then, the simulated energy yield is calculated and compared to the measured energy yield of bifacial modules. The results show a small difference between the simulated and measured energy yield for the time period between October 2019 and June 2020 with a total variation of 4.65% in the total energy yield.

# Preface

This thesis is the final work of my MSc Sustainable Energy Technology program at the Delft University of Technology. During the last year of my master degree I was pleased to be part of the PVMD group of TU Delft and end my studies with a great and challenging thesis topic regarding bifacial modules. Ever since I joined TU Delft I was very intersted in solar systems and after following the PV systems course I was sure that the modelling of photovoltaic systems was the direction that appealed to me the most. Therefore, the idea to develop a new model to calculate the energy rating of bifacial modules as my thesis project was immediately triggered my interest. However, this project would not have the expected outcome without the help of several people. This preface is to thank the people I have worked with during this year who helped and guided me to complete my master thesis.

First and foremost, I would like to thank my daily supervisor Dr. Malte Vogt for the time he dedicated to me. The weekly meetings we had motivated me and encouraged me repeatedly. His guidance through this project and the feedback he gave me was absolutely invaluable allowing me to improve my work and my results. Additionally, even in this challenging times with the pandemic his attitude was very supportive and understanding and I am really grateful for that.

I would also like to express many thanks to my supervisor Dr. Rudi Santbergen for his continuous support and his willingness to evaluate and discuss my findings when that was necessary. In addition, I am thankful to Dr. Hesan Ziar for sharing with me valueable data that helped me to validate my model. I would also like to thank Dr. Olindo Isabella and Dr. Ricardo Guerra Marroquim for being part of the thesis committee.

Finally, I would like to thank one of my best friends, Neophytos, for the unforgettable memories and experiences we shared in the last two years and for his support. I would also like to give my highest gratitude to my family for their love and support throughout these two challenging years.

*Giorgos Pilis*
*Delft, July 2021*

# Contents

# Nomenclature

The next list describes several abbreviations and symbols that will be later used within the body of the document.

**Abbreviations**

| | |
|---|---|
| $AL$ | Angular Losses |
| $AM$ | Air Mass |
| $AOI$ | Angle of Incidence |
| $BF$ | Bifacial Factor |
| $BGA$ | Bifacial Gain in Energy |
| $BoS$ | Balance of System |
| $CSER$ | Climate Specific Energy Rating |
| $DHI$ | Diffuse Horizontal Irradiance |
| $DNI$ | Direct Normal Irradiance |
| $DOY$ | Day Of Year |
| $GHI$ | Global Horizontal Irradiance |
| $LCOE$ | Levelized Cost Of Electricity |
| $LST$ | Local Solar Time |
| $SR$ | Spectral responsivity |
| $SVF$ | Sky View Factor |
| $TC$ | Temperature Coefficient |
| $VF$ | View Factor |

**Other Symbols**

| | |
|---|---|
| $\alpha$ | Ground albedo |
| $\alpha_r$ | Angular losses coefficient |
| $\alpha_s$ | Sun altitude |
| $\beta$ | Module tilt |
| $\Delta$ | Brightness index |
| $\delta$ | Declination angle |
| $\epsilon$ | Clearness index |
| $\eta$ | Efficiency |
| $\nu$ | Wind speed |
| $\phi$ | Location latitude |

$\theta_z$ Sun zenith angle

$A_i$ Anisotropic index

$A_M$ Module azimuth

$A_s$ Sun azimuth

$B$ Direct in-plane irradiance

$CC$ Number of cells per column of the module

$CW$ Cell width

$D$ Diffuse in-plane irradiance

$E$ Energy

$E_o$ Extraterrestrial irradiance

$F_1$ and $F_2$ Brightness coefficients

$G$ In-plane irradiance

$G_{sc}$ Solar constant

$H_p$ Annual front side irradiance

$HG$ Height of the module from the ground

$I_{cir}$ Circumsolar irradiance

$I_{iso}$ Isotropic diffuse irradiance

$MW$ Module width

$P$ Power

$R$ Reflectance

$SL$ Shadow length

$T$ Temperature

# 1

# Introduction

One of the main threats that humanity is currently facing is the climate change and the global warming effect. Earth's climate has changed dramatically since industrialization due to the significant increase of greenhouse gas emissions. This effect is known as "greenhouse effect" where certain gases in the atmosphere trap heat radiating from earth toward space. One of the most important greenhouse gases is the carbon dioxide ($CO_2$) which is mainly released when burning fossil fuels and according to NASA [1], this is the most important long-lived "driver" of climate change. Burning fossil fuels was the way to generate electricity in the past and along with the high energy demand of the last years humans have increased the atmospheric $CO_2$ concentration by 47%. This resulted in tremendous consequences for the planet such as increase of the global temperatures, melting of glaciers and rise of the sea level [1].

To address this serious problem, the amount of $CO_2$ emissions released in the atmosphere has to be reduced and that can be achieved by using other sustainable sources such us solar and wind energy rather than fossil fuels for energy supply. In addition, according to the Paris agreement the European Union (EU) aims to be climate-neutral by 2050 which means that all the energy will be generated by sustainable energy sources with zero greenhouse gas emissions. A great source of renewable energy which will be discussed in this report is the solar energy.

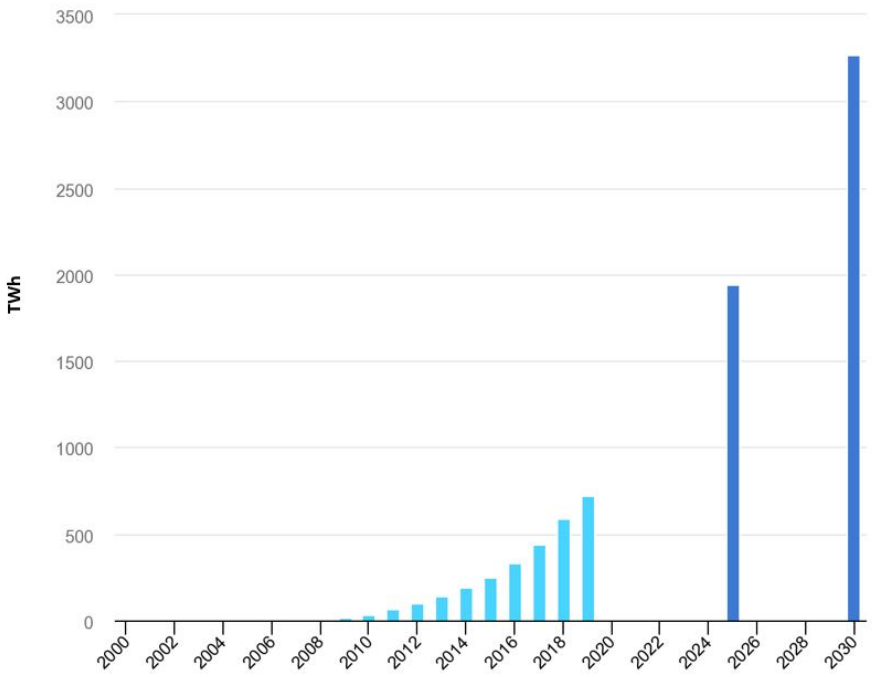


Figure 1.1: Solar PV energy generation as projected by the IEA. Retrieved by [2]

According to the International Energy Agency (IEA) the share of solar PV electricity generation has substantially increased in the last decade from 11.7 TWh in 2008 to 555 TWh in 2018 as can be seen in the Figure 1.1. The increase of solar energy generation is expected to keep rising in the following years reaching to almost 3300 TWh in 2030 [2].

Over the last few years the Photovoltaic (PV) modules which convert sunlight into electric energy have seen a dramatic drop in cost. Therefore, more PV modules are now installed and the increase of energy generated by PV modules can be attributed to a numerous factors which are listed below:

- PV modules can be installed at any climate since they generate electricity from sunlight
- Energy can be produced even in cloudy weather locations
- Relatively low cost of the PV modules
- Low maintenance costs

Even the fact that the cost of PV modules has significantly dropped, the balance of system (BoS) costs are still high, reaching to approximately 63-77% of the total system costs. The BoS includes the land area cost, installation costs, mounting structure costs and the costs of all the components of the system except the PV modules. Therefore, to further decrease the total cost of the system as well as the levelized cost of electricity (LCOE), it is of foremost importance to increase the energy yield per unit area of PV modules. This can be achieved by using more efficient solar modules, cooling down the modules, using single-axis tracking to allow the panels to follow the sun over a day or using bifacial PV modules which generate power from both sides [3]. This work is focused on bifacial PV modules.

## 1.1. Bifacial modules

Today, most of the PV panels which are used are monofacial. The rear side of monofacial modules is opaque, since a non-transparent electrode, usually aluminum foil is used, making it impossible for the irradiance to reach the rear side of the cells. This can be seen in Figure 1.2 [4] where the solar cells are sandwiched by an encapsulant with a glass panel on the top side of the module and a non-transparent white sheet on the rear side of the module. On the other hand, bifacial PV modules are characterized by their ability to collect light from the front and rear side of the module and produce solar power from both sides. Because of their great benefits, a lot of research has been conducted on the development and assessment of bifacial PV modules [5] with more than 400 papers being published since 1979 [6]. As is directly implied in the name, bifacial PV modules are constructed in such a way so both the front and the rear side of the modules are exposed to sunlight. In bifacial modules the front side performs as the traditional mono-facial modules. However, the difference between the two technologies is on the backside, where in bifacial modules, a transparent glass panel is installed making both sides of the module transparent to solar light as shown in Figure 1.3. Additionally, compared to the standard mono-facial panels, bifacial panels can generate up to 30% more energy yield [7].

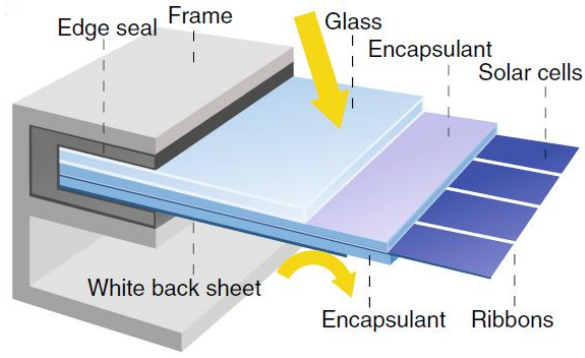


Figure 1.2: Monofacial module[4]

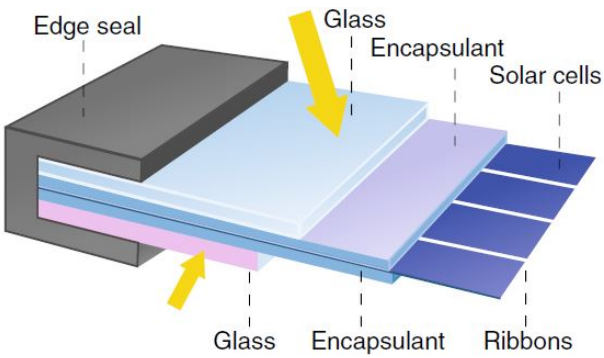


Figure 1.3: Bifacial module [4]

Bifacial PV modules were used in the past [8] in space applications but they were too expensive for terrestrial applications. Since nowadays the cost of solar modules is significantly lower than previous

years, low cost bifacial PV modules can be developed and used even for small scale applications. Consequently, the conventional mono-facial modules will be replaced by bifacial modules dominating the market in less than 6 years from now as can be seen in Figure 1.4 [9]

However, even the fact that bifacial PV modules are already in use, power rating values under one-sun illumination are still undefined. This is partly because there is no standard definition of rear irradiance when the irradiance on the front side of the module is $1000W/m^2$. An important parameter which is used for bifacial modules is the *bifacial gain in energy (BGE)* as shown in Equation 1.1. The BGE is defined as the fraction between the amount of energy generated by the rear and the front side of the module.

$$BGE(\%) = \frac{Rear[kWh]}{Front[kWh]} \tag{1.1}$$

Another parameter which is used to characterized the efficiency of bifacial modules is *bifaciality* (BF) also known as *bifacial ratio*. The definition of bifaciality is given in Equation 1.2 where the relative efficiency of the rear side of the module is related to the efficiency of the front side of the module.

$$BF(\%) = \frac{n_{rear}}{n_{front}} \tag{1.2}$$

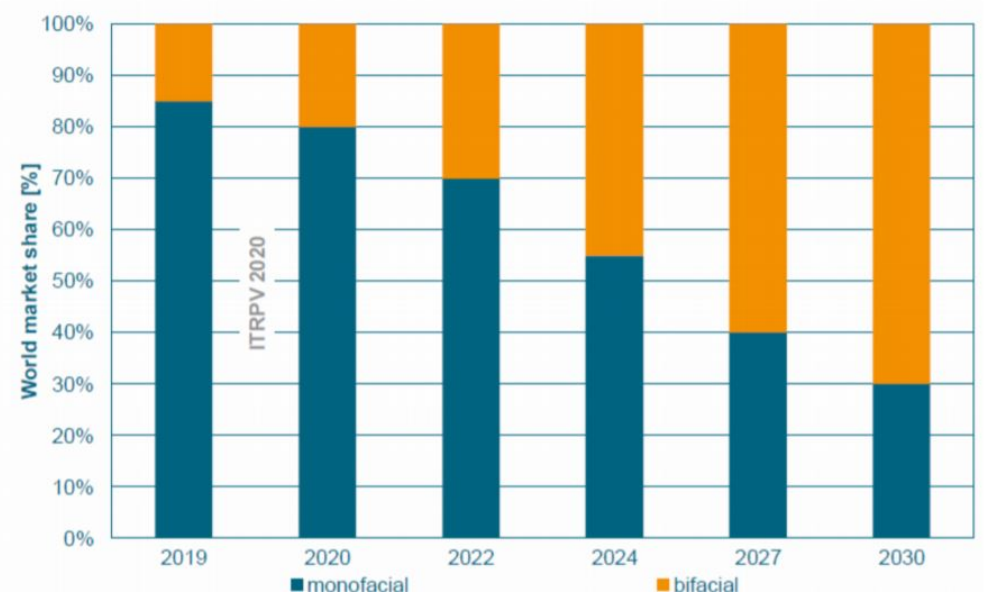


Figure 1.4: Market share of bifacial solar cells in the PV market as projected by the ITRPV roadmap 2020, [9]

## 1.2. Motivation: Why is energy rating important?

An important parameter which is always provided in the data-sheet by the manufacturing companies, is the efficiency of solar panels. It shows how much of solar energy shining on a PV module can be converted into usable electricity and is the most commonly used parameter to compare the performance of different PV technologies. The efficiency depends on the spectrum, the intensity of the incident sunlight and also to the module temperature. Therefore, it is measured under carefully controlled conditions known as Standard Test Conditions (STC) which are the following:

- Module temperature ($T_{mod}$) - 25°C
- Solar irradiance (G) - 1000 W/$m^2$
- Air mass spectrum (AM) - 1.5

Note that, these conditions at which the efficiency is measured rarely occur under real operating conditions and as a result efficiency cannot be used to compare the behaviour of a PV module or a system in different climate conditions. Additionally, the efficiency of a PV module changes with temperature

and irradiance. More specifically, when the module temperature increases due to higher irradiance for example, its efficiency will decrease, leading to lower power generation. On the other hand, when the irradiance increases, the efficiency of a PV module can increase since more photons will reach the module surface leading to higher power output [10].

In Figure 1.5, the module temperature ($T_{mod}$) and the incident irradiance on a bifacial PV module under real operating conditions are illustrated with blue colour, where each point corresponds to one hour of a year (*365* days * *24* hours= *8760* blue points). In addition, a red point point is shown in the figure. The red point indicates the same conditions as in STC and obviously this is far from real operating conditions. Consequently, consumers cannot evaluate the performance of the PV module under such climate conditions with the irradiance given in the data-sheet.

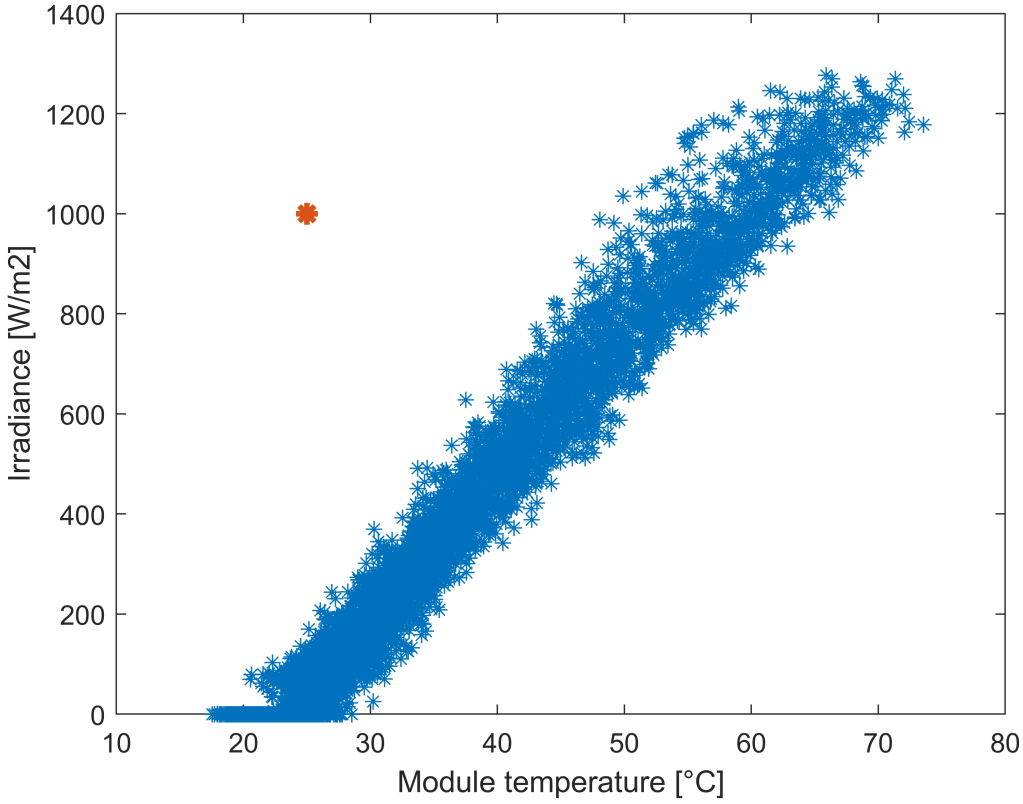


Figure 1.5: Real operating conditions in tropical humid climate for a year

On the contrary, energy rating takes into account all points under real operating conditions shown in Figure 1.5 giving the opportunity to consumers to realistically evaluate PV modules performance in such climates and compare different modules. In other words, energy rating shows how efficient a PV module is within a year, using as reference value the efficiency of the module measured in STC.

As discussed in the following subsection, energy ratings have been established only for mono-facial PV modules, but not for bifacial modules. Thus, developing a reliable energy rating model for PV bifacial modules is of great interest.

for the preparation and publication of International Standards for all electrical, electronic and related technologies

## 1.3. Energy rating

In August 2018, the International Electrotechnical Commission (IEC), a worldwide organization for the preparation and publication of International Standards, has finalized the IEC61853 standard series with the publication of the last two parts (part 3 [11] and part 4 [12]). The IEC 61853 series describes all the necessary steps for the calculation of the energy rating of monofacial modules and has been published under the general title: *Photovoltaic (PV) module performance testing and energy rating*.

This standard serves as a tool to compare the behaviour of a specific PV technology under various climatic regions, or to compare the performance of different PV technologies under the same climatic conditions. Therefore, it can be used from PV installers and manufacturers to decide which is the most suitable PV technology under specific climate conditions based on the energy yield and energy rating of the module.

At this point, it is of significant importance to clearly distinguish the difference between energy yield and energy rating since these concepts are often confused.

The energy yield is the amount of energy generated by a specific PV module or system at the DC side, taking into account the inclination and orientation angles as well as the location of the system. The energy yield is measured in kWh per unit of time usually per year and in the case of bifacial modules, energy yield is the total energy generated from both sides of the module.

On the other hand, energy rating is a way to assess the productivity of a PV module under various climate conditions. It is directly depended on the characteristics of the PV module but is independent of the installation details. It is commonly expressed as annual average Module Performance Ratio (MPR) or Climate Specific Energy Rating (CSER) as given in the following equation [13]:

$$CSER = \frac{E_{year}/H_{year}}{P_{stc}/G_{stc}} = \frac{G_{stc} \cdot E_{year}}{P_{stc} \cdot H_{year}} \tag{1.3}$$

where, $CSER$ [dimensionless] is the annual performance ratio of a PV module,
$E_{year}$ [kWh] is the total energy produced by the PV module over a year,
$G_{stc}$ [W/m2] is the irradiance at Standard Test Conditions (STC)
$P_{stc}$ [W] is the maximum power of the PV module measured in STC
$H_{year}$ [kWh/m2] is the total of the hourly in-plane irradiation over a year

This is the ratio of the energy produced by the module over a time period (usually a year) in the reference climate to the energy that would have been produced if the module was operating with efficiency obtained under Standard Test Conditions (STC:25°C, 1000W/m2, AM1.5) [13]. Note that the energy rating does not provide an accurate yield estimation as progressive degradation or transient behaviour such as light induced changes or thermal annealing effects are not taken into account.

When CSER=1, it means that the PV module operates with the same efficiency as it was measured under STC, while CSER values less than 1 indicate lower efficiency in the reference climate than in STC. The opposite applies when the CSER is higher than 1. Since CSER is derived from the definition of the performance ratio (PR) of the PV system it is important to understand what is the difference between the two. The main difference is that for the calculation of CSER the DC power generated by a module operating at its maximum power point is used while for the PR calculation the final AC power is used. Another difference, is that PR can be used to compare PV modules or PV plants at different locations all over the world, while CSER can only be calculated for the reference climates which are mentioned at the end of this section.

The Standard series (IEC 61853) contains all the necessary requirements for the the determination of PV module energy yield and energy rating taking into account various meteorological datasets and various mathematical models. All these aspects are described in four parts which the standard is composed from as follows:

- $IEC61853-1$: The methodology to measure the maximum power output at various levels of irradiance and module temperature is described. The units of power is in *Watts* and the irradiance spectral distribution should correspond to AM1.5 [14].
- $IEC61853-2$ The module temperarure is measured taking into account incident irrradiance, ambient temperature and wind speed. Also, the spectral responsivity and incidence angles are measured to consider the effects of varying angles of incidence and sunlight spectra [15].
- $IEC61853-3$ The methodology for the calculation of PV module energy rating is analyzed taking into account the angle of incidence and spectral effects as well as the module temperature under different climate profiles defined in the last part of the standard series [11].
- $IEC61853-4$ Six reference climate profiles are used to describe the working conditions of PV installations where the data are defined for a whole year and are tabulated as an hourly datasets

[12]. The climate profiles are listed as follows:
→ High elevation above 3000m
→ Subtropical arid
→ Subtropical coastal
→ Temperate coastal
→ Temperate continental
→ Tropical humid

Note, this standard applies only for mono-facial modules and not for bifacial modules.

## 1.4. Research Questions and Objectives

The main questions of this thesis are the following:
***1. How can the energy rating of bifacial PV modules be calculated?***
***2. Can the energy rating be used to assess the productivity of bifacial modules?***

To answer these questions, the following objectives are formulated:
**Objective I:** Develop a model to calculate rear side irradiance on bifacial PV modules
**Objective II:** Extend mono-facial PV module energy rating to bifacial modules
**Objective III:** Validation of the model using real time data

## 1.5. Thesis Structure

The structure of the report is as follows. Firstly, in chapter 2 the theoretical background retrieved from scientific articles is provided, giving all the necessary information and explaining all terms which are used later in this work. In addition, existing view factor models which are used for the calculation of the rear side irradiance for bifacial modules are discussed and compared. Thereafter, chapter 3 is focused on the modelling of the rear side irradiance on bifacial modules while the techniques used in this model are discussed. Then, the results of the model are illustrated while the effect of spectral albedo is examined. Building on information acquired from the rear irradiance model, the calculation procedure for the energy yield and energy rating for mono-facial modules is analysed in chapter 4. Since this work is focused on bifacial PV modules, the standard IEC61853 is adjusted accordingly to obtain the energy rating of bifacial modules as well. However, since no standard method has been developed for the calculation of the energy rating of bifacial modules different approaches are analysed. Chapter 5 lays out the validation procedure to assess the precision of the proposed model. For the validation, real time data measured in ambient conditions in Weurt, Eastern Netherlands are used and compared with the simulation results. Finally, in chapter 6, the most important outcomes of this work are summarised along with a recommendations section for possible improvements of the model.

# 2

# Literature review

In this chapter the theoretical background retrieved from scientific articles is provided explaining the most important terms which are used in this work. Section 2.1 analyzes irradiance composition and gives a brief introduction of view factor (*VF*) and ray-tracing techniques. Section 2.2, section 2.3 and section 2.4 analyze different methods for the calculation of the direct, diffuse and reflected irradiance towards module's surfaces respectively and thereafter, in section 2.5 the impact of reflection losses on module's surfaces is assessed. Then, existing view factor models used for the calculation of the rear side irradiance are discussed and compared in section 2.6. Finally, in section 2.7 the methodology used in IEC61853 standard for the estimation of energy rating and energy yield of a PV module is described, while other approaches used to simulate the power output and the performance of a PV module are discussed.

## 2.1. Irradiance composition

When a PV module or a system is exposed to ambient conditions the calculation of incoming irradiance becomes complex. Shading (which can also be partial), reflection of irradiance from other objects and transmission losses are just some of the many factors which increase the complexity of the irradiance model leading to inaccurate results of the irradiance received by the PV module/system. The total irradiance falling on a PV module which is also known as plane-of-array (POA) irradiance is given by the following equation:

$$G_m = G_m^{dir} + G_m^{diff} + G_m^{refl} \tag{2.1}$$

where,

- $G_m^{dir}$ is the direct irradiance which is used to describe solar irradiance traveling on a straight line from the sun down to the surface of the earth without any reflection at any other surface
- $G_m^{diff}$ is the diffuse irradiance which describes the sunlight that has been scattered by molecules and particles in the atmosphere such as clouds, but still made it down to the surface of the earth
- $G_m^{relf}$ is the reflected irradiance which describes the sunlight that has been reflected by a non-atmospheric surface such as the ground and finally reached the module surface.

Note that the direct irradiance has a specific line of direction towards the earth while the diffuse irradiance can follow any direction. Therefore, shadows on the ground surface during the day are produced only when the direct irradiance is blocked. Finally, the direction of ground reflected irradiance depends on the ground surface and can follow different mechanisms of reflection [16]. In this work Lambertian reflection is assumed where the irradiance is reflected with the same intensity towards all directions. A graphical representation of each component of the total irradiance falling at the surface of a PV module is illustrated in Figure 2.1.

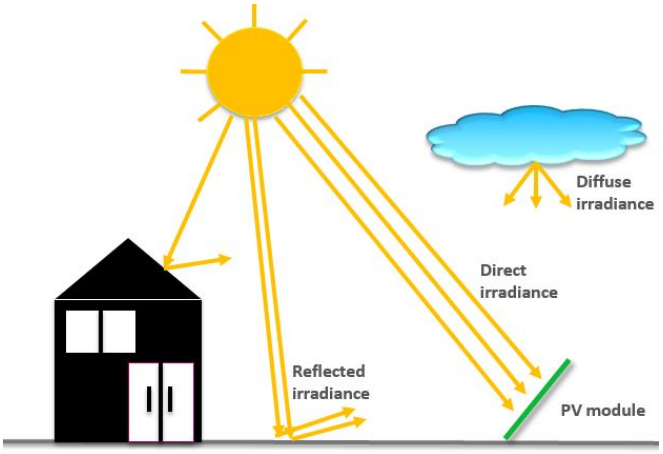


Figure 2.1: Graphical representation of irradiance components

The total irradiance on the front or the rear side of a PV module consist of the direct irradiance, the diffuse irradiance and ground reflected irradiance but the contribution of each one of these components to the total irradiance differs for the front and the rear side of the module.

The R&D department of Electricite de France (EDF) showed through a series of experiments and simulations the effect of ground albedo on the total irradiance on PV modules [17]. As expected more irradiance can be reflected from the ground when a material with high albedo is used. However, as can be seen on the left hand side of figure 2.2, most of the irradiance incident on the front side of a module comes from direct irradiance followed by the diffuse irradiance and finally by the ground reflected irradiance. Therefore, the effect of the albedo value is not significant for the front side irradiation and in many cases it can be neglected. Nevertheless, the opposite happens on the rear side of a module. The rear side irradiance is strongly influenced by the albedo since the ground reflected irradiance is the main source of rear irradiance, while the direct irradiance has the least contribution as can be seen in the following Figure 2.2 [17].

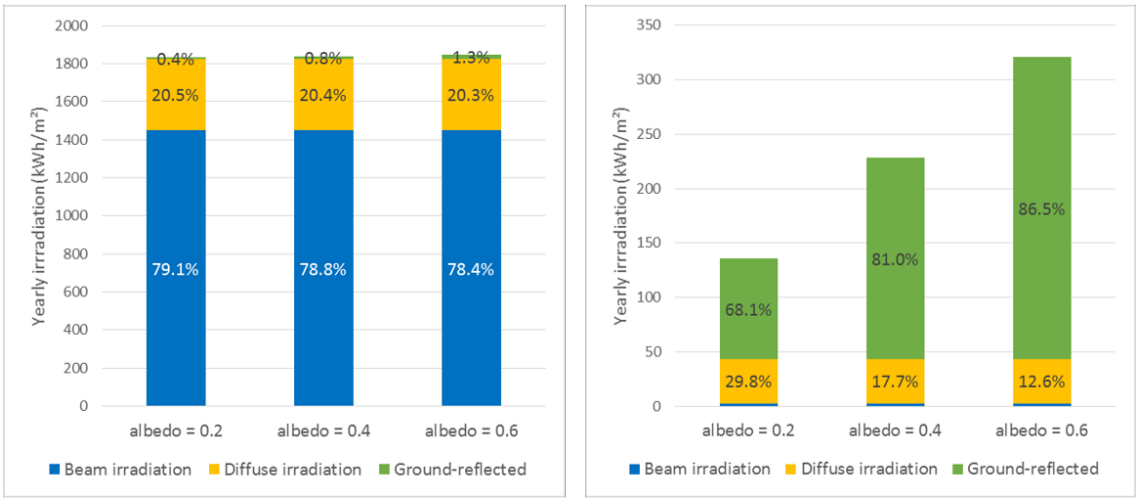


Figure 2.2: Contribution of irradiance components to the front (left) and rear (right) side of a bifacial PV module.

For the calculation of the irradiance on the front or the rear side of PV modules, two methods can be followed. The first method, is based on view-factors. View factors, also termed as configuration factors, is the fraction of irradiance reflected from surface 2 (e.g. the ground) to a receiving surface 1 (e.g. surface of the PV module). A view factor model implicitly assumes that all reflecting surfaces are Lambertian and therefore irradiance is scattered isotropically [18]. The definition of view factor is given

by the following formula [19]:

$$VF_{1\to2} = \frac{1}{A_1}\int_{A_1}\int_{A_2}\frac{cos(\theta_1)cos(\theta_2)}{\pi s^2}dA_2dA_1 \tag{2.2}$$

where $\theta_1$ and $\theta_2$ are the angles between the light ray and the surface normal between the two differential areas ($n_1$ , $n_2$). These parameters can be seen in Figure 2.3.

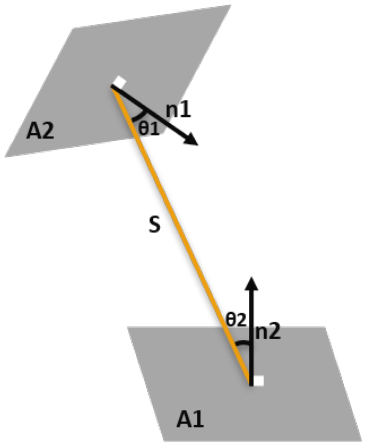


Figure 2.3: Graphical representation of View factor

When view factors are applied, the **Summation** rule [19] can be used, which means that the summation of all the $VF_{1\to2}$ from surface 1 to all the surrounding surfaces has to be equal to unity. This is derived from the conversation of energy and it is given by the following formula:

$$\sum_{j=1}^{N} VF_{i\to j} = 1 \tag{2.3}$$

Also a rule known as **reciprocity relationship** [19] can be used where the $VF_{i\to j}$ can be easily found if the $VF_{j\to i}$ is known. Note that if the $A_i$=$A_j$ then $VF_{i\to j}$=$VF_{j\to i}$.

$$A_1VF_{1\to2} = A_2VF_{2\to1} \tag{2.4}$$

Finally, the **superposition** rule [19] is implemented when not a lot of data are available. Therefore, this method is used to calculate the VF from surface 1 to a surface with two intermediate points 2 and 3. This is formalised in Equation 2.5 and a graphical representation is shown in Figure 2.4

$$VF_{1\to(2,3)} = VF_{1\to2} + VF_{1\to3} \tag{2.5}$$

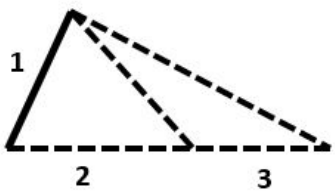


Figure 2.4: Graphical representation for the superposition rule

This method is straightforward to implement and it is mainly used for small scale systems. Various commercial software use this approach to calculate the incident irradiance on both sides of a PV module as discussed later in this chapter [20].

The second method is called ray-tracing which is more accurate than the view factor method and it can handle systems with complex geometries. This technique is used in computer graphics by monitoring the intensity, direction and absorption of light rays emitted through the landscape of interest to generate a realistic image. In addition, obstacles such as walls are also considered, since light rays can be reflected into different directions. However, some additional functions can be implemented to limit the number of bounces and avoid possible infinite loops. Ray-tracing can be split up into two different methods namely forward and backward ray-tracing. The difference between the two is that in forward ray-tracing a ray is traced from the source of light to the PV module while in the backward ray-tracing the ray is monitored from the PV module back to the source [16]. In that way, using backward ray-tracing all necessary rays that reach the module surface are traced while in forward ray-tracing rays which will never reach the module are also traced making the model slower and more complex. One of the most famous software which use backward ray tracing is RADIANCE [21].

## 2.2. Direct irradiance

The direct irradiance incident on the surface of the PV module can be obtained using the following formula:

$$G_m^{dir} = DNI * cos(AOI) \tag{2.6}$$

where DNI is the direct normal irradiance and AOI is the angle of incidence between the surface normal and the incident direction of sunlight and has a range between $\pm 90°$. The AOI depends on the solar position and it is therefore necessary to know both azimuth and altitude of the sun at any given time. Note, the direct irradiance has a finite value only when the sun is above horizon otherwise $G_m^{dir} = 0$. Since, this project is focused on bifacial modules is important to mention that the direct irradiance on the rear side of the module is different from front side irradiance since different angle of incidence is used. More specifically, values of direct irradiance on the rear side of the module are expected only when the sun is behind the module - mainly during sunrises and sunsets.

## 2.3. Diffuse irradiance

In contrast to direct irradiance, diffuse irradiance is the light coming from the sky and can follow any direction to reach a PV module. However, it is more complex to be modeled since sky conditions have to be taken into account. Multiple models have been developed for the calculation of the diffuse irradiance and selection of models are described in the following subsections.

### 2.3.1. Liu and Jordan Isotropic sky diffuse model

The Liu and Jordan model was developed in 1960 and is the fundamental model on which all the other models are based and built on [22]. This approach calculates the diffuse irradiance using a sky view factor (SVF) assuming that the sky is always clear and its brightness is the same which in reality it is not true. The following equation is used to calculate diffuse irradiance on the PV module.

$$G_m^{diff} = DHI * SVF \tag{2.7}$$

where the DHI is the diffuse horizontal irradiance measured in $[\frac{W}{m^2}]$ and $SVF$ is the sky view factor which shows how much sky is ”seen” by the surface of interest. Note that for horizontal PV module where the tilt is zero degrees, the $SVF$ is equal to one, meaning that the whole sky dome can be seen by the front side of the module. When the module tilt is vertically positioned $(90°)$, the $SVF$ equals 0.5 as half of the sky can be seen by the surface of the module.

This model is based on the assumption that the intensity of the diffuse radiation is uniform over the sky dome and as a result it is classified as isotropic sky model. However, in reality the sky is anisotropic and in the following subsections other models which take into account the anisotropic factor are discussed.

### 2.3.2. Hay and Davies Isotropic sky diffuse model

In 1980, Hay and Davies [23] have developed a new model in order to calculate the diffuse irradiance more precisely. More specifically, they separated the diffuse irradiance into two parts, the isotropic and

circumsolar component while a new anisotropic index $A_i$ was introduced. To get a better understanding on what the circumsolar irradiance is, it is helpful to remember that around the sun there is a solar disk which is very bright. The irradiance coming from this bright region is called circumsolar diffuse irradiance and according to Hay and Davies the direction of the circumsolar component is the same as that of direct irradiance.

The diffuse irradiance taking into account the aforementioned parameters is calculated as follows [24]:

$$G_m^{diff} = DHI * [A_i * R_b + (1 - A_i) * SVF] \tag{2.8}$$

where $A_i$ and $R_b$ can be found from the following equations respectively:

$$A_i = \frac{DNI}{E_o} \tag{2.9}$$

$$R_b = \frac{cos(AOI)}{cos(\theta_z)} \tag{2.10}$$

The $E_o$ term is the extraterrestrial irradiance or otherwise the irradiance at the top of the earth's atmosphere whereas the term $\theta_z$ is the solar zenith angle.

### 2.3.3. Hay, Davies, Klucher and Reindl Isotropic sky diffuse model

The sky diffuse irradiance model was taken one step further by Reindl, which an additional factor for the calculation of the diffuse irradiance was added to account for horizon brightening [25]. This model is also known as HDKR model since Hay and Davies, Klucher and Reindl contributed to its development. The HDKR model formulation for sky diffuse radiation is shown in the following formula [26]:

$$G_m^{diff} = DHI * [A_i * R_b + (1 - A_i) * SVF * (1 + \sqrt{\frac{DNI * cos(\theta_z)}{GHI}} * sin^3(\frac{\beta}{2}))] \tag{2.11}$$

where GHI is the global horizontal irradiance and $A_i$ is the same anisotropic index which was used in Hay and Davies model. The additional component of Equation 2.11 addresses the cloudiness factor as a square root of the direct in-plane irradiance share in the global irradiance while the $sin^3(\frac{\beta}{2})$ function shows that the influence of the horizon component is low for small and medium tilt angles. However, its influence grows significantly as the tilt increases, reaching maximum when the surface becomes vertical as suggested by Temps and Coulson [27]. This component leads to higher irradiance values compared to Hay and Davies model.

### 2.3.4. Perez Anisotropic sky diffuse model

In contrast with the aforementioned sky diffuse models the Perez model is a fully anisotropic approach. The diffuse irradiance is separated in isotropic, circumsolar and horizon component but at the same time new empirical coefficients are introduced. In this model, two empirically fitted functions which describe the sky conditions are used, $F_1$ and $F_2$ for circumsolar and horizon diffuse radiation respectively. $F_1$ and $F_2$ are also called brightness coefficients which depend on the position of the sun, the brightness of the sky dome, and its clearness. In other words, the key parameters are: (1) the solar zenith angle $(\theta_z)$, (2) the diffuse horizontal irradiance $(DHI)$ and (3) a new parameter $\epsilon$ which indicates the clearness of the sky [25]. According to Perez model, the diffuse irradiance on a tilted module can be described by the following equation[28]:

$$G_m^{diff} = DHI[(1 - F_1) * VF_{mod \to sky} + F_1(\frac{\alpha}{b}) + F_2 sin(\beta)] \tag{2.12}$$

As can be seen from Equation 2.12, $F_1$ factor is corrected with the ratio of another two factors $\alpha$ and $b$. The first term is connected with the angle of incidence (AOI) of the circumsolar radiation on a module surface while the $b$ term depends on the zenith angle of radiation $(\theta_z)$ as can be seen in the following expressions respectively.

$$\alpha = max(0, cos(AOI)),\ b = max(cos(85°), cos(\theta_z)) \tag{2.13}$$

$$F_1 = max[0, (f_{11} + f_{12}\Delta + \frac{\pi\theta_z}{180^\circ} f_{13})] \tag{2.14}$$

$$F_2 = f_{21} + f_{22}\Delta + \frac{\pi\theta_z}{180^\circ} f_{23} \tag{2.15}$$

In equations 2.14 and 2.15 the $f$ coefficients can be defined after the sky clearness index $\epsilon$ is obtained. The sky clearness index is expressed as follows:

$$\epsilon = \frac{(DHI + DNI)/DHI + k\theta_z^3}{1 + k\theta_z^3} \tag{2.16}$$

where $k$ is a constant equal to 1.041 and the solar zenith angle $\theta_z$ is given in radians. Perez provided tables at which the $f$ coefficients can be found for specific bins of clearness $\epsilon$ [29]. More specifically, 8 values of clearness bins $(\epsilon)$ are provided ranging from 1 (clear skies) to 8(overcast skies).

Finally, the sky brightness index $(\Delta)$ in equations 2.14 and 2.15, is a function of the air mass, hourly diffuse irradiation, and normal incident extraterrestrial irradiation as it shown in the following formula:

$$\Delta = \frac{DHI * AM}{E_o} \tag{2.17}$$

The *AM* can be calculated using Equation 2.18 while the definition of $E_o$ is given in Equation 2.19.

$$AM = \frac{1}{cos(\theta_z)} \tag{2.18}$$

$$E_o = E_{sc}(1.000110 + 0.034221cos(b) + 0.001280sin(b) + 0.000719cos(2b) + 0.000077sin(2b)) \tag{2.19}$$

where, b=2$\pi$(DOY/365) and *DOY* is the day of the year. The term $E_{sc}$ is the solar constant which according to the literature is equal to 1361$W/m^2$ [30].

## 2.4. Reflected irradiance

The calculation of reflected irradiance is the most complex and requires more investigation. To simplify the geometry of the system used in this project, it is assumed that irradiance is reflected only from the ground and not from nearby objects such as other PV arrays and buildings. In this section some methods used for the computation of reflected irradiance models are explained.

### 2.4.1. Isotropic ground reflected irradiance

This is the most simple way to calculate ground reflected irradiance since isotropic irradiance is assumed. For example, the irradiance reflected from the ground to the front surface of the module is given by the following equation:

$$G_m^{refl_{front}} = \alpha * GHI * VF_{F\rightarrow ground} \tag{2.20}$$

where $\alpha$ is the albedo of the ground material, $GHI$ is the gloabal horizontal irradiance and the last term $VF_{F\rightarrow ground}$ is the view factor from the front side of the module to the ground. In other words, the view factor indicates the ground area seen by the front side of the PV module.

A similar equation can be used for the calculation of the ground reflected irradiance at the rear side of the module:

$$G_m^{refl_{rear}} = \alpha * GHI * VF_{R\rightarrow ground} \tag{2.21}$$

However, the calculation of the rear side irradiance is more complicated as the shadow cast of the module on the ground surface should be taken into account. According to the literature, several models have been developed taking into account this effect [18]. The shadow of the module will significantly affect the energy output of a module as different amount of irradiance is reflected from shaded and unshaded ground surface areas.

This method assumes isotropic irradiance on the ground surface, whereas in real conditions this assumption is not true. Therefore, in the next subsection a more precise method is examined.

### 2.4.2. Advanced ground reflected irradiance model

The ground shadow cast from PV modules can significantly reduce the illumination onto the ground resulting in lower reflected irradiance at the both sides of the PV module. The shading effects using these model can be divided in two categories: $(1)$ Self-shaded direct and circumsolar diffuse irradiance, $(2)$ Self-shaded isotropic diffuse irradiance.

The first category, refers to the area where the ground does not receive direct $(DNI)$ and circumsolar irradiance $(I_{cir})$ due to the shadow cast of the PV module, while the rest of the ground can contribute to the reflected $DNI$ and $I_{cir}$. A graphical representation is illustrated in Figure 2.5$(\alpha)$, and the irradiance reaching the module based on these factors can be evaluated by[31]:

$$G_m^{refl_{DNI+I_{cir}}} = \alpha(DNIcos(\theta_z) + I_{cir}cos(\theta_{z_{cir}})) * (\frac{1 - cos(\beta_{F/R})}{2} - VF_{sh\to F/R} * \frac{SL}{HG}) \tag{2.22}$$

where $\alpha$ is the ground albedo coefficient (Lambertian diffuse reflector), $\theta_{z_{cir}}$ is the zenith angle of the circumsolar irradiance, $SL$ is the length of the shadow cast by the solar module, *HG* is the module height from the ground and finally $VF_{sh\to F/R}$ is the view factor from the shaded region of the ground to the front or the rear side of the module.

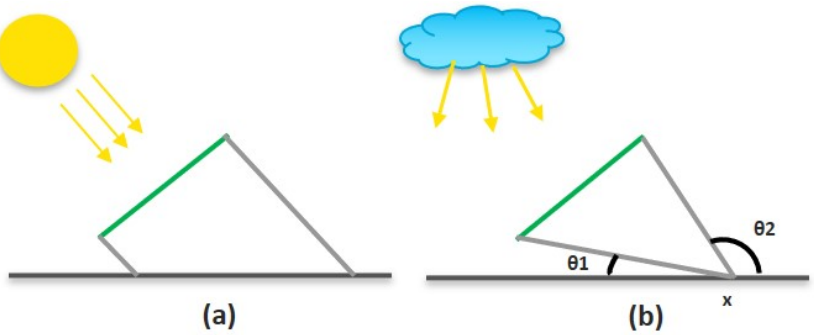


Figure 2.5: Shadow effect on (a)Self-shaded direct and circumsolar diffuse irradiance, (b)Self-shaded isotropic diffuse irradiance

On the other hand, only the isotropic diffuse irradiance $I_{iso}$ can reach the ground and be reflected as can be seen in Figure 2.5$(b)$. The $I_{iso}$ depends on the ground position $(x)$ and thus the view factor from each ground position towards the sky should be calculated based on the following formula[31]:

$$VF_{x\to sky} = 1 - (cos(\theta_1) + cos(\theta_2))/2 \tag{2.23}$$

where $\theta_1$ and $\theta_2$ are labeled in Figure 2.5$(b)$. Since, the total irradiance reaching the module should be calculated, the ground reflected irradiance must be integrated based on the limits of our reflector[32] otherwise an infinitely ground reflector can assumed. Note also that the superposition rule is applied here for the calculation of the view factor from position *x* to the front/rear side of the module as follows:

$$VF_{x\to sky} + VF_{x\to F/R} = 1 \tag{2.24}$$

$$G_m^{refl_{I_{Iso}}} = \frac{1}{HG} * a * I_{iso} \int_{-\infty}^{+\infty} VF_{x\to sky} * VF_{x\to F/R}\, dx \tag{2.25}$$

Finally, the total ground reflected irradiance reaching the rear side of the module is equal to:

$$G_m^{refl} = G_m^{refl_{DNI+I_{cir}}} + G_m^{refl_{I_{Iso}}} \tag{2.26}$$

It should be noted that these equations can be used for the calculation of ground reflected irradiance on the front and the rear side of a module accordingly.

## 2.5. Angular losses

In the case of modelling irradiance under real operating conditions, unexpected losses occur since the standard test conditions are rarely present. One of the main losses which arises when PV modules operate in real conditions are the angular losses in reference to their behaviour in STC conditions. The reason of these losses is the change of the angle of incidence (AOI>0º) since normal incidence is assumed at standard test conditions. As a consequence, reflection losses can become significant affecting the absorbed irradiance and thus the energy generation of PV modules. These losses are strongly dependent on the orientation of the module, the local latitude and the climate characteristics.

The loss factor due to the change in the AOI is defined as "angle of incidence modifier", IAM, which in the case of the beam component is defined as the fraction of the transmittance ($\tau$) at an angle $\theta$ and the normal transmittance at an angle of 0º as follows:

$$IAM(\theta) = \frac{\overline{\tau}(\theta)}{\overline{\tau}(0)} = \frac{\overline{R}(\theta) - \overline{A}(\theta)}{\overline{R}(0) - \overline{A}(0)} \tag{2.27}$$

where $\theta$ is the AOI, $\overline{\tau}$ is the weighted transmittance, $\overline{R}$ is the weighted reflectance and finally $\overline{A}$ is the weighted absorptance. Note that these weighted parameters are obtained using the product of the spectral response of the PV module and the spectral distribution of the radiation at AM1.5G. A selection of models used for the calculation of IAM are discussed in this section.

### 2.5.1. ASHRAE IAM model

This model was developed by Souka and Safat in 1996 which was later adopted by the ASHRAE (American Society of Heating, Refrigeration, and Air Conditioning) and thus known as the ASHRAE incidence modifier, [33]. This is the simplest approach for the calculation of IAM since only one parameter $b_0$ is needed.

$$IAM = 1 - b_0\left(\frac{1}{cos(\theta) - 1}\right) \tag{2.28}$$

This function is simple to use but suffers from discontinuity at 90º and not good fitting results for high angles of incidence. In Figure 2.6, the IAM as a function of AOI is shown for two values of $b_0$.

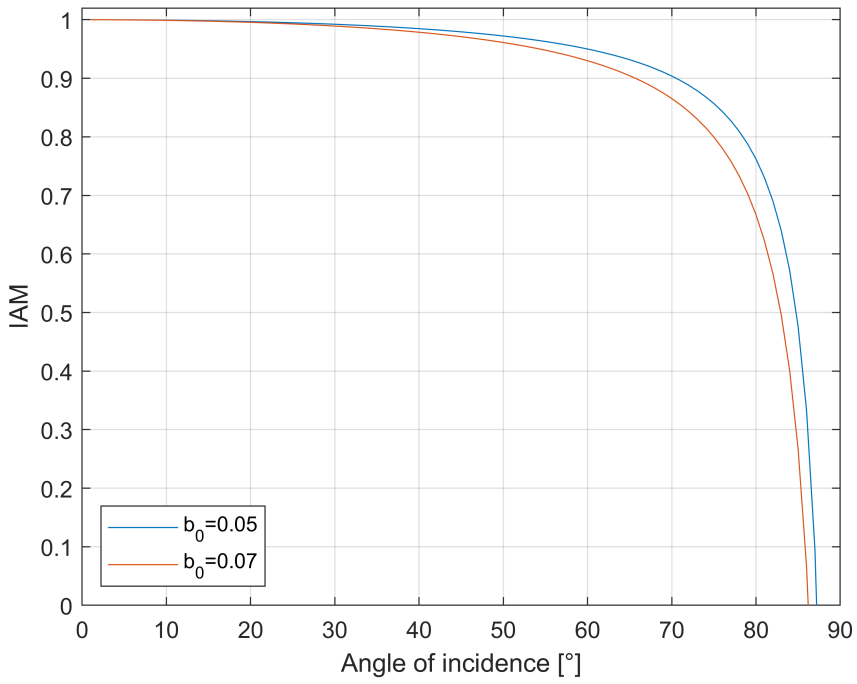


Figure 2.6: IAM as a function of the angle of incidence for the ASHRAE model for two values of $b_0$

### 2.5.2. Physical IAM model

This model was published by De Soto et al. in 2006 and it is based on Snell's and Bougher's laws, [34]. The first step in this model is to calculate the angle of refraction ($\theta_r$) using the Snell's law:

$$\theta_r = arcsin(\frac{1}{n}sin(\theta)) \tag{2.29}$$

where, *n* is the index of refraction of the glass cover whereas the 1 is the refraction index of the air. The reflection losses are calculated using the Frensel coefficients and finally the transmittance of the cover glass of the module is given in Equation 2.30.

$$\tau(\theta) = \exp(\frac{-K \cdot L}{cos(\theta_r)})(1 - \frac{1}{2}(\frac{sin(\theta_r - \theta)^2}{sin(\theta_r + \theta)^2}) + \frac{tan(\theta_r - \theta)^2}{tan(\theta_r + \theta)^2})) \tag{2.30}$$

where K is the extinction coefficient glass [1/m] and L is the glass thickness [m].

Then, the transmittance at an angle of 0º is determined using Equation 2.31.

$$\tau(0) = \lim_{\theta \to 0} \tau(\theta) = exp(-K \cdot L)[1 - (\frac{1-n}{1+n})^2] \tag{2.31}$$

Typical input parameters for the glass cover of a PV module are:

- n=1.526
- K=4$\frac{1}{m}$
- L=0.002m

Finally, the $IAM(\theta)$ was obtained using Equation 2.27 and the resulted IAM as a function of the angle of incidence is shown in Figure 2.7.

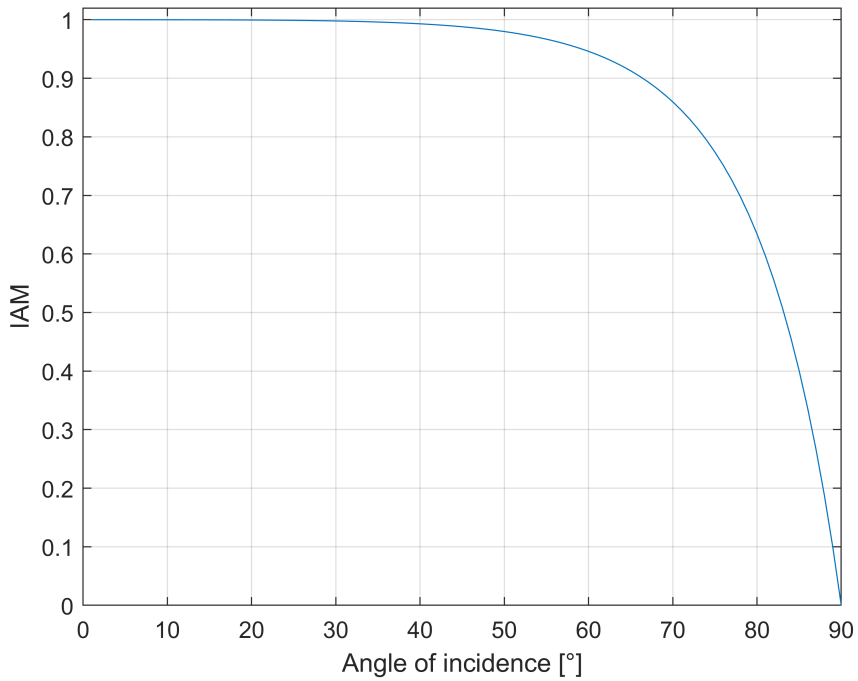


Figure 2.7: IAM as a function of the angle of incidence for the physical model,[34]

### 2.5.3. Martin and Ruiz IAM model

According to Martin and Ruiz [35],[36], the angular losses on a PV module due to reflection is given in the following equation

$$AL(AOI) = 1 - [\frac{1 - \overline{R}(AOI)}{1 - \overline{R}(0)}] \tag{2.32}$$

where the second term of this equation corresponds to the relative angular transmission of the module. The relative angular transmission of light is named as ”angular factor” ($f_{I\alpha}$) and is defined as the ratio of the short-circuit current ($I_{sc}$) at an angle $\alpha$ and the product of the short-circuit current at normal incidence (AOI=0º) and the cosine of the angle. This angular factor is the incident angle modifier (IAM).

$$f_{I\alpha} = \frac{I_{sc}(AOI)}{I_{sc}(0)cos(AOI)} \cong \frac{1 - \overline{R}(AOI)}{1 - \overline{R}(0)} \tag{2.33}$$

The following mathematical model was then proposed for the reflectance of a PV module considering both crystalline (c-Si) and amorphous silicon (a-Si) technologies, with or without anti-reflective coatings.

$$\overline{R}(AOI) = \overline{R}(0) + [1 - \overline{R}(0)][\frac{exp(-cosAOI/\alpha_r) - exp(-1/\alpha_r)}{1 - exp(-1/\alpha_r)}] \tag{2.34}$$

where $\alpha_r$ is the angular losses coefficient, an empirical dimensionless parameter. This model was applied to the analysis of various PV modules leading to adequate result in all cases. Thus, the expression of the angular losses and the angular factor $f_{I\alpha}$ become as shown in equations 2.35 and 2.36 respectively:

$$AL(AOI) = 1 - [\frac{1 - exp(-cosAOI/\alpha_r)}{1 - exp(-1/\alpha_r)}] \tag{2.35}$$

$$f_{I\alpha} = \frac{1 - exp(-cosAOI/\alpha_r)}{1 - exp(-1/\alpha_r)} \tag{2.36}$$

## 2.6. View factor irradiance models

In this section, existing models which use the view factor technique to obtain the irradiance on the rear side of PV modules are discussed and compared.

### 2.6.1. PVsyst

This software was initially developed at the University of Geneva in 1992 and is used for bifacial PV modules since 2017 [37]. PVsyst is used for modelling the irradiance on both sides of a PV module with the help of a 2-D bifacial view-factor model and can be used for fixed tilt systems or for horizontal axis tracking systems. The sky diffuse irradiance component incident on the rear side of the module is calculated in 2-D, using a VF indicating the part of the sky which can be ”seen” by the rear side of a module [20]. For the calculation of the diffuse irradiance on the rear side of the PV module the Hay and Davies model is used. However, the calculation of the beam irradiance depends on the geometrical parameters of the system [38] and happens to be higher than zero when the sun is above horizon. For the calculation of the ground reflected irradiance, the view factor being used from the ground to the module surface is divided into two parts. The first part is for the irradiance reflected from the shaded ground surface and the second part for the unshaded ground surfaces as it is shown in the following formula [37]:

$$G_m^{refl_{rear}} = \alpha * GHI * VF_{Unshaded->mod} + \alpha * DHI * VF_{Shaded->mod} \tag{2.37}$$

where $\alpha$ is the ground albedo which is assumed to be constant. Note that the light reflected from the ground is isotropic (Lambertian reflection) and no reflection from neighbor rows or surrounding objects is considered. In addition, this model assumes that the irradiance incidence on the unshaded and shaded ground surfaces are uniform and equal to GHI and DHI respectively. It is also assumed that the arrays are infinitely long since the PV modules have the same orientation and are spaced equally.

For more accurate results the irradiance is calculated for five points at the rear side of a module and then averaged over them [37] while the non-uniformity of the backside illumination can be added

using an ”empirical mismatch factor”. Finally, to take into account possible shadows at the rear side of the module (e.g. due to the mounting structure and the junction box), a shading factor is used.

### 2.6.2. NREL VF

NREL has developed a software used for the estimation of the backside irradiance for a row or multiple rows of bifacial PV modules. This model is based on the use of 2D view-factors and can be used for fixed tilt systems or single axis-tracking configurations. Additionally, the effects of shading by other rows of of PV modules assuming no differences in the backside irradiance along the row's length [32] are included in the model. As already mentioned, the rear side irradiance is significantly more difficult to be determined due to shadows from the array to the ground and a restricted view of the sky. Therefore, the targets of this model assuming infinite length of the modules are the following [32]:

- Identify the shaded ground area by the PV array. Using the PV array dimensions and orientation, the sun position at each time-stamp can be obtained and shadows are projected in the row-to-row $(rtr)$ dimension. Finally, the $rtr$ is divided into $n$ segments (e.g 100 segments) which each segment can be shaded or unshaded.
- Calculate the irradiance received by the ground taking into account any shading effects and restricted view of the sky. This model uses the Perez sky model (see section 2.3.4) and using the following equation, the irradiance falling on the ground for each of the $n$ segments can be determined. Note that the $I_{hor}$ can be ignored for the ground.

$$GrIrr = A(DNI + I_{cir}) + VF_{ground->sky} * I_{sky} \tag{2.38}$$

where, $A = cos(\theta_z)$ when the ground segment is unshaded or $A = cos(\theta_z) * Transparentfraction$ when the ground segment is shaded. The transparent fraction refers to spacing between cells and modules leading to additional light reaching the ground [39]. Finally, $VF_{ground \rightarrow sky}$ can be calculated using the following formula. An illustration is shown in Figure 2.8.

$$VF_{ground->sky} = \frac{1}{2}(cos(\theta_{s1}) - cos(\theta_{s2})) \tag{2.39}$$

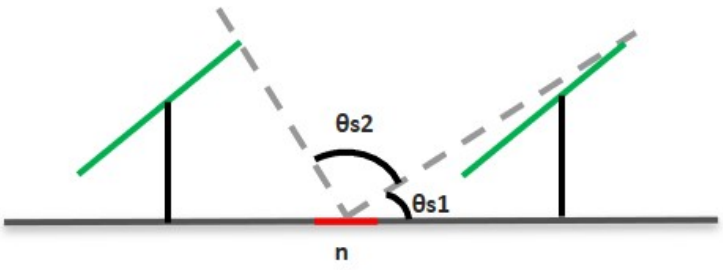


Figure 2.8: VFs for the diffuse sky radiation incident on a ground segment

- Calculate the backside irradiance (BSI) of a PV module which takes into account the irradiance from the sky, the reflected irradiance from the ground and the reflected irradiance from the front surface of the PV modules on the row behind. This model assumes that only the diffuse irradiance is reflected from the modules behind and for the calculation of the diffuse irradiance component of the BSI, the field-of-view is divided into 180 one-degree segments $(i)$. Then, for each segment, the product between the irradiance received by the segment, the VF and the AOI correction is calculated and summed for all segments. The total BSI is determined by the following equation:

$$BSI = b * F_b(DNI + I_{cir}) + \sum_{i=1}^{180\circ} VF_i * F_i * I_i \tag{2.40}$$

where $b = cos(AOI)$. If $b$ value is negative then it is assumed that $b = 0$. $F_b$ is the AOI correction using the air-glass model of Sjerps-Koomen. $VF_i$,and $F_i$ is the view factor and the AOI correction

of the $ith$ one-degree segment respectively while $I_i$ is the irradiance viewed by the $ith$ one-degree segment. A schematic representation of the VF for each $ith$ one-degree segment is presented in Figure 2.9

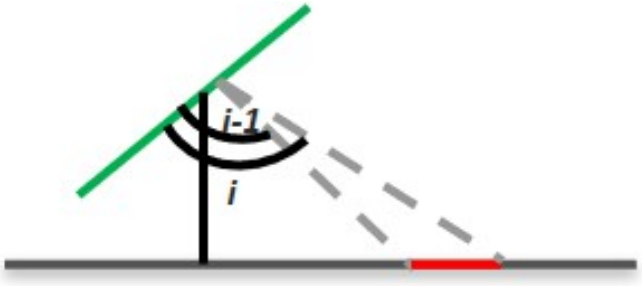


Figure 2.9: Field-of-view of the ground for a one-degree segment

### 2.6.3. MoBiDiG

MoBiDiG (Modelling of Bifacial Distributed Gain) is a simulation tool developed at ISC Konstanz in Germany and it is able to model the energy yield of both fixed and single axis tracking systems for monofacial or bifacial PV systems [20]. In this model the direct, diffuse and ground reflected irradiance are calculated as follows. The calculation of the direct irradiance on the front or the rear side of a module requires the geometrical properties of the system such as the position of the sun and the tilt of the module while the diffuse irradiance component is determined using the Perez model. Finally, the ground reflected irradiance at each cell within the backside of the module is modelled using a quasi 3D view factor concept. This method calculates separately the reflected irradiance from the shaded and unshaded areas of the ground taking into account the layout of the PV system. The model calculates the rear side irradiance for 12 positions on the module and an averaged value over the whole module is finally obtained. A more detailed description of this model has been carried out in previous work [40].

### 2.6.4. BIGEYE

The BIGEYE is a simulation model developed by TNO to predict the yield of both fixed tilt and single-axis tracking bifacial PV systems without any limitations to tilt angles and orientations [20]. The direct irradiance is calculated similarly to the MoBiDiG tool. For the calculation of the diffuse irradiance the Perez model is used to determine the isotropic ad and circumsolar part of the diffuse irradiance. However, the view factors showing how much sky and ground is ”seen” by each surface of the PV module are fully 3D and numerically calculated. This software is also taking into account that the light reaching the ground (both direct and diffuse light) is not uniform. Additionally, other effects such us self-shading, shading from nearby objects and homogeneous transparency of the modules are considered [41]. Since the irradiance incident on the ground is not uniform, the ground is separated in multiple parts. Therefore, the ground reflected irradiance is calculated by multiplying the ground albedo with the integrated irradiance at each part and with view-factor between the plane of the module and the examined location of the ground. In that way, the effect of the shade that is created on the ground by the panels in the system and the presence of the mounting structure at the rear leading to non-uniform irradiance are treated by the model. Since the VFs are numerically calculated, the specific length of the arrays, the distance between arrays and the different tilt angles of the modules in a field can be taken into account. BIGEYE calculates the rear irradiance using the average of four points on the module surface.

An overview of the aforementioned models can be seen in Table 2.1.

| Features | PVsyst | NREL VF | MoBiDiG | BIGEYE |
|---|---|---|---|---|
| Simulation model | 2D | 2D | Quasi 3D view factor model | 3D |
| 1-axis tracking | ✓ | ✓ | ✓ | ✓ |
| Anisotropic diffuse irradiance | ✗ | ✓ | ✓ | ✓ |
| Irradiance non-uniformity | ✓[1] | ✓ | ✓ | ✓ |
| IAM for backside reflections | ✗ | ✓ | N/A | N/A |
| Spectral-corrected backside irradiance | ✗ | ✗ | N/A | N/A |
| Light transmitted between cells | ✓ | ✓ | N/A | ✓ |
| Shading losses | ✓[2] | N/A | N/A | ✓ |
| Length of rows | Infinite | Infinite | Finite | Finite |
| Edge effects modeled | ✗ | ✗ | ✗ | ✓ |
| Irradiance change along rows height | ✗ | ✓ | ✓ | ✓ |
| Irradiance change along rows length | ✗ | ✗ | N/A | ✓ |

[1] An empirical mismatch factor is used (10%)
[2] A shading factor is used

Table 2.1: Irradiance model comparison

## 2.7. Energy rating of mono-facial PV modules

The price and productivity of PV modules are commonly assessed based on their efficiency and maximum power output measured in STC conditions. However, the amount of electricity produced by the PV module and return of investment costs depends on the working conditions of the module which are usually far from STC conditions. Therefore, the energy rating is used to evaluate the performance of PV modules under real operating conditions. As mentioned in the previous section, for the calculation of energy rating the energy yield of the module should be obtained. In this section, the methodology used in IEC61853 standard for the estimation of energy rating (CSER) and energy yield of a PV module is described while other approaches used to simulate the performance and the power output of a PV module are discussed.

### 2.7.1. Methodology according to IEC61853

According to this standard, the PV module power output and the energy rating are estimated considering six predefined climates representative of real operating conditions. Each standard reference climate profile consists of hourly data in tabulated form for a complete year including the following parameters: broadband irradiance ($G$), spectrally resolved global in-plane irradiance, ambient temperature ($T_{amb}$), wind speed ($v$), solar elevation angle ($\alpha_s$) and the angle of incidence between the sun rays and the normal to the module's front surface ($AOI$).

The complete methodology to estimate CSER for a PV module under each reference climate is illustrated in as shown in Figure 2.10. This methodology can be divided into four calculation steps which are described in detail within this section and are the following:

1. Angle of incidence effects
2. Spectrum effects
3. PV module temperature effect
4. PV module efficiency and power output

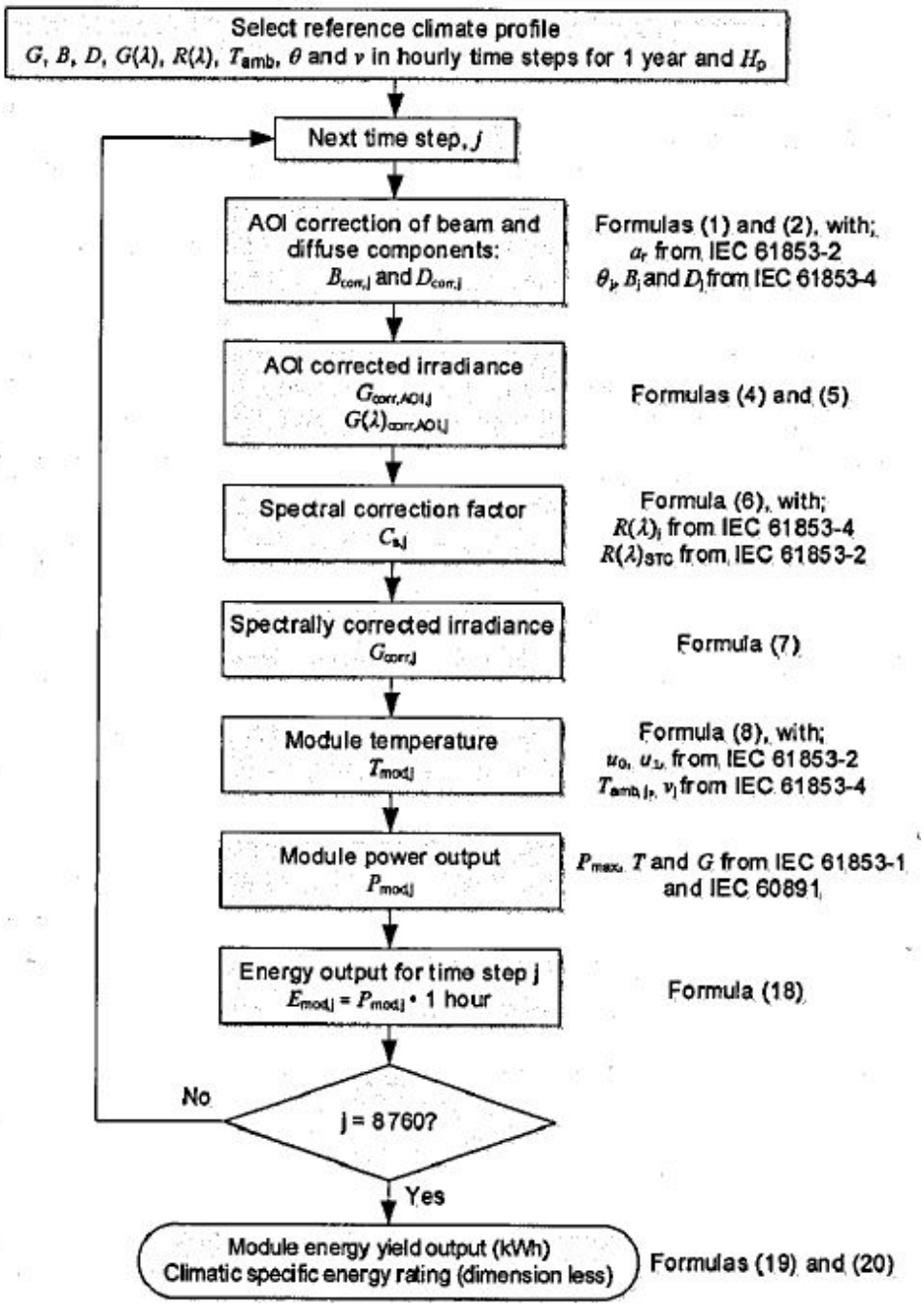


Figure 2.10: Flowchart of calculation procedure, [11]

1. **Angle of incidence effects**
   In order to precisely calculate the energy output of the module, the effect of the angle of incidence (*AOI*) is considered for the determination of the reflected irradiance. This correction depends on the AOI of solar radiation which often differs substantially from normal incidence which is assumed in STC leading to non-precise calculation of the PV module energy generation [42].

   The angular corrected in-plane global irradiance is calculated using Martin and Ruiz equations mentioned in section 2.5.

$$G_{corrAOI,j} = [B_{f,j} * (1 - F_B)] + [D_{f,j} * (1 - F_D)] \tag{2.41}$$

   where $B_{f,j}$ and $D_{f,j}$ are the uncorrected direct and diffuse irradiance components incident on the

front side of the module at hour *j* respectively. Additionally, $F_B$ and $F_D$ are the angular losses factors for the beam and diffuse irradiance respectively and are calculated as follows:

$$F_{B_{f,j}} = \frac{exp(-cosAOI/\alpha_r) - exp(-1/\alpha_r)}{1 - exp(-1/\alpha_r)} \tag{2.42}$$

$$F_{D_{f,j}} \cong exp[-\frac{1}{\alpha_r}(c_1(sin\beta + \frac{\pi - \beta - sin\beta}{1 + cos\beta}) + c_2(sin\beta + \frac{\pi - \beta - sin\beta}{1 + cos\beta})^2)] \tag{2.43}$$

where $\beta$ is the tilt of the module and $\alpha_r$ is the an empirical factor coefficient obtained in part 2 of the standard (IEC61853-2).

The sum of $F_{B_{f,j}}$ and $F_{D_{f,j}}$ is the total hourly in-plane irradiance on the front side of the module corrected for the angle of incidence effects ($G_{corr,AOI,j}$) which is required for the spectral correction effect.

2. **Spectrum effects**
The spectral correction is applied to the short-circuit current ($I_{sc}$) since the change in the $I_{sc}$ when different spectrum is applied can be used as an equivalent change to the irradiance obtaining $G_{corr}$. The hourly spectral correction factor $C_{s,j}$ is calculated using the following equation:

$$C_{s,j} = \frac{1000 \int_{\lambda_s}^{\lambda_e} SR(\lambda) G_{corr,AOI,j}(\lambda) d\lambda}{G_{corr,AOI,j} \int_{\lambda_s}^{\lambda_e} SR(\lambda) G_{STC}(\lambda) d\lambda} \tag{2.44}$$

where, $G_{corr,AOI,j}$ is the AOI-corrected in-plane irradiance at hour *j*, $G_{corr,AOI,j}(\lambda)$ is the spectrally resolved in-plane irradiance corrected for AOI at hour *j* and $G_{STC}(\lambda)$ is the spectral intensity of the reference spectrum (AM 1.5G) as measured in IEC60904-3 [43] (see Figure 2.11). Finally, *SR* is the spectral responsivity of the module given by IEC61853-2 [15] as shown in Figure 2.12.

The spectral responsivity (*SR*) is the ratio of the current generated by the PV module to the power of light incident on the PV module. Usually the spectral response is limited at long wavelengths because the semiconductor of the module cannot absorb photons with energies below the band gap. On the other hand, for very short wavelengths the spectral response also drops since the photons energy is large, and hence the ratio of photons to the power of light is reduced. Note that, photons with energies above band gap are not utilized by the module leading to higher temperatures of the module.

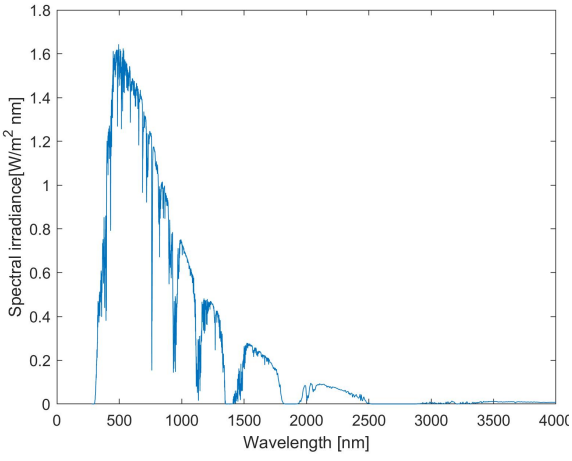


Figure 2.11: Reference solar spectrum AM1.5G

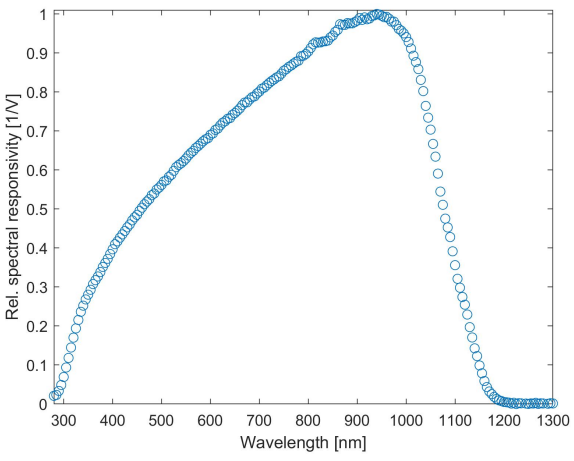


Figure 2.12: Module spectral response

After the calculation of the hourly spectral correction factor $C_{s,j}$, the corrected in-plane irradiance $G_{corr,j}$ for both the AOI and spectrum effects can be obtained as shown in Equation 4.15

$$G_{corr,j} = C_{s,j} * G_{corr,AOI,j} \tag{2.45}$$

3. **PV module temperature effect**
   The effect of module temperature is one of the main factors that affects the power generation and it is therefore required for the estimation of the PV power output. An analytical formula developed by Faiman was used to predict module temperature $T_{M,j}$ [44] for each hour $j$ as shown in Equation 4.16.

$$T_{M,j} = T_{amb,j} + \frac{G_{corr_{AOI,j}}}{u_0 + u_1 v_j} \tag{2.46}$$

   where, $T_{amb,j}$ is the ambient temperature, provided in climatic datasets of IEC 61853-4
   $v_j$ is the wind speed that dictates conductive cooling extracted from IEC61853-4
   $u_0$ and $u_1$ are empirical fitting parameters reported in IEC61853-2
   $G_{corr_{AOI,j}}$ is the front side in-plane global irradiance corrected for the AOI effects

4. **PV module efficiency and power output**

   Considering the hourly values of the corrected irradiance for the AOI and spectrum effects along with the module temperature, the PV module output can be obtained from the efficiency values derived from the power matrix provided in IEC61853-1. However, since the power values in the table are given at different temperature and irradiance conditions than the calculated parameters in the reference climate conditions, interpolation and/or extrapolation of the power table is performed. A more detailed analysis of the interpolation and extrapolation method is discussed in section 4.2. Then, the power output is calculated per hour which can be easily translated into the annual energy yield. Finally, using Equation 1.3, the *CSER* of monofacial modules can be determined for each one of the reference climates.

### 2.7.2. Fraunhofer ISE model

Another model was developed by Fraunhofer Institute for Solar Energy Systems (ISE) in 2015 [45] to simulate the power output and the module performance ratio (MPR) of a PV module. The MPR value illustrates how much of the energy that could be generated at STC is actually produced in real operating conditions. This model, is based on historical data and the data-sheets of the PV module provided by manufacturers. The practical MPR is calculated as follows:

$$MPR = \frac{\eta_{STC,measured}}{\eta_{STC,nominal}} f_{AOI} f_{spectral} f_G f_T f_{stability} \tag{2.47}$$

where $\eta_{STC,nominal}$ is the efficiency of the module as stated in the data sheet, $\eta_{STC,measured}$ is the measured STC efficiency, $f_{AOI}$ is the relative influence due to the angle of incidence (AOI) effects, $f_{spectral}$ accounts for the relative spectral influence, $f_G$ is the relative irradiance influence, $f_T$ is the relative temperature influence and finally $f_{stability}$ is an influence factor used to take into account possible degradation effects. The calculation of the influencing factors of the MPR are described and discussed in the following:

1. Angle of incidence effects
2. Spectral effects
3. PV module temperature calculation
4. Irradiance and temperature effects
5. Stability effects

1. **Angle of incidence effects**
   The $f_{AOI}$ factor accounts for reflection losses which occur at different AOI from perpendicular irradiance. Therefore, the magnitude of these losses depends on the AOI and thus the position of the sun for the specific location, the tilt and orientation of the PV module as well as on the ratio of direct and diffuse irradiance. Additionally, the module reflection characteristics are taken into account where in this approach the standard glass PV modules are used. These characteristics correspond to an ”air-glass” configuration as given by Martin and Ruiz model [35]. The total reflection losses are obtained with respect to the reflection characteristic separately for the direct and diffuse irradiance components. For the direct in-plane irradiance, the AOI and module reflection behaviour are combined for each time step. On the other hand, for the case of diffuse in-plane irradiance, the reflection losses are estimated to be 3.5% for all time steps, with the assumption that the diffuse irradiance component is isotropic as described in [45]. Finally, the sum of the direct $B_{POA}$ and diffuse $D_{POA}$ in-plane irradiance components corrected for the AOI effects result to the total in-plane irradiance $G_{POA}$. This methodology is therefore used for the calculation of AOI effects but the relevant equations are not published.

2. **Spectral effects**
   For the calculation of spectral losses, a spectral impact factor $f_{spectral}$ is considered as indicated in section 3.3 of [45]. This factor accounts the fact that spectral irradiance is not constant and as a result PV modules can utilize only a part of the spectral irradiance. In this approach the ”spectral impact” is defined as the relative difference between the measured annual irradiation measured by a pyranometer and the spectrally effective annual irradiation available for a PV module type. The effective irradiance is obtained using the product of the spectral mismatch factor (obtained in IEC60904-7 [46]) with the irradiance measured by the pyranometer.

3. **PV module temperature calculation**
   In this model, the module temperature is obtained in a simplified way where in contrast to the IEC-61853 standard the wind speed and module properties are not considered. The PV module temperature is calculated from the ambient temperature $T_{amb}$ given by SolarGIS time series [47] and an irradiance dependent value of $25K$ at $1000W/m^2$:

$$T_M = T_{amb} + 25K\frac{G_{POA}}{1000W/m^2} \tag{2.48}$$

   where $T_M$ is the module temperature and $G$ is the incident irradiance on the PV module.

4. **Irradiance and temperature effects**
   For modelling the PV module efficiency at 25°C for various irradiance levels different from STC, a simple model developed by Heydenreich et al. [48] was used:

$$\eta(G_{POA}, T_{STC}) = \alpha G_{POA} + bln(G_{POA}+1) + c(\frac{ln^2(G_{POA}+e)}{G_{POA}+1} - 1) \tag{2.49}$$

   where *a, b, c* are parameters describing the low light behaviour and $e$ is the Euler’s number. The *a, b* and $c$ parameters can be obtained from two sources: A) technical data-sheets of the PV module and B) laboratory measurements

   To calculate the module performance at irradiance and temperatures different form STC another equation proposed by Heydenreich et al. [48] was used :

$$\eta(G_{POA}, T_M) = \eta(G_{POA}, T_{STC})(1 + TC(T_M - T_{STC})) \tag{2.50}$$

   where $TC$ is a temperature coefficient of the PV module which can be found from technical data-sheets or it can be obtained as an empirical value from long-term monitoring data.

   In order to obtain $f_G$ and $f_T$, the influence on produced energy is calculated for each time step taking into account the corrected irradiance for the AOI effects. These factors can be obtained as follows:

$$f_G = 1 - \frac{\sum_{i=0}^{N} G_i(\eta_{STC} - \eta(G_i, T_{stc}))}{\sum_{i=0}^{N} G_i \eta_{stc}} \tag{2.51}$$

$$f_T = 1 - \frac{\sum_{i=0}^{N} G_i(\eta(G_i, T_{stc}) - \eta(G_i, T_{mod,i}))}{\sum_{i=0}^{N} G_i \eta(G_i, T_{stc})} \tag{2.52}$$

where, $G$ is the irradiance and $N$ is the number of available time steps.

5. **Stability effects**
   The stability of the electrical characteristics and reliability of the module over the expected lifetime of a PV module (about 25 years) is a very important influencing factor for the expected module lifetime energy. According to Jordan and Kurtz [49], the degradation rates ranging from no degradation to more than 2% around a median of 0.5%. However, since the determination of the degradation rate is time-consuming, costly and sometimes difficult to estimate, a stability factor $f_{stability}$ equal to 1 is used in this model. Therefore, the results refer only to the first year of operation of the PV system.

### 2.7.3. Linear Performance Loss Analysis

The Linear Performance Loss Analysis ($LPLA$) is an alternative approach developed by TUV Rheinland to calculate module performance ratio ($MPR$) [50]. The difference of this approach compared to IEC61853 standard is that LPLA is mainly focused on the performance of the PV module relative to its efficiency measured in STC than on the hourly simulation results defined in the standard. The LPLA approach calculates the $MPR$ of a PV module for defined operating conditions, taking into account relevant influencing factors of the yield performance:

1. Temperature losses
2. Low irradiance losses
3. Spectrum effects
4. Angle of incidence losses
5. Soiling losses

For the calculation of $MPR$, each influencing factor is separately obtained as shown in Equation 2.53,
.

$$MPR = 1 + \Delta MPR_{TEMP} + \Delta MPR_{LIRR} + \Delta MPR_{SL} + \Delta MPR_{AOI} + \Delta MPR_{SOIL} \tag{2.53}$$

These $\Delta MPR$ factors express the deviation of outdoor performance to the efficiency in STC and can be negative or positive numbers for losses or gains respectively. For the calculation of the aforementioned impact factors some data defined in the IEC61853 standard are required. The PV module measurements such us the spectral response measurements are necessary as defined in part 2 of the standard. In addition, the power matrix measurements defined in IEC-61853-1 can be reduced (Irradiance 100-1100 $W/m^2$ at 25°C). Finally, the weather data sets are listed in a different way and are short compared to IEC61853-4. At this point, the methods used for the estimation of each factor shown in Equation 2.53 are discussed.

1. **Temperature losses**
   To calculate temperature losses $\Delta MPR_{TEMP}$ the temperature coefficient ($TC$) as well as the operating temperature of the module are used. Note that the temperature coefficient is measured in the laboratory and it is supplied by manufacturers while the module operating temperature is measured in the field. The temperature losses $\Delta MPR_{TEMP}$ are obtained using the following equation [50]:

$$\Delta MPR_{TEMP} = TC(\overline{T}_{M,G} - 25°C) \tag{2.54}$$

where $T_{M,G}$ is the average annual module temperature weighted with irradiance:

$$\overline{T}_{M,G} = \frac{\int_t T_M G_{POA}\, dt}{\int_t G_{POA}\, dt} \tag{2.55}$$

2. **Low irradiance losses**
As mentioned earlier in this chapter the short-circuit current ($I_{sc}$) is almost linear to the irradiance. On the other hand, power output of PV modules have a non-linear behaviour with irradiance and as a consequence it is important to estimate the energy generation for different irradiance levels. The $\Delta MPR_{LIRR}$ is calculated as follows [50]:

$$\Delta MPR_{LIRR} = \left(\frac{\int_t p(G_{POA}) G_{POA}\, dt}{\int_t G_{POA}\, dt}\right) - 1 \tag{2.56}$$

where $p(G_{POA})$ is the low irradiance behaviour measured in the lab for seven irradiances from 100-1100 W/$m^2$ at 25°C

$$p(G_{POA}) = \frac{P_{max,Meas} G_{STC}}{P_{max,STC} G_{Meas}} \tag{2.57}$$

3. **Spectrum effects**
The spectrum difference from the reference spectrum mentioned in STC can lead to losses or gains in the energy output of the module. The spectral correction is obtained using a spectral mismatch factor according to IEC60904-7 [46]. The $\Delta MPR_{SL}$ is calculated as follows [50]:

$$\Delta MPR_{SL} = \frac{\int \overline{E}_{SUN}(\lambda) \cdot SR_{MOD}(\lambda)\, d\lambda}{\int \overline{E}_{SUN}(\lambda) \cdot SR_{PYR}(\lambda)\, d\lambda} \times \frac{\int E_{STC}(\lambda) \cdot SR_{PYR}(\lambda)\, d\lambda}{\int E_{STC}(\lambda) \cdot SR_{MOD}(\lambda)\, d\lambda} - 1 \tag{2.58}$$

where, $E_{STC}$ is the reference irradiance spectrum (AM1.5G), $\overline{E}_{SUN}$ is the average annual spectral irradiance, $SR_{PYR}$ is the spectral response of the pyranometer and $SR_{MOD}$ is the spectral response of the module.

4. **Angle of incidence losses**
The energy yield of a PV module can be obtained using the sum of the direct and diffuse irradiance components for various angular bands. For the calculation of $\Delta MPR_{AOI}$ the following equation is applied [50]:

$$\Delta MPR_{AOI} = \left(\frac{\int_t p(AOI) G_{POA}(AOI)\, dt}{\int_t G_{POA}\, dt}\right) - 1 \tag{2.59}$$

where $p(AOI)$ is the performance factor for the angular response of a flat sample measured in the laboratory:

$$p(AOI) = \frac{P_{max}(AOI)}{P_{max,STC}} \tag{2.60}$$

5. **Soiling losses**
The soiling losses accounts for the accumulation of snow, dust, leaves and bird droppings on the surface of PV panels resulting to lower performance of the module. Therefore, these losses depend on the climate conditions where the system is located as well on the cleaning procedure. For this reason, a constant factor coefficient can be used for each climate taking also into account the coating at the surface of the PV module (e.g anti-soiling coating).

After the calculation of $MPR$, the operating efficiency $\eta_{op}$ of the module can be obtained as follows:

$$\eta_{op} = MPR \times \eta_{STC} \tag{2.61}$$

This approach is easy to implement and the calculation of MPR is simplified compared to the methodology described in IEC-61853.

# 3

# Rear irradiance model

For the calculation of the energy rating, the irradiance reaching the rear side of the module is required. As discussed in the first chapter of this report two methods can be used for modelling rear side irradiance, one is ray-tracing and the other is view factor method. In this work, the view factor approach is used and a 2D geometric model is developed in MATLAB based on the available data for the reference climates. Since, the goal of the project is to calculate the energy rating, some simplifications were introduced to the irradiance model but at the same time keeping it sufficient enough for the problem. In this model a single standalone crystalline silicon (c-Si) module in two dimensions is assumed, which is equivalent to an infinitely long row of modules in three dimensions.

In this chapter the first objective mentioned in section 1.4 regarding the modelling of the rear side irradiance is examined. In the first section of this chapter, the coordinate system used in this work is defined while in section 3.2 the input data given in the IEC61853 standard are discussed. In section 3.3, section 3.4 and section 3.5 the procedure followed for the calculation of the rear side irradiance is explained. Thereafter, in section 3.6 the methodology used to obtain the spectrally resolved irradinace incident on the rear side of the module is described. Finally, in section 3.7 the results of the model are illustrated and discussed using a constant albedo value while in the last section of this chapter the effect of spectral albedo is examined.

## 3.1. Coordinate system

Before going into the details of the model it is of great importance to define the coordinate system. For convenience sake, a horizontal coordinate system is used to describe the position of the sun and the geometry of the system. Using this coordinate system the position of the sun is expressed by two angles, $altitude\ \alpha_s\ and\ azimuth\ A_s$.
The $altitude\ \alpha_s$ is the elevation of the sun measured in degrees above the horizontal plane. Its angular range is between -90° and 90°, where the negative values indicate that the sun is below horizon and thus not visible. The azimuth angle $A_s$ however, is the angular displacement from south of the projection of direct radiation on the horizontal plane. Its angular range is between -180° $\leq A_s \leq$ 180°,with zero due south, east negative, and west positive [51].

This coordinate system is used to precisely calculate the DNI using a 3D model approach as explained later in this chapter. An illustration of the coordinate system and the position of the sun is shown in Figure 3.1, where throughout the day the position of the sun and thus $\alpha_s$ and $A_s$ change.

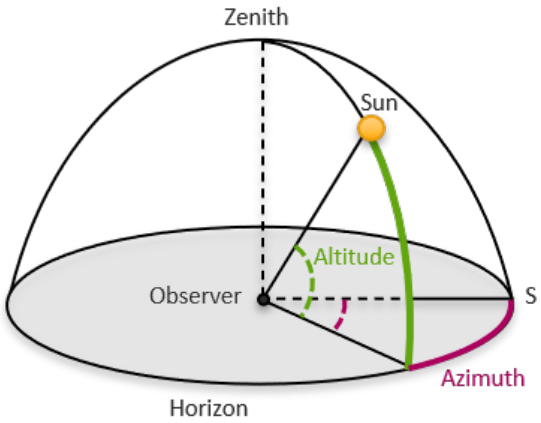


Figure 3.1: Horizontal coordinate system

## 3.2. Available data in IEC-61853 standard

At this section, the available data for the reference climate conditions which are given by the standard are discussed. The modules are mounted in a fixed position on free-standing racks facing the equator with an inclination angle of $20°$ from horizontal. In addition, the data for each climate are tabulated as hourly values for one full year and the parameters which are reported for each climate are the following:

- Date (Year/Month/Day)
- Hour (LST - Local Solar Time)
- Ambient temperature ($T_{amb}$)
- Wind speed at module height
- Sun elevation ($\alpha_s$)
- Sun incidence angle $AOI$
- Global horizontal irradiance ($GHI$)
- Direct horizontal irradiance ($B_h$)
- Global in-plane irradiance ($G$)
- Direct in-plane irradiance ($B$)
- Spectrally resolved global in-plane irradiance ($W/m^2$) for a set of discrete bands ($G(\lambda)$), with band intervals given in the tabulated data sets

In the following table the $latitude\ \phi$ and the yearly global in-plane irradiance for all reference climates is shown as given by $IEC61853-4$. Note, this standard is only applicable for mono-facial modules and thus $H_p$ corresponds to the total irradiance incident on the front side of the module.

| **Climate type** | **Latitude ($\phi$)** | **Total yearly global in-plane irradiance $H_p[kWh/m^2]$** |
|---|---|---|
| Tropical humid | 1°S | 1677.7 |
| Subtropical arid (dessert) | 33°30'N | 2295.5 |
| Subtropical coastal | 33°22'N | 1496.6 |
| Temperate coastal | 56°N | 972.9 |
| High elevation (above 3000 m) | 34°N | 2139.1 |
| Temperate continental | 57°N | 1266.0 |

Table 3.1: List of climatic data sets

The diffuse in-plane irradiance $D$ at the $j^{th}$ hour is not given in the data sets but it is easily obtained from the global in-plane irradiance $G$ and the direct in-plane irradiance $B$ as follows:

$$D_j = G_j - B_j \tag{3.1}$$

The same data are used for the calculation of the rear side irradiance. However, the calculation of the rear side irradiance requires DNI and As as an additional inputs. These are not explicitly given in the standard and the procedure to derive them is explained in the following.

First, the DNI is obtained using Equation 3.2:

$$DNI = B_h/cos(\theta_z) \tag{3.2}$$

where $\theta_z$ is the sun zenith angle $\theta_z = 90 - \alpha_s$. It is also important to know the position of the sun in the sky at the specific location for each hour of the year. As a result the sun azimuth angle $A_s$ is determined for each hour of the year using the following formula:

$$A_s = sign(\omega)|cos^{-1}(\frac{cos(\theta_z)sin(\phi) - sin(\delta)}{sin(\theta_z)cos(\phi)})| \tag{3.3}$$

where, $\omega$ is the hour angle, $\phi$ is the location latitude in degrees and $\delta$ is the declination angle. The hour angle ($\omega$) is an expression of time, expressed in degrees, from the solar noon. The rotation of the earth is 15° per hour and thus $\omega = 15°(LST - 12)$. By convection it is equal to zero at solar noon (when the sun reaches the highest point in the sky); negative in the morning and positive during the afternoon. The sign function in Equation 3.3 is therefore equal to +1 if $\omega$ is positive and -1 if $\omega$ is negative.

The declination angle $\delta$ is calculated using the following formula and a schematic representation is shown in Figure 3.2. This angle depends on the tilt of the earth on its axis of rotation as well as to the rotation of the earth around the sun. Note that, -23.45° ≤ $\delta$ ≤ 23.45°

$$\delta = (180\pi)(0.006918 - 0.399912cos(B) + 0.070257sin(B) - 0.006758cos(2B) + 0.000907sin(2B) - 0.002697cos(3B) + 0.00148sin(3B))$$

where B is given in Equation 3.4 and *n* is the day of the year.

$$B = (n-1)\frac{360}{365} \tag{3.4}$$

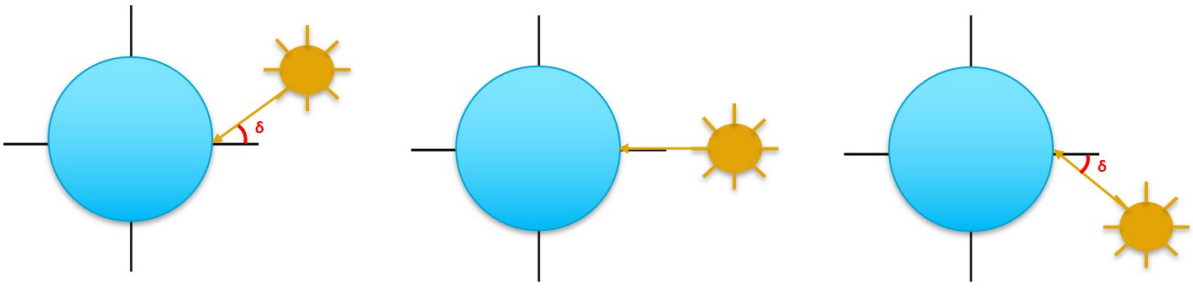


Figure 3.2: **Left**: $\delta_{max}$=23.45° on June 22, **Center**:$\delta_{max}$=0° on March 22 and September 22, **Right**: $\delta_{max}$=-23.45° on December 22

Using this procedure the direct normal irradiance $DNI$ and the *Sun azimuth angle* $A_s$ are calculated for each hour of the year for all the reference climates. As a result, all the necessary data for the calculation of the rear side irradiance are obtained and in the next sub-sections the procedure used to calculate each irradiance component is analyzed.

## 3.3. Direct irradiance

The direct in-plane irradiance on the rear side of a module is given by

$$B_r = DNI * cos(AOI_r) \tag{3.5}$$

where $AOI_r$ is the angle between the rear surface normal of the module and the incident direction of sunlight. Note, the subscript $r$ corresponds to the rear side of the module and the definition of the $AOI_r$ is the following, [52]:

$$AOI_r = cos^{-1}(cos(\theta_z)cos(\beta_r) + sin(\theta_z)sin(\beta_r)cos(A_s - A_{M_r})) \tag{3.6}$$

The $AOI_r$ is a function of $A_s$ and as a result the $AOI_r$ is obtained for any position of the sun at any instant time. For the rear side of bifacial modules, the tilt $\beta_r$ and azimuth angles $A_{M_r}$ are equal to (180°-$\beta_{front}$) and ($A_{M_{front}}$+180°) respectively. Note that when $AOI_r > 90°$, it means that direct sunlight cannot reach the rear side of the module. Therefore, two conditions must apply for the direct irradiance at the rear side of the module. First, its angular range should be $AOI_r \in$ [-90°,90°] and second, the sun should be visible - above the horizon $\alpha_s$>0°. In figure 3.3, the 3 dimensional system with the corresponding angles necessary for the calculation of DNI and $AOI_r$ is shown.

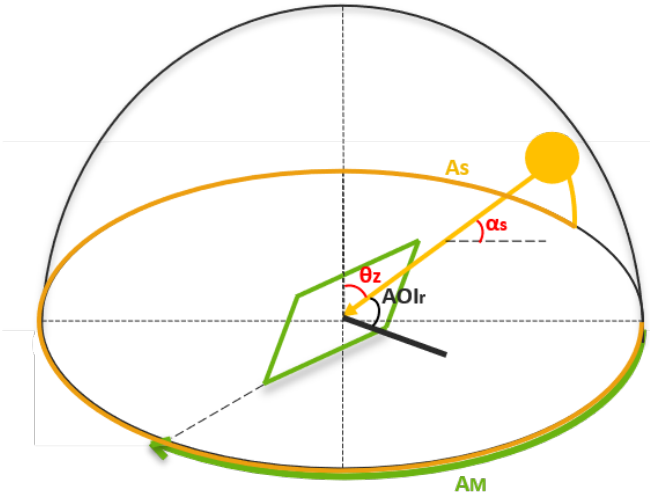


Figure 3.3: Angle of incidence at the rear side of the module

## 3.4. Diffuse irradiance

To determine the diffuse irradiance incident on the rear side of the module the same model used for the front side of the module is selected. Therefore, the Perez model is used to decompose the DHI into its circumsolar ($D_{r_{(circ)}}$), sky ($D_{r_{(sky)}}$), and horizon ($D_{r_{(hor)}}$) components as explained in subsection 2.3.4. The circumsolar irradinace is the outcome of light scattering by aerosols under clear sky while the diffuse irradiance which comes out from the earth horizon at $\theta_z = 90°$ is called horizon brightening. Finally, the isotropic irradiance component is included to form an overall anisotropic diffuse irradiance spectrum. However, the contribution of circumsolar, isotropic and horizon component have a different impact on the rear side irradiance of the module and consequently different approaches are used for each one of these components as follows:

$$D_{r_{(iso)}} = DHI(1 - F_1) * VF_{r \to sky} \tag{3.7}$$

$$D_{r_{(circ)}} = DHI * F_1(\frac{\alpha}{b}) \tag{3.8}$$

$$D_{r_{(hor)}} = DHI * F_2 sin(\beta_r) \tag{3.9}$$

where $VF_{r\rightarrow sky} = (1 - cos(\beta_r))/2$ is the view factor from the rear side of the module towards the sky. The total diffuse irradiance on the rear side of the module is given by the following equation:

$$D_r = D_{r_{(iso)}} + D_{r_{(circ)}} + D_{r_{(hor)}} \tag{3.10}$$

## 3.5. Ground reflected irradiance

Since no information regarding the exact location and the system are given in the standard, a simplified approach is used to calculate the reflected irradiance. The method presented here, is an application of view factors for a 2D geometry of a single standalone module located in a free horizon area. Therefore, no light is reflected form other surfaces such as building or nearby PV modules. The average value of the ground albedo is selected to be a constant value of 0.2, a usual assumption whenever the local albedo is not measured or known (see, e.g [53] and the references therein). In addition, the shadow cast effect is taken into account and hence some geometric characteristics of the system have to be determined, that is the module length *(ML)* and the height of the lowest point of the module from the ground *(HG)*. In this simulation the following geometry parameters are considered:

| | |
|---|---|
| Number of cells | 6×12 |
| Cell width [cm] | 16.17 |
| Height from ground [m] | 1.00 |
| Module length in landscape orientation [m] | 1.02 |
| Module length in portrait orientation [m] | 2.02 |

Table 3.2: Geometric characteristics of the system

The shadow of the module can significantly affect rear side irradiance and thus it could not be neglected. Figure 3.4, shows the side view of a module with the necessary parameters needed for the calculation of the shadow length of an elevated PV module tilted at an angle $\beta$. Note that the horizontal dashed line is a projection of the ground where the black color corresponds to the shaded part while the yellow colour to the unshaded part of the ground.

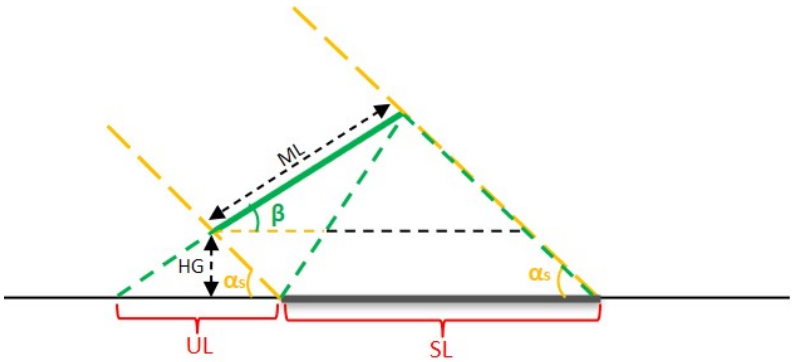


Figure 3.4: Schematic showing of the side view and the shadow length of an elevated PV module

Since the module is elevated, it should be taken into account that some part of the ground beneath the module is not shaded. Using some trigonometric operations, the *unshaded length (UL)* shown in Figure 3.4 is obtained, while *shadow length (SL)* is determined using Equation 3.11 [52]. As can be observed, the $SL$ of the module varies with time along the day since it is a function of sun position and also depends on module orientation, and module length.

$$SL = ML[cos(\beta) + sin(\beta)cot(\alpha_s)cos(A_M - A_s)] \tag{3.11}$$

The proposed model takes the shadow effect into account only when the sun is at the front of the module (as illustrated with red in Figure 3.5) resulting a shadow behind the module. This assumption is used to reduce the computational time since any shadow in front of the module affects the front side irradiance. It should be considered, that the irradiance on the front side of the module is calculated

and provided by IEC-61853 standard where the component of reflected irradiance is neglected and therefore, no further calculations are required.

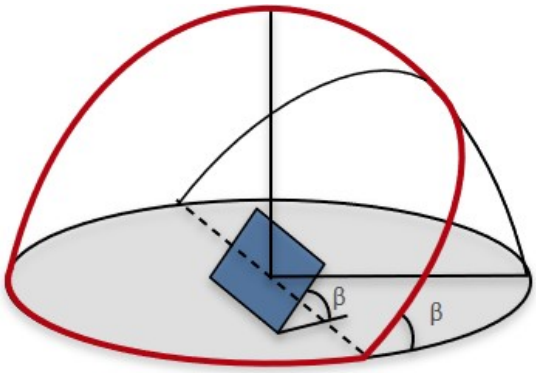


Figure 3.5: Celestial hemisphere

For the calculation of the view factors, a distinction is made between the shaded and unshaded grounds. According to J. Appelbaum [54], the view factor from the rear side of a single collector row to the shaded and unshaded grounds are given by equation 3.14 and 3.15 respectively.

$$VF_{r\to grd.s} = \frac{ML + SL - [ML^2 + SL^2 - 2ML * SLcos(\beta)]^{1/2}}{2ML} \tag{3.12}$$

$$VF_{r\to grd.us} = \frac{MLcos(\beta) - [ML^2 + SL^2 - 2ML * SLcos(\beta)]^{1/2} - SL}{2ML} \tag{3.13}$$

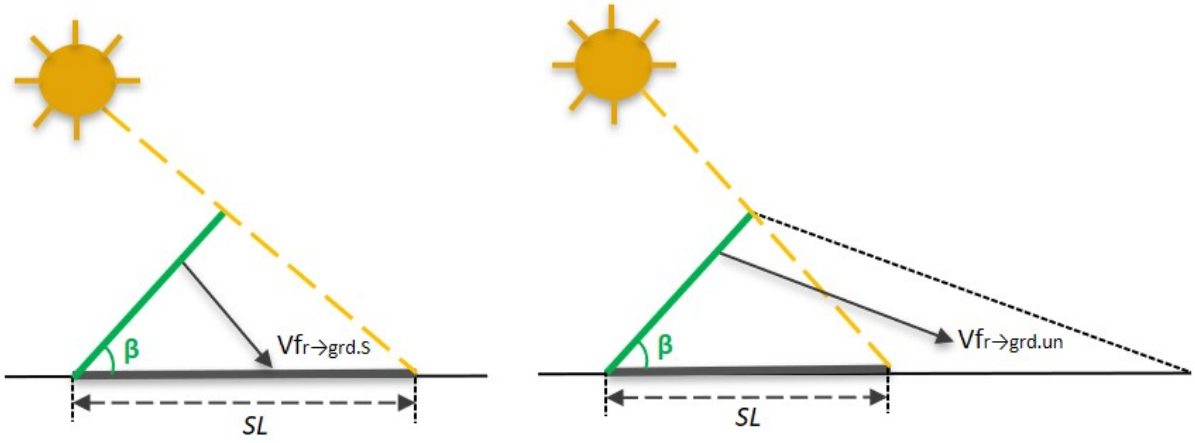


Figure 3.6: View factor from the rear side of collector attached to the ground to shaded (*left*) and not shaded grounds (*right*)

Note, these view factor equations were established for modules which are attached to the ground. However, as already mentioned, the examined modules are now elevated from the ground ($HG$) and as a result part of the ground behind the PV modules may not be shaded, at any instant of time. Thus, equations 3.14 and 3.15 should be adjusted as follows:

$$VF_{r\to Shaded} = VF_{r\to grd.s} - VF_{r\to us(1)} \tag{3.14}$$

$$VF_{r\to Unshaded} = VF_{r\to us(1)} + VF_{r\to grd.us} \tag{3.15}$$

To get a better understanding of these equations and relative parameters, Figure 3.7 was developed.

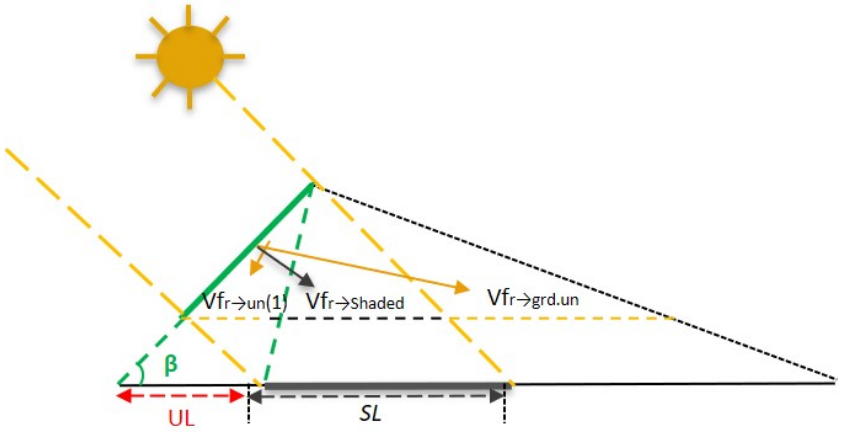


Figure 3.7: View factor from the rear side of an elevated module to the shaded (*left*) and not shaded grounds (*right*)

To verify the results, the summation rule is used where the sum of the view factors of the rear side of the collector should always equal to unity as shown in Equation 3.16. An illustration of all the view factors used in this model is shown in Figure 3.8.

$$VF_{r\rightarrow sky} + VF_{r\rightarrow Shaded} + VF_{r\rightarrow Unshaded} = 1 \tag{3.16}$$

For the calculation of the rear side irradiance some assumptions are used. First, it is assumed that the light reflected from the ground is isotropic (lambertian reflection). Additionally, the irradiance on the unshaded part of the ground is assumed equal to the *GHI* whereas for the shaded areas the *DHI* is used due to the obstruction of the direct sunlight. Finally, the assumption that the modules are completely opaque is implemented in the model meaning that no light can be transmitted through the module.

Using the aforementioned *VFs* and assumptions, the hourly ground reflected irradiance on the rear side of the modules is obtained.

$$G_r^{refl} = \alpha * DHI * VF_{r\rightarrow Shaded} + \alpha * GHI * VF_{r\rightarrow Unshaded} \tag{3.17}$$

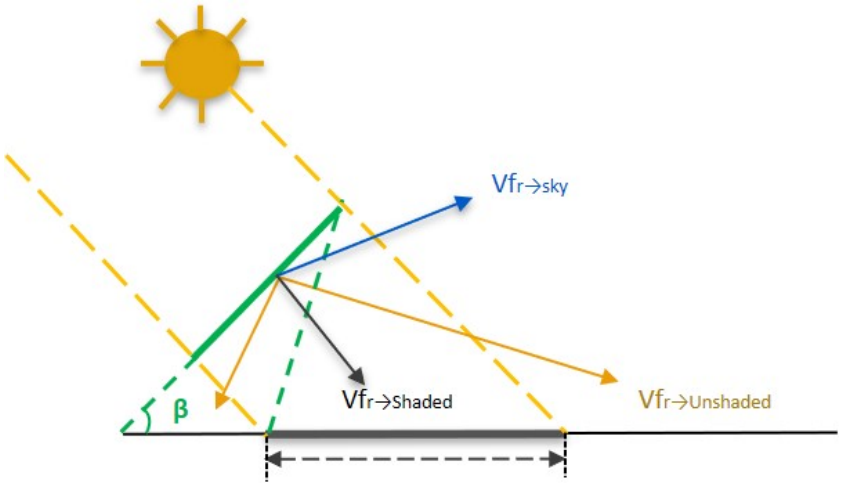


Figure 3.8: View factors to sky and ground, rear side of collector- shaded and not shaded grounds

## 3.6. Spectrally resolved rear irradiance calculation

In this section, the spectrally resolved irradinace incident on the rear side of the module ($G_{rear}(\lambda)$) is calculated. $G_{rear}(\lambda)$ is used for the correction of the the rear-side irradiance for the spectrum effects

as explained in the following chapter (subsection 4.2.2). However, according to the standard, necessary information such as the exact locations of the systems are not available, making it impossible to calculate $G_{rear}(\lambda)$. More precisely, the only available spectral information is the front-side in-plane irradiance. Therefore, the only way to obtain the spectral irradiance on the rear side of the module is to use this spectrum of the front side for the rear side of the module as follows.

Since the hourly values of DHI and GHI are available in the standard, the DHI($\lambda$) and GHI($\lambda$) can be obtained using the scaling method.

$$DHI(\lambda) = \frac{DHI}{G_f} G_f(\lambda) \tag{3.18}$$

$$GHI(\lambda) = \frac{GHI}{G_f} G_f(\lambda) \tag{3.19}$$

Similarly, using the hourly values of direct ($B_r$) and diffuse irradiance ($D_r$) obtained from the irradiance model, the spectrally resolved direct ($B_r(\lambda)$) and diffuse irradiance ($D_r(\lambda)$) incident on the rear side of the module are obtained.

$$B_r(\lambda) = \frac{B_r}{G_f} G_f(\lambda) \tag{3.20}$$

$$D_r(\lambda) = \frac{D_r}{G_f} G_f(\lambda) \tag{3.21}$$

After the calculation of both DHI($\lambda$) and GHI($\lambda$), the ground reflected irradiance on the rear side of the module can be estimated.

$$G_r^{refl}(\lambda) = \alpha(\lambda)(DHI(\lambda) * VF_{r\rightarrow grd.s} + GHI(\lambda) * VF_{r\rightarrow grd.us}) \tag{3.22}$$

Note that instead of fixed albedo value, spectral albedo can also be used as discussed in section 3.8. Finally, the spectrally resolved irradiance incident on the rear side of the module is obtained as follows:

$$G_{rear}(\lambda) = B_r(\lambda) + D_r(\lambda) + G_r^{refl}(\lambda) \tag{3.23}$$

In the case where all the necessary data are available, the spectral correction coefficient can be estimated more precisely. The data which are currently not defined in the standard and are necessary for the calculation of the rear-side spectral irradiance are the following:

- Spectrally resovled global horizontal irradiance GHI($\lambda$)
- Spectrally resovled diffuse horizontal irradiance DHI($\lambda$)

Note, that these data might be available to the people who created the standard. Consequently, if these data will be published in the near future the following procedure can be used tackle the effect of spectral mismatch at the rear side of the module. Assuming that both GHI($\lambda$) and DHI($\lambda$) are given in the standard the rear in-plane irradiance can be obtained besed on these two variables. First of all, the spectrally resovled direct horizontal irradiance $B_h(\lambda)$ can be obtained as follows:

$$B_h(\lambda) = GHI(\lambda) - DHI(\lambda) \tag{3.24}$$

Then, the Bh($\lambda$) can be used in the irradiance model to obtain DNI($\lambda$) and finally calculate the direct component of irradiance incident on the rear side but spectrally resolved ($B_r(\lambda)$). Similarly, the DHI($\lambda$) can be used to obtain the diffuse spectrally resolved irradiance component ($D_r(\lambda)$) and using both GHI($\lambda$) and DHI($\lambda$) as well as the reflectance of the ground $\alpha$, the spectral ground reflected irradiance incident in the rear side of the module can be determined. The combination of all three spectral irradiance components per wavelength range are equal to the total spectrally in-plane irradiance $G_{rear}$ measured in [$W/m^2nm$] as shown in Equation 3.23.

## 3.7. Irradiance model results

In this section, the results of the rear irradiance model are analysed. More specifically, only the results of one of the reference climates are illustrated in this section, while the results for the rest of the climates can be found in Appendix B. Generally, Europe is characterized by temperate climates where most of the western Europe including the Netherlands has *temperate coastal climate* featuring mild summers and cool but not cold winters depending on their latitude. Consequently, the temperate coastal climate was chosen to be examined as it is one of the most common climates in terms of population and therefore the results are of a great interest.

Before heading to the results of the model, it is important to mention that the impact of ground clearance (height of the module from the ground) and the effect of the transparent area of the module to the total irradiation were investigated. In the simulations, the height of the module from the ground (ground clearance) which is not specified in the standard is selected to be constant at *HG=1m* and the module is assumed to have 0% transparent area. Note that the elevation of the module from the ground is not randomly chosen. This parameter was adjusted in the simulations as shown in Figure 3.9 where the annual irradiance on the rear side of the module for different ground clearance values is presented. As shown in the figure, both portrait and landscape orientations of the module are analysed shown with blue and orange colour respectively.

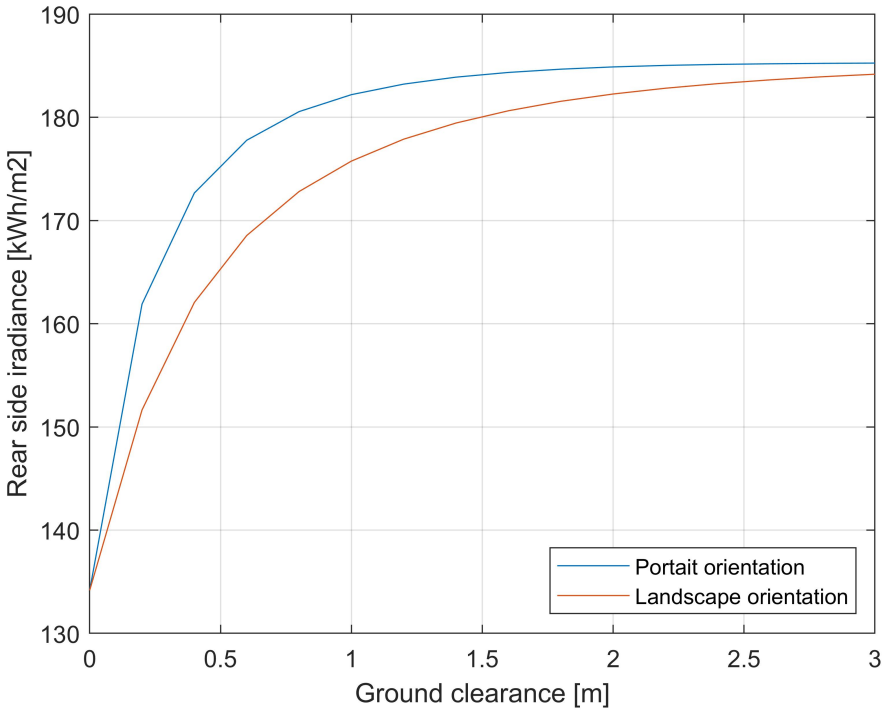


Figure 3.9: Annual rear side irradiance for various ground clearance values

As can be observed, the irradiance on the rear side of the module strongly depends on the ground clearance. However, at sufficient height the impact of ground clearance on the rear side irradiance is minimized. These results are in agreement with the literature where it was found that the uniformity of the irradiance on a module surface increases at sufficient height (usually at *HG*≥*1*m) while at the same time the impact of the module transparent area on the rear side irradiance is minimised [55]. As shown in the figure above, when modules are installed in portrait orientation the impact of ground clearance on the rear side irradiance is minimized at higher heights ($HG \geq 1$m), while for the case of landscape orientation this impact is minimized at higher heights ($HG \geq 1.5$m). In the following simulation results the modules are assumed to be installed in portrait orientation at 1m from the ground surface with 0% transparent area.

In Figure 3.10 the monthly in-plane irradiance on monofacial and bifacial modules for the temperate coastal climate is shown. Note, that the incident irradiance on the front side of monofacial module was measured and provided by the IEC-61853 while the rear irradiance incident on the rear side of bifacial module was calculated as previously described in this chapter. As can be seen in the figure, the highest amount of irradiance is absorbed in July for both types of modules and as it was expected more irradiance is absorbed from bifacial than monofacial modules over the year.

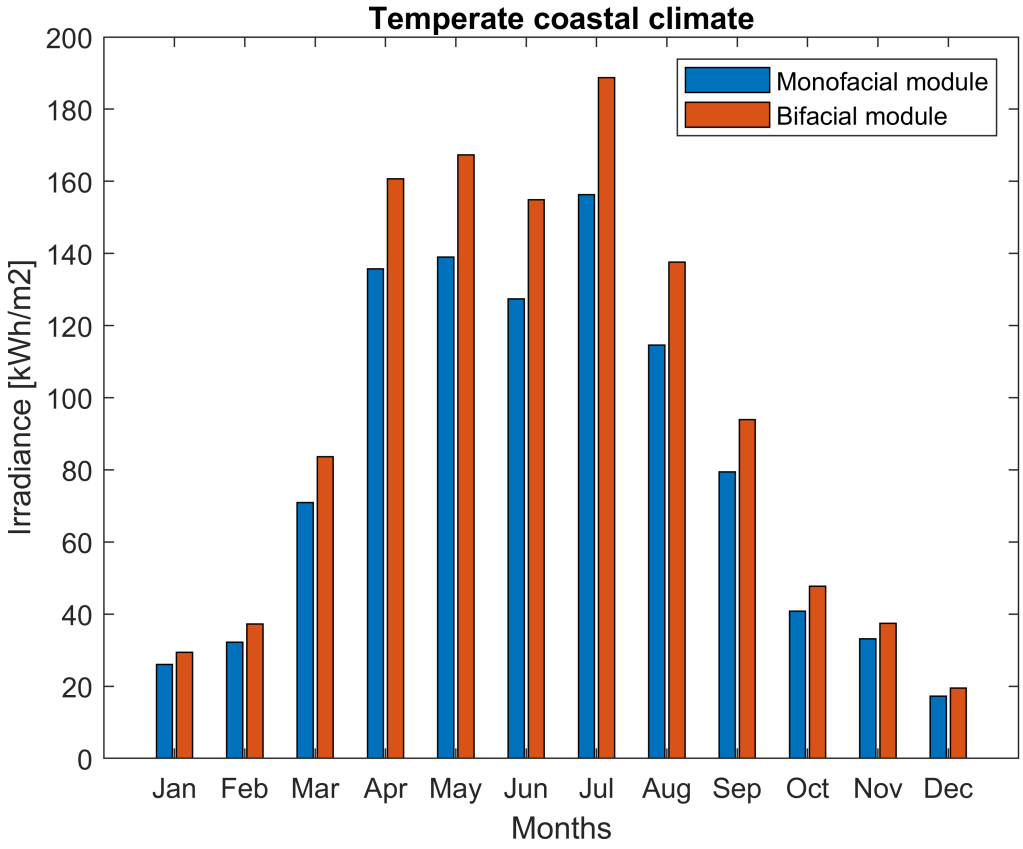


Figure 3.10: Monthly irradiance on monofacial and bifacial modules over a year

An overview of the total irradiance for all the reference climates can be seen in Table 3.3 where the yearly irradiance is shown and compared for both bifacial and monofacial modules.

| **Climate type** | **Irradiance on monofacial modules [kWh/m$^2$]** | **Irradiance on bifacial modules [kWh/m$^2$]** |
|---|---|---|
| Tropical humid | 1677.7 | 2003.1 (+19.4%) |
| Subtropical arid (dessert) | 2295.5 | 2656.2 (+15.7%) |
| Subtropical coastal | 1496.6 | 1755.3 (+17.3%) |
| Temperate coastal | 972.9 | 1148.7 (+18.1%) |
| High elevation (above 3000 m) | 2139.1 | 2483.6 (+16.1%) |
| Temperate continental | 1266.0 | 1472.2 (+16.3%) |

Table 3.3: Yearly Irradiance

In tropical humid climate, the largest difference in the irradiance level between monofacial and bifacial modules was observed, whereas in subtropical arid climate this difference was the lowest. More specifically, in tropical climate, the irradiance on bifacial modules was higher than monofacial by 19.4% while in subtropical arid climate the difference was just 15.7%. These results imply that it would be advantageous to install bifacial modules especially in areas with tropical humid climate but also in any other

climates since more irradiance can be collected than monofacial modules. However, more research is required to identify whether the installation of bifacial modules will be efficient enough or not. In other words, an optimization method should be developed where the energy output of the system and other parameters such as the land area cost and the mounting structure costs should be taken into account.

Figure 3.11 shows the contribution of direct (blue), diffuse (orange) and ground reflected irradiance (yellow) at the rear side of a module for a year. Obviously most of the light comes from ground reflection (88.3%), where a constant albedo value of 0.2 was used. Later in this work, other albedo values are used in the model to investigate their impact to the total in-plane irradiance. On the other hand, the direct irradiance has the least contribution with 0.5% and diffuse irradiance accounted for 11.2% of the total irradiance. Consequently, the ground reflected irradiance cannot be neglected as in the case of monofacial modules and thus, a more detailed analysis is required when installing bifacial modules.

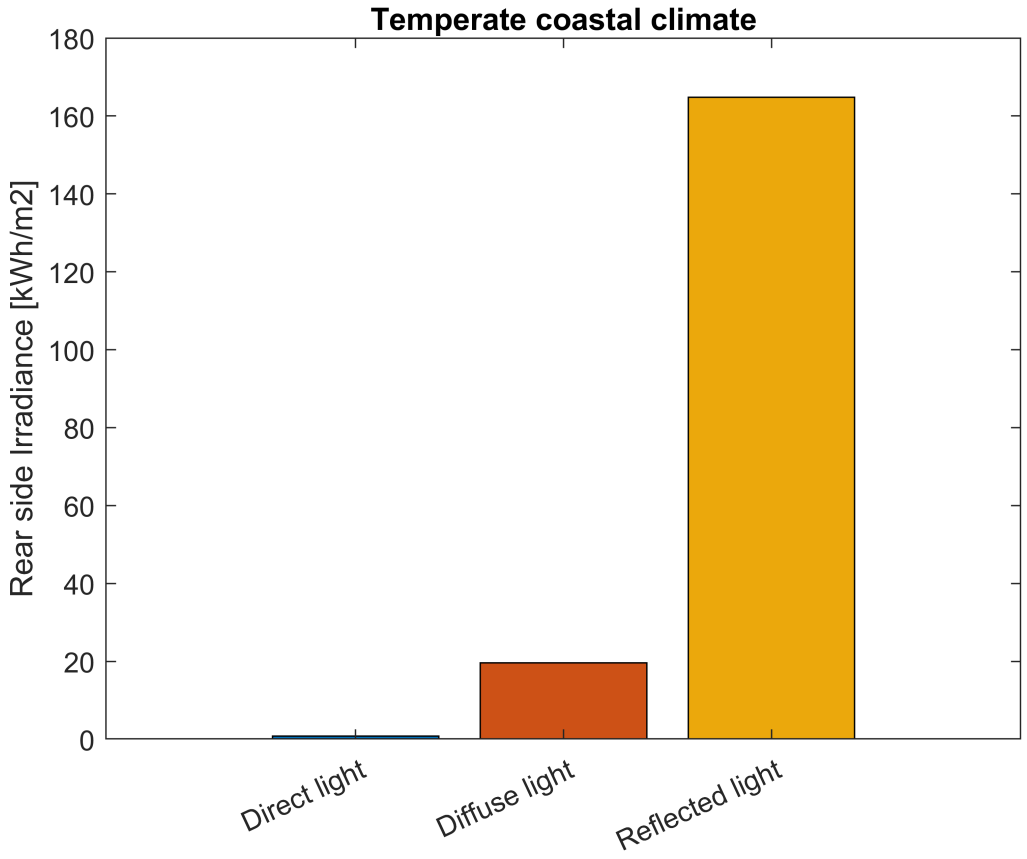


Figure 3.11: Annual rear side irradiance composition

Finally, in Figure 3.12, the distribution of the irradiance components at each month of the year are demonstrated. It can be seen that between May and July the contribution for direct, diffuse and ground reflected irradiance is the highest. This can be attributed to the fact that the days are much longer than nights leading to more irradiation at the rear side of the module during that period. Also, since the sun's rays hit the earth at a more direct angle, more sunlight can be reflected to the module.

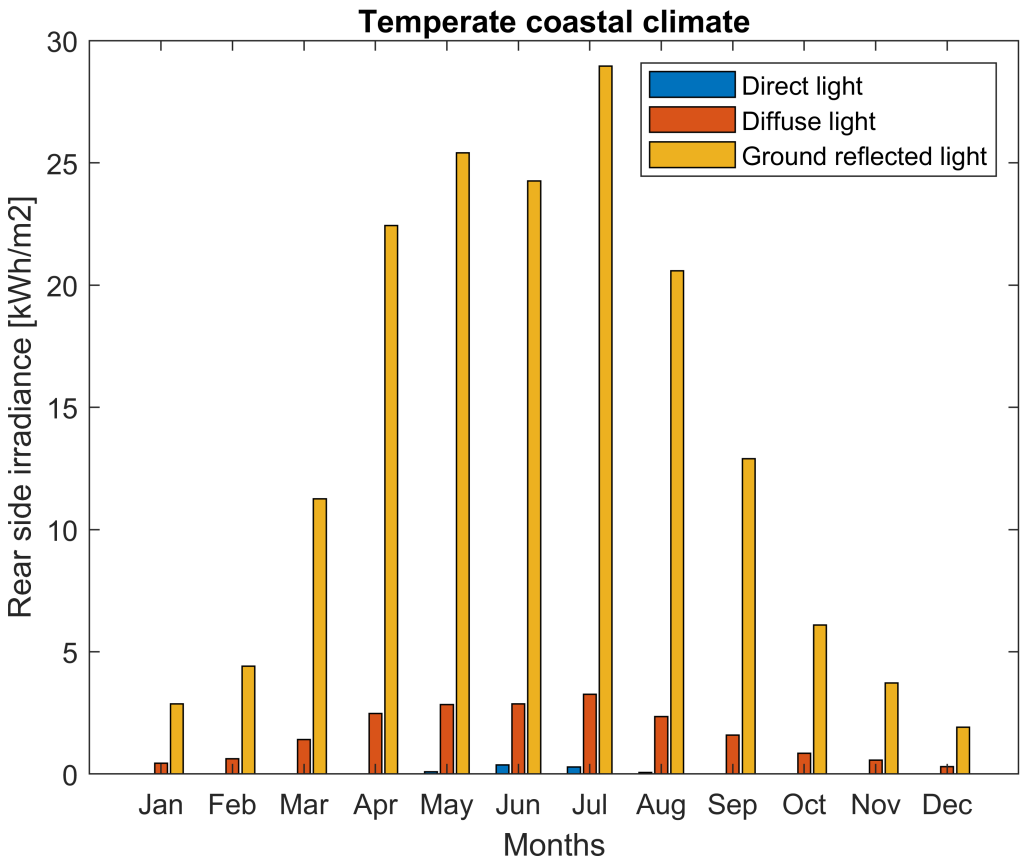


Figure 3.12: Monthly rear side irradiance composition

## 3.8. Spectral albedo calculation

In this section, the irradiance model developed for the calculation of the rear side irradiance is extended to calculate the rear irradiance using spectral albedo values from various ground materials. Until now, the simplest albedo model with a constant value $\alpha = 0.2$ is used in the model. However, this assumption is not always suffice to obtain the amount of reflected light with high accuracy and might lead to considerable errors in the results. As a result, a more advanced model for the ground reflectivity is used.

According to the law of conservation of energy, the total energy of an isolated system remains constant and consequently the irradiance that it is not reflected is either absorbed or transmitted. Since irradiance is a spectral quantity, its contribution to the ground reflectivity must be taken into account. This is the so called spectrally-integrated albedo $\alpha_{SI}$ which is defined as the ratio of the area under the reflected irradiance curve and the area under the incoming spectral irradiance as shown in Equation 3.25

$$\alpha_{SI} = \frac{G_{reflected}}{G_{received}} = \frac{\int A(\lambda)G(\lambda)d\lambda}{\int G(\lambda)d\lambda} \tag{3.25}$$

where A($\lambda$) is the spectral reflectivity and G($\lambda$) is the incoming global spectral irradiance. The integration limits are usually between 300nm to 4000nm, since almost 100% of the reference irradiance spectrum defined by AM1.5G is within this wavelength range [56], [57]. It should be noted that in reality, the irradiance spectrum $G(\lambda)$ changes over time as it depends on the sky conditions and the position of the sun leading to change of the air mass (AM). This also affects the reflectivity $\alpha_{SI}$ because some materials reflect more light at specific wavelengths than other wavelengths.

To include $\alpha_{SI}$ in the model, the global in-plane spectrally resolved irradiance $G_F(\lambda)$ given in the standard for each climate is used while the spectral reflectivity A($\lambda$) is obtained using the online ECOSTRESS spectral library developed by NASA [58]. Since the ground material is not defined in the standard, the following materials are selected to be examined:

- Green grass
- Black paint
- Construction Asphalt
- Gray Sandstone rock (gravel)
- Snow
- Red brick

After the calculation of $A(\lambda)$ and $G(\lambda)$, the ground reflectivity is obtained. A graphical represantation of $A(\lambda)$ for green grass and $G(\lambda)$ for the temperate coastal climate given in the standard are illustrated in figures 3.13 and 3.14 respectively.

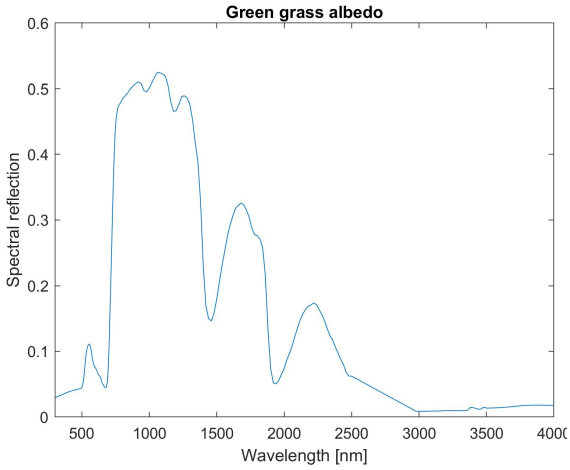


Figure 3.13: Spectral reflectivity of green grass

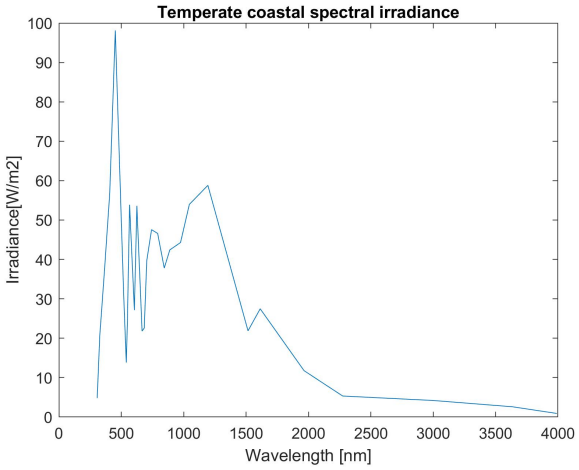


Figure 3.14: Global in-plane spectral irradiance

By definition, $A(\lambda)$ is lower than unity for all wavelengths leading to the conculsion that the value of $\alpha_{SI}$ will always be lower than unity as was expected.

However, this approach for averaging albedo data neglects the spectral response of the module. To take this effect into account, the short circuit current ($I_{sc}$) of the module which is directly dependent on the spectrally resolved in-plane irradiance ($G_F(\lambda)$) and the spectral response $SR(\lambda)$ of the PV module will be used.

$$I_{sc} = \int SR(\lambda) G_F(\lambda) \tag{3.26}$$

According to Andrews R. ad Pearce J. [56], the ratio between the $I_{sc}$ developed due to albedo irradiation and to the $I_{sc}$ developed using the total irradiation on the module surface, a new albedo called spectrally responsive albedo was defined. The definition of the spectrally responsive albedo ($\alpha_{SR}$) which is also implemented in the model is the following:

$$\alpha_{SR} = \frac{\int SR(\lambda) A(\lambda) G_F(\lambda) d\lambda}{\int SR(\lambda) G_F(\lambda) d\lambda} \tag{3.27}$$

As can be seen from the above equation, $\alpha_{SR}$ is a function of SR which is differs between PV module technologies. This is the main disadvantage of using $\alpha_{SR}$ as it should be recalculated when different technologies are considered. Usually the integration limits are from 300nm to 4000nm (as for $\alpha_{SI}$) but since c-Si modules are used in the model, a wavelength range between 300nm to 1200nm was selected to further reduce the simulation time. This is because the SR of c-Si modules is zero for wavelengths above 1200nm and thus no light can be absorbed (see Figure 2.12).

The spectrally resolved in-plane irradiance ($G_F(\lambda)$) at each climate condition was available for a set of discrete bands and using the interpolation method the $SR(\lambda)$ and $A(\lambda)$ were obtained for the same wavelength ranges. Then, following equation 3.27, $\alpha_{SR}$ was calculated for each hour of the year as shown in the figure below.

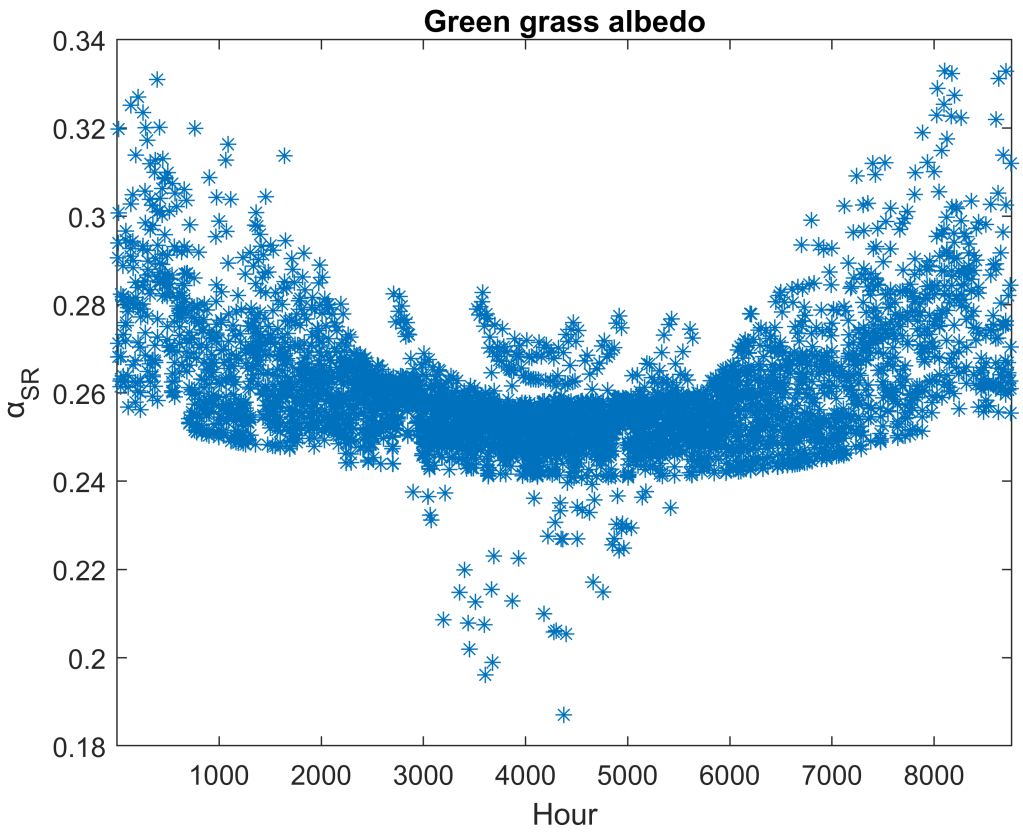


Figure 3.15: Spectral responsive albedo under temperate coastal climate conditions

As shown in Figure 3.15, the spectral responsive albedo of green grass under temperate coastal conditions is not constant over time. Implementing these albedo values into the rear irradiance model, different amount of irradiance is reflected from the ground towards the rear side of the module as will be analysed in the next section.

### 3.8.1. Spectral albedo effects

As mentioned previously, using equations 3.25 and 3.27, $\alpha_{SI}$ and $\alpha_{SR}$ can be obtained for each hour of the year. To compare the effect between these values on the ground reflected irradiance, the weighted average $\alpha_{SI}$ and weighted average $\alpha_{SR}$ are calculated over the course of the year. In addition, the weighted average spectral integrated albedo using the reference spectrum of AM1.5g ($\alpha_{SI_{AM1.5g}}$) is calculated. The weighted albedo values for the selected ground materials are listed in Table 3.4 under all climate conditions.

| Climate | Ground type | $\alpha_{SI_{AM1.5g}}$ | $\alpha_{SI}$ | $\alpha_{SR}$ | $I_{SI_{AM1.5g}}$ $[kWh/m^2]$ | $I_{SR}$ $[kWh/m^2]$ |
|---|---|---|---|---|---|---|
| Tropical humid | Green grass | 0.23 | 0.22 | 0.25 | 370 | 392 |
| | Black paint | 0.03 | 0.03 | 0.03 | 84 | 84 |
| | Asphalt | 0.08 | 0.08 | 0.08 | 148 | 148 |
| | Gray gravel | 0.43 | 0.42 | 0.43 | 655 | 660 |
| | Snow | 0.87 | 0.82 | 0.91 | 1307 | 1371 |
| | Red brick | 0.21 | 0.22 | 0.20 | 337 | 319 |
| Subtropical arid | Green grass | 0.23 | 0.23 | 0.26 | 411 | 456 |
| | Black paint | 0.03 | 0.03 | 0.03 | 92 | 92 |
| | Asphalt | 0.08 | 0.08 | 0.08 | 163 | 163 |
| | Gray gravel | 0.43 | 0.42 | 0.43 | 728 | 740 |
| | Snow | 0.87 | 0.79 | 0.91 | 1454 | 1518 |
| | Red brick | 0.21 | 0.24 | 0.20 | 374 | 365 |
| Subtropical coastal | Green grass | 0.23 | 0.23 | 0.26 | 294 | 324 |
| | Black paint | 0.03 | 0.03 | 0.03 | 67 | 68 |
| | Asphalt | 0.08 | 0.08 | 0.08 | 118 | 118 |
| | Gray gravel | 0.43 | 0.44 | 0.44 | 520 | 531 |
| | Snow | 0.87 | 0.80 | 0.91 | 1037 | 1087 |
| | Red brick | 0.21 | 0.24 | 0.20 | 268 | 260 |
| Temperate coastal | Green grass | 0.23 | 0.23 | 0.26 | 200 | 220 |
| | Black paint | 0.03 | 0.03 | 0.03 | 47 | 48 |
| | Asphalt | 0.08 | 0.08 | 0.08 | 82 | 82 |
| | Gray gravel | 0.43 | 0.42 | 0.43 | 351 | 356 |
| | Snow | 0.87 | 0.81 | 0.91 | 697 | 728 |
| | Red brick | 0.21 | 0.24 | 0.20 | 182 | 177 |
| High elevation | Green grass | 0.23 | 0.24 | 0.27 | 391 | 444 |
| | Black paint | 0.03 | 0.03 | 0.03 | 87 | 87 |
| | Asphalt | 0.08 | 0.08 | 0.08 | 155 | 155 |
| | Gray gravel | 0.43 | 0.42 | 0.43 | 694 | 707 |
| | Snow | 0.87 | 0.77 | 0.91 | 1388 | 1445 |
| | Red brick | 0.21 | 0.25 | 0.21 | 356 | 352 |
| Temperate continental | Green grass | 0.23 | 0.24 | 0.26 | 234 | 262 |
| | Black paint | 0.03 | 0.03 | 0.03 | 55 | 56 |
| | Asphalt | 0.08 | 0.08 | 0.08 | 96 | 96 |
| | Gray gravel | 0.43 | 0.42 | 0.43 | 412 | 420 |
| | Snow | 0.87 | 0.79 | 0.91 | 818 | 854 |
| | Red brick | 0.21 | 0.24 | 0.21 | 213 | 209 |

Table 3.4: Weighted averages of albedos with the resulted irradiance values

As expected, the $\alpha_{SI_{AM1.5g}}$ changes according to the ground material but it remains the same for all climate conditions since the same sky spectrum (AM1.5G) is used. In addition, as listed in Table 3.4, the average weighted albedo values ($\alpha_{SI_{AM1.5g}}$, $\alpha_{SI}$, $\alpha_{SR}$) of black paint and asphalt under all climate conditions are the same while the average albedos of green grass, grey gravel and red brick show a variation smaller than 0.04. At last, the average albedo value of snow show deviations up to 0.12 depending on the climate. Note that this behaviour is similar for all climates.

The blue curve shown in figure 3.16 and 3.17 represents the spectral reflectance of green grass and snow respectively which were taken from the Ecostress Spectral Library provided by NASA Jet Propulsion Laboratory [58]. In addition, the flat lines represent the $\alpha_{SI}$, $\alpha_{SR}$ and $\alpha_{SI_{AM1.5g}}$ with red, black and purple colours respectively for both green grass and snow. As can be seen in figure 3.16, the minor difference between $\alpha_{SI}$ and $\alpha_{SI_{AM1.5g}}$ is not visible as their difference is less than 0.01 (see Table 3.4).

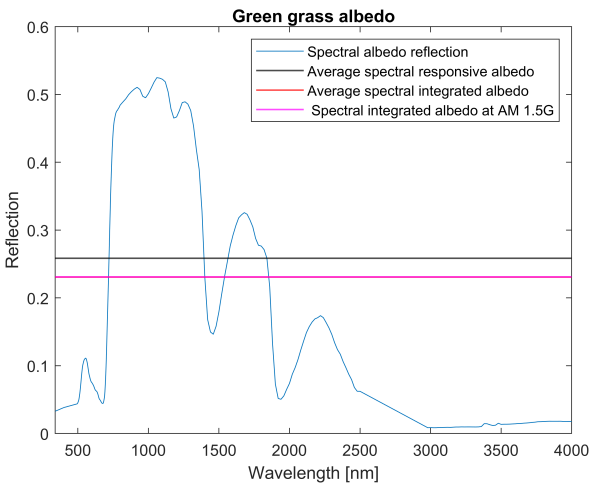


Figure 3.16: Green grass reflection under temperate coastal climate conditions

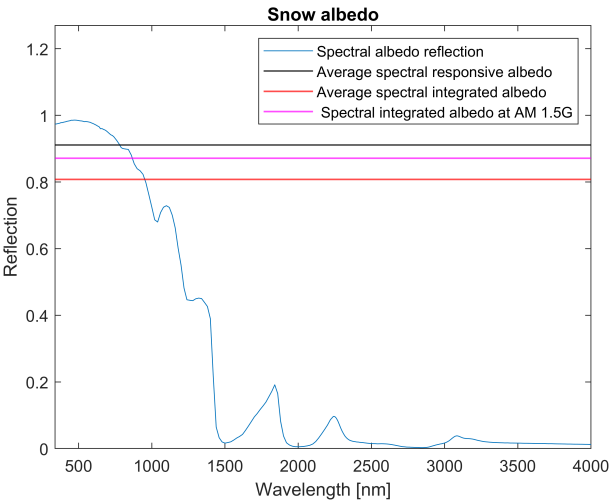


Figure 3.17: Snow reflection under temperate coastal climate conditions

In Table 3.4 the annual rear side in-plane irradiance using the spectral integrated albedo under the reference spectrum AM1.5g ($I_{SI_{AM1.5g}}$) and the spectrally responsive albedo ($I_{SR}$) for each ground material is illustrated. As can be observed, materials with higher albedo, can reflect more light towards the module. In that case, six materials were compared and as it was expected most of irradiance is reflected when ground is covered with snow while the least irradiance is reflected when ground is painted black. Therefore, when designing a PV system with bifacial modules, it is significantly important to carefully decide which material should be placed underneath the modules to achieve optimum efficiency. Additionally, as shown in the table, the use of improper albedo values can lead to under or over-prediction of system irradiance and energy yields, leading to improper optimization of the PV system. As a result, the values of weighted albedos are crucial for the calculation of the rear side in-plane irradiance and thus the energy rating.

## 3.9. Conclusions

In this chapter, the model used for the calculation of the irradiance incident on the rear side of a PV module is described using the data acquired from IEC-61853 standard. The in-plane irradiance is separated into direct, diffuse and ground reflected irradiance where different models are used for their estimation. To calculate the direct irradiance on the rear side of the module, the AOI is required. For the calculation of the rear side diffuse irradiance component the Perez model is used. Finally, the irradiance reflected from the ground towards the rear side of the module is obtained using the view factor technique where a distinction is made between the view factors to shaded and unshaded grounds. Additionally, the effect of mounting height of the module is examined and found that the uniformity of the irradiance on a module surface increases at sufficient height (usually at $HG \geq 1$m). According to the results of the model it can be concluded that bifacial modules can absorb 15-19% more irradiance than monofacial modules. In addition, the effect of the spectral albedo is examined where it is shown that the use of improper albedo values can lead to under/over prediction of the system irradiance by around 4% depending on the climate conditions and the ground material.

# 4

# Energy rating

Currently, no methods have been developed for the calculation of energy rating of bifacial modules while the IEC-61853 standard can be used to obtain the energy rating of monofacial modules. This chapter is focused on the second objective mentioned in section 1.4 to extend this standard towards bifacial modules. More specifically, in section 4.1, the energy rating as obtained in IEC-61853 standard is illustrated, while in section 4.2 the methodology to estimate the energy rating of bifacial modules is discussed, including the correction of the rear side irradiance and the calculation of power output of the module. Finally, in section 4.3 and 4.4 two approaches used for the calculation of energy rating of bifacial modules are described and compared with the energy rating of monofacial modules while different bifacialities are introduced in the model.

## 4.1. Energy rating obtained in IEC-61853

In this section, the energy rating obtained using the methodology described in part 3 of IEC-61853 standard is described. As discussed in the previous chapter, this methodology is based on hourly data of a full year but it is important to note that these data are not enough to precisely estimate the energy output of a PV module in a specific location. To provide an accurate estimation of the energy yield, additional information about the specific site are required including climatic data for several years, more data regarding the presence of shadows and dust on the modules as well as details about the installation configuration. According to the standard, several simplifications were considered in the energy rating process of monofacial modules. The CSER of monofacial modules is defined as shown in Equation 4.1, where the subscript ”std” indicates that this methodology is the one described in the standard.

$$CSER_{Mon_{std}} = \frac{E_{year_{front}} G_{STC}}{P_{STC} H_{year_{front}}} \tag{4.1}$$

As shown in Equation 4.1, the annual energy rating of monofacial modules ($E_{year_{front}}$) is required and it is calculated using the methodology described in subsection 2.7.1. $H_{year_{front}}$ is the incident irradiance on the front side of the module as given in the datasheet while $P_{STC}$ and $G_{STC}$ are the maximum power and irradiance in STC.

In Figure 4.1, the energy rating of monofacial modules for the reference climates is illustrated. As can be observed, the difference in the CSER between climates suggests that the same modules can be more efficient in some climates compared to others. For example, in high elevation and temperate coastal climates the modules found to be more productive than the other climates meaning that their performance is closer to the efficiency measured in STC .

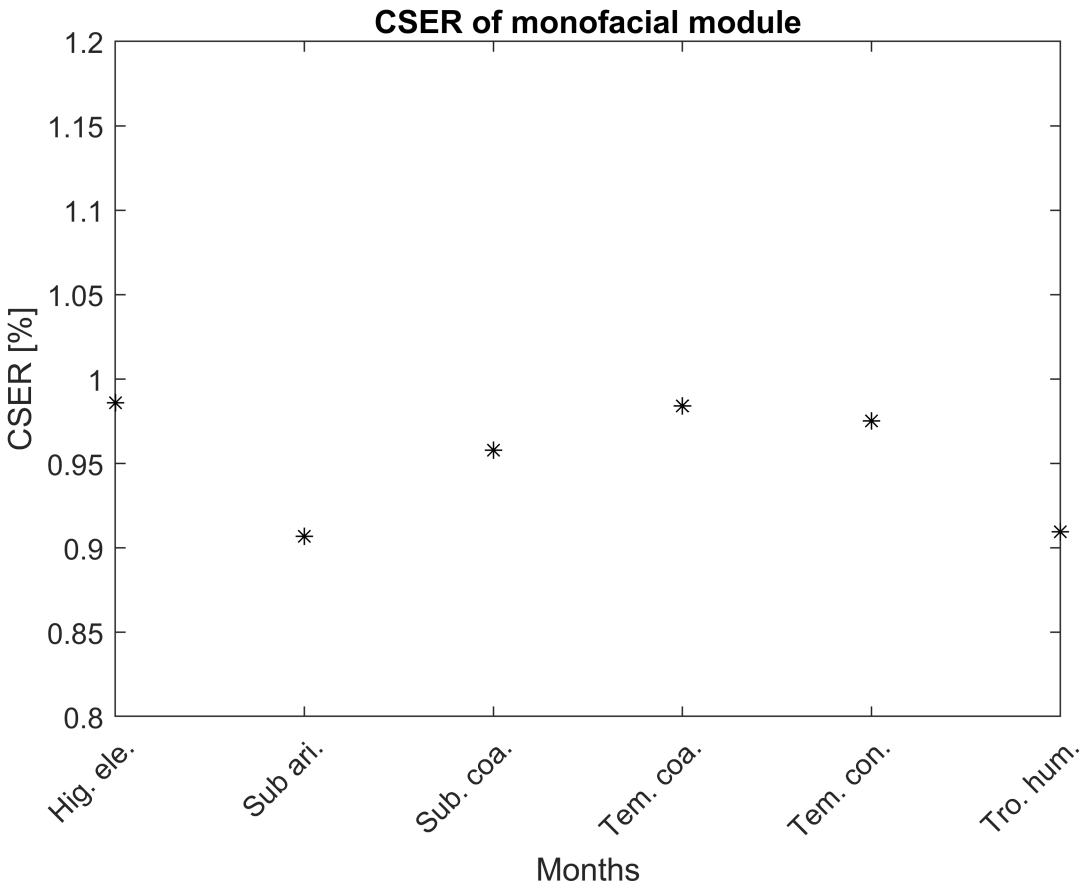


Figure 4.1: CSER of monofacial modules according to IEC61853

## 4.2. Energy rating of bifacial modules

For the calculation of the energy rating of bifacial modules a similar methodology with the one described in IEC61853-3 is followed. As seen above, there are several assumptions and simplifications in the calculation of the energy rating of monofacial modules already and even more assumptions are necessary for bifacial modules. Since bifacial modules receive additional irradiance from the rear side, the calculation procedure should be adjusted accordingly.

In the flowchart shown in Figure 4.2, the procedure used for the estimation of energy yield and energy rating of bifacial modules is illustrated. Two colours can be distinguished in this flowchart. The gray color refers to calculation steps regarding the front side of the module while the light blue color refers to the rear side of the module. Note, that the steps shown in grey color agree with the procedure mentioned in IEC61853-3.

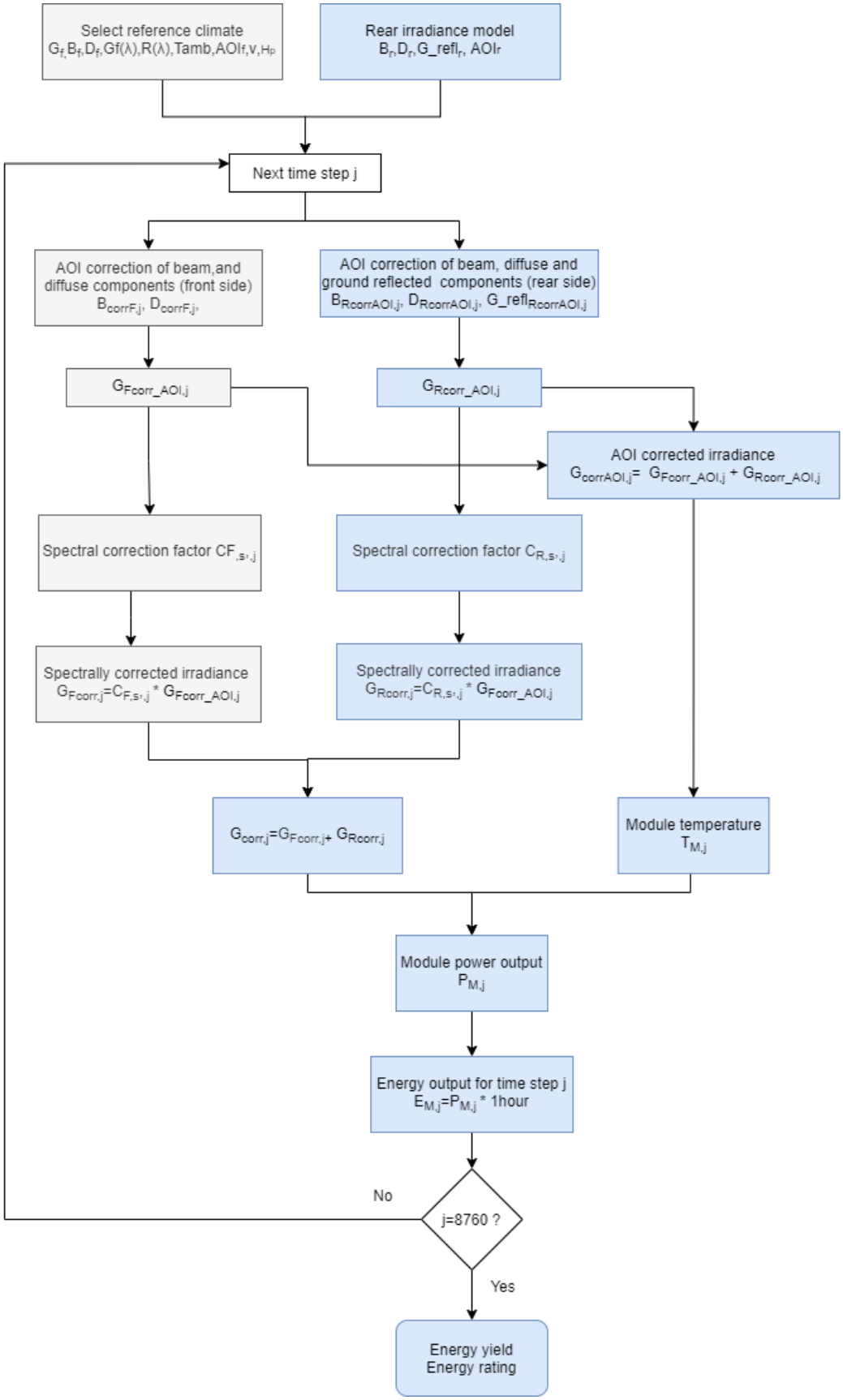


Figure 4.2: Flowchart for the calculation of energy rating for bifacial modules

As can be seen in the flowchart, in order to calculate the energy rating of bifacial modules additional input data are required. More specifically, the hourly values of direct, diffuse and ground reflected irradiance obtained from the irradiance model discussed in chapter 3 are introduced in the model. Then, the rear side irradiance should be corrected for the angular and the spectral mismatch losses. Finally, using the corrected in-plane irradiance and the module temperature, the power output of the module can be obtained and used for the calculation of energy rating.

### 4.2.1. Correction of rear side irradiance due to angular incidence effects

After the selection of one of the available climates given by the standard and the calculation of the rear irradiance components, the next step is the correction of the rear side irradiance for the AOI effects. To take into account the reflection losses on the rear surface of the module due to the change in the angle of incidence, the Martin & Ruiz equations are applied where different factors are used for each radiation component (direct, diffuse, albedo).

The direct irradiance corrected for the AOI is given by the following equation:

$$B_{R_{corrAOI}} = (1 - F_{B_r}) * B_r \tag{4.2}$$

$$F_{B_r} = \frac{exp(-cosAOI_r/\alpha_r) - exp(-1/\alpha_r)}{1 - exp(-1/\alpha_r)} \tag{4.3}$$

where $F_{B_r}$ is the angular loss factor of the solar radiation direct component from the rear surface of the module. Note, the same angular loss factor as the one used in the standard is applied ($\alpha_r = 0.146$).

On the other hand, the diffuse irradiance component obtained using the Perez model consists of circumsolar, horizon brightening and isotropic diffuse light. Each of these components require different correction factors as follows:

$$D_{Riso_{corrAOI}} = (1 - F_{D_r}) * D_{r_{iso}} \tag{4.4}$$

$$D_{Rcirc_{corrAOI}} = (1 - F_{B_r}) * D_{r_{circ}} \tag{4.5}$$

$$D_{Rhor_{corrAOI}} = (1 - F_{B_r}) * D_{r_{hor}} \tag{4.6}$$

$$F_{D_r} \cong exp[-\frac{1}{\alpha_r}(c_1(sin\beta_r + \frac{\pi - \beta_r - sin\beta_r}{1 + cos\beta_r}) + c_2(sin\beta_r + \frac{\pi - \beta_r - sin\beta_r}{1 + cos\beta_r})^2)] \tag{4.7}$$

where $F_{D_r}$ is the angular losses factor of the solar radiation diffuse component. The total diffuse irradiance corrected for the AOI effects on the rear side of the module is:

$$D_{R_{corrAOI}} = D_{Riso_{corrAOI}} + D_{Rcirc_{corrAOI}} + D_{Rhor_{corrAOI}} \tag{4.8}$$

A similar correction factor is used for the case of the ground reflected irradiance as shown in the following formula:

$$G_{Rrefl_{corrAOI}} = (1 - F_{A_r}) * G_r^{refl} \tag{4.9}$$

$$F_{A_r} \cong exp[-\frac{1}{\alpha_r}(c_1(sin\beta_r + \frac{\beta_r - sin\beta_r}{1 - cos\beta_r}) + c_2(sin\beta_r + \frac{\beta_r - sin\beta_r}{1 - cos\beta_r})^2)] \tag{4.10}$$

where $F_{A_r}$ is the angular losses factor of the solar radiation ground-reflected (albedo) component.

After the correction of all the irradiance components for the AOI effects, the total irradiance incident on the rear side of the module can be obtained using Equation 4.11

$$G_{R_{corr\_AOI}} = B_{R_{corrAOI}} + D_{R_{corrAOI}} + G_{Rrefl_{corrAOI}} \tag{4.11}$$

Finally, the total corrected in-plane irradiance incident on both sides of a bifacial module is obtained.

$$G_{corr_{AOI}} = G_{R_{corr\_AOI}} + G_{F_{corr\_AOI}} \tag{4.12}$$

In Figure 4.3, the total irradiance (front and rear) before and after the correction for the angular losses is illustrated.

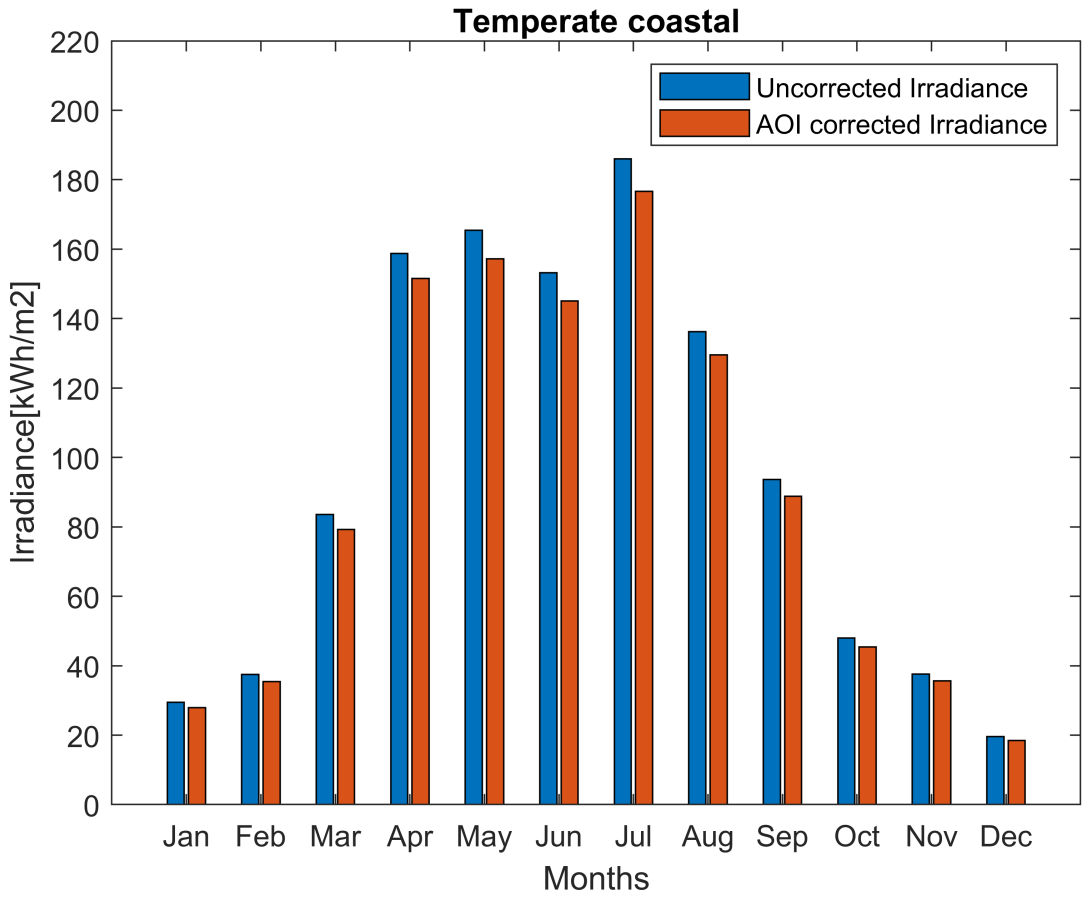


Figure 4.3: Irradiance before and after correction of the AOI

### 4.2.2. Spectrally corrected irradiance at the rear side of a module

As mentioned earlier, in IEC 61853 the spectrum mismatch between the AM1.5G and the in-plane irradiance on the front side of the module is taken into account using a spectral correction coefficient. However, in the case of bifacial modules a new definition should be introduced including the spectral response at the rear side of the module and the albedo beneath the module. However, in order to be able to estimate the spectrum mismatch, some assumptions are used in the model as will be explained in the following.

First, the module spectral responsivity (SR) of the rear side is assumed to be the same as the front side. In reality, the SR of the front and the rear side of a module are different. This is because an anti-reflective coating is usually applied on the front side of modules to reduce the amount of sunlight reflected off PV modules, capturing more of the sun's irradiance and thus delivering higher energy output. On the other hand, on the rear side of the module a standard glass is used without the anti-reflective coating to reduce the cost of the module.

Also, the AM1.5G spectrum defined in IEC 60904-3 is used for monofacial modules. However, bifacial modules receive two different spectra, one incident on the front side of the module and another at the rear side of the module. Nevertheless, no reference spectrum AM1.5R is defined for the rear-side of the module and according to the literature, in power rating of bifacial PV modules, the reference spectrum AM1.5G can be used to obtain spectral mismatch for both sides without significant errors [59]. Additionally, proposing a different spectrum for the rear side, multiple complications such as additional spectral matching rating solar simulators and other would be introduced to the industry. Therefore,

the spectral correction is performed independently for both sides of the module using the reference terrestrial spectrum of AM1.5G. The spectral correction factor given in Equation 2.44 was adjusted for the rear side of the module as follows:

$$C_{R,s,j} = \frac{1000 \int_{\lambda_s}^{\lambda_e} SR(\lambda) G_{R_{corr,AOI,j}}(\lambda) d\lambda}{G_{R_{corr,AOI,j}} \int_{\lambda_s}^{\lambda_e} SR(\lambda) R_{STC}(\lambda) d\lambda} \tag{4.13}$$

Using the same integration limits as in the front side (300nm to 4000nm) the spectrally corrected rear irradiance at each hour *j* of the year is calculated:

$$G_{Rcorr} = C_{R,s,j} G_{R_{corr,AOI,j}} \tag{4.14}$$

Finally, the total irradiance corrected for the AOI and spectrum effects can be obtained.

$$G_{corr} = G_{Fcorr} + G_{Rcorr} \tag{4.15}$$

### 4.2.3. Calculation of module temperature and power output

It is well known that the instantaneous temperature of a PV module depends on multiple parameters such as, the incoming irradiance on the PV module (both and front irradiance in case of bifacial modules), the module's electrical, optical and thermal properties, and its heat exchange with the surroundings. In this model, the same analytical formula mentioned in IEC61853 standard for monofacial modules is used for the calculation of module temperature for each hour of the year $T_{M,j}$. However, since bifacial modules are investigated in this work, the total irradiance absorbed from both sides of the module corrected only for the AOI effects as calculated using Equation 4.12 should be taken into consideration:

$$T_{M,j} = T_{amb,j} + \frac{G_{corr_{AOI,j}}}{u_0 + u_1 v_j} \tag{4.16}$$

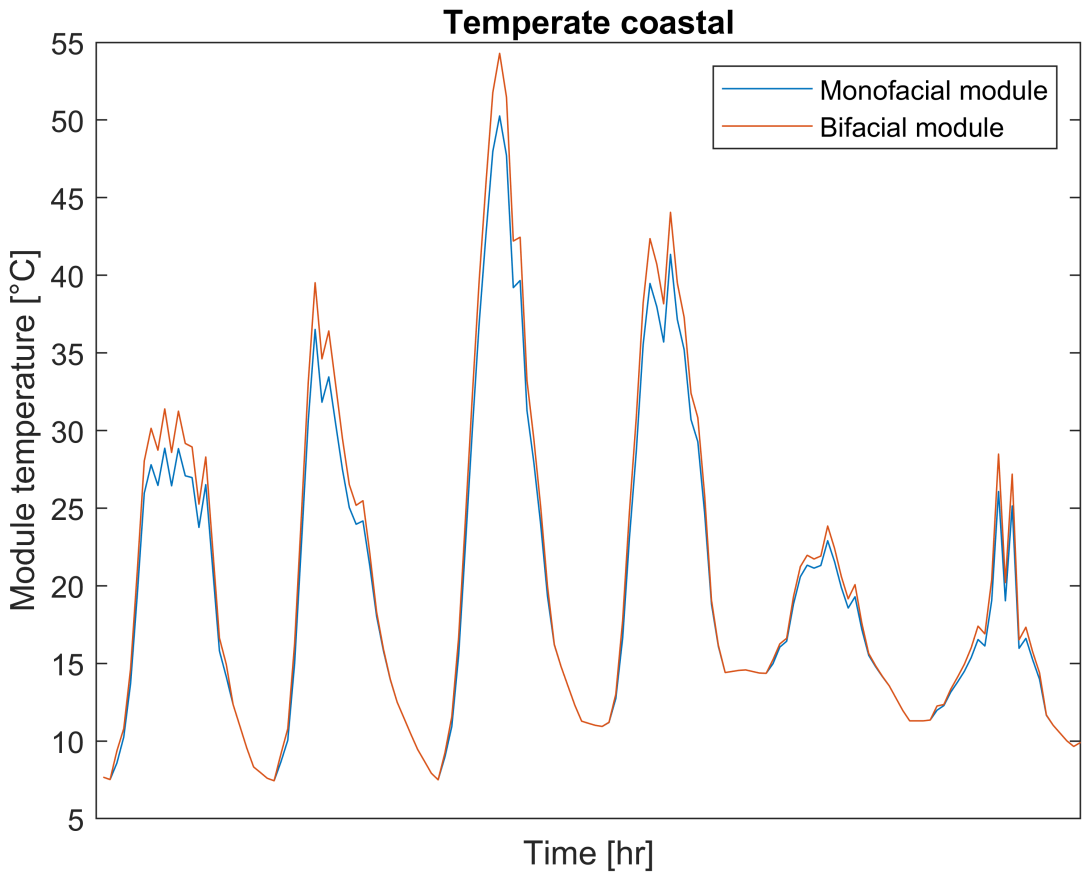


Figure 4.4: Module temperature for a week

In Figure 4.4, the temperature of monofacial and bifacial modules for the first week of July is shown. As it was expected, the temperature of bifacial modules can reach slightly higher values than monofacial, due to higher irradiance absorption. This can also be seen in Figure 4.5 where the hourly temperature of bifacial and monofacial module is plotted in y-axis and x-axis respectively.

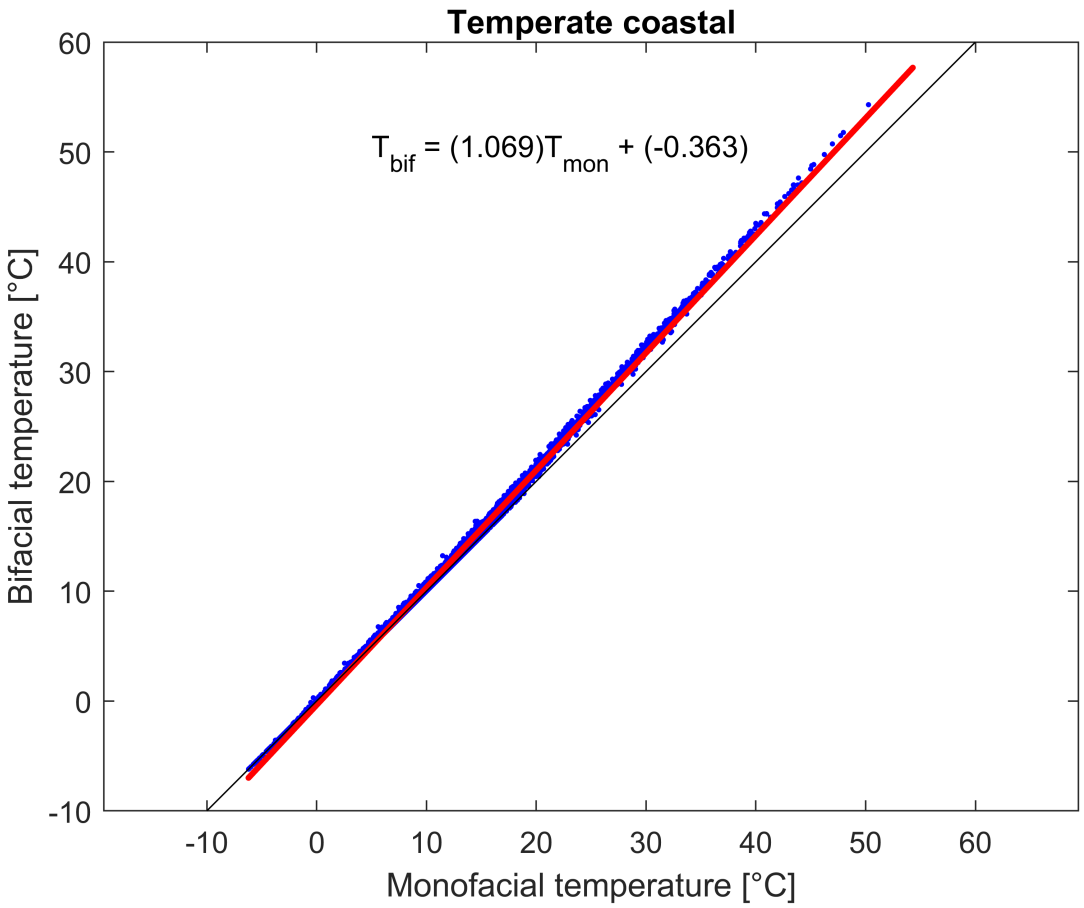


Figure 4.5: Bifacial module temperature as a function of monofacial module temperature

The blue dots in the Figure 4.5 represent the hourly temperature and the red line is a linear function which provides the ”best” fit of the data points. However, looking at the figure in more detail, it can be observed that the fitting of the red line is worse at low temperatures compared to higher temperatures. Therefore, the fitting line is not applicable for low temperatures since it is shown that $T_{bif}$<$T_{mon}$ which is not true. According to the data (blue dots), the $T_{bif}$ should be equal to $T_{mon}$ at low temperatures while at higher temperatures $T_{bif}$>$T_{mon}$. A black line with equation $T_{bif}$=$T_{mon}$ is also shown in the graph which can be used as reference or for the purpose of comparison. The equation of the red line is given in the graph which describes a line with slope 1.069 and y-intercept -0.363°C.

In the following table, the linear function and the temperature of monofacial and bifacial modules are presented for each climate profile. Note that $\overline{T}_{mon}$ and $\overline{T}_{bif}$ shown in the last two columns of Table 4.1 account for the average annual module temperature weighted with irradiance since some data points contribute more than others to the final average. For instance, during night, the contribution of temperature to the final average is not as important as during day since no irradiance reach the module. As shown in the last columns of the table, the temperature of bifacial modules is higher than monofacial modules for all climates. This can also be seen from the slope of equations, where *'a'* is always higher than unity.

| **Climate type** | **Linear function ($T_{bif}$=a$T_{mon}$+b)** | $\overline{T}_{mon}$**[°C]** | $\overline{T}_{bif}$**[°C]** |
|---|---|---|---|
| Tropical humid | $T_{bif}$=1.133$T_{mon}$-2.998 | 45.1 | 48.0 |
| Subtropical arid (dessert) | $T_{bif}$=1.069$T_{mon}$-0.873 | 43.0 | 45.6 |
| Subtropical coastal | $T_{bif}$=1.055$T_{mon}$-0.513 | 33.3 | 35.2 |
| Temperate coastal | $T_{bif}$=1.069$T_{mon}$-0.363 | 21.6 | 22.8 |
| High elevation (above 3000 m) | $T_{bif}$=1.061$T_{mon}$+0.776 | 14.9 | 17.2 |
| Temperate continental | $T_{bif}$=1.037$T_{mon}$+0.291 | 24.5 | 26.3 |

Table 4.1: Linear function and weighted temperature

After the calculation of $G_{corr_{AOI}}$ and $T_M$ for each hour of the year, the next step is to obtain the module power output. For this purpose, the power matrix measured in IEC61853-1 can be used. The power matrix consists of 22 power values where each power value is measured at different module temperature $T$ and irradiance $G$. More specifically, the temperature range is between 15°C and 75°C while the range for irradiance is between $100 W/m^2$ and $1100 W/m^2$. The power matrix is the following:

| | **Temperature** | | | |
|---|---|---|---|---|
| **Irradiance [W/m$^2$]** | **15°C** | **25°C** | **50°C** | **75°C** |
| **100** | 26.60 | 25.77 | NA | NA |
| **200** | 54.06 | 53.80 | NA | NA |
| **400** | 114.89 | 110.46 | 99.24 | NA |
| **600** | 174.09 | 167.57 | 150.84 | 133.80 |
| **800** | 232.89 | 224.16 | 202.05 | 179.35 |
| **1000** | 291.31 | 280.47 | 252.45 | 246.06 |
| **1100** | NA | 308.05 | 277.36 | 246.06 |

Table 4.2: Power matrix

where ”NA” means that the power output at these conditions is not available because these combinations of irradiance and module temperature are quite uncommon to occur, and hard to measure.

Then, each power value in the power matrix is divided with the corresponding irradiance $G$ to obtain the efficiency of the PV module for the given temperature and irradiance $\eta(G,T)$. The calculated parameters $G_{corr}$ and $T_M$ are then used in combination with the power matrix to determine the efficiency of the module at the specific conditions $\eta(G_{corr},T_M)$. The $G_{corr}$ is the sum of the front and the rear side irradiance corrected for the AOI and spectral effects. Note that, the bifaciality of the module was assumed to be equal to 1, meaning that the efficiency between the front and the rear side of the module is the same. This is technologically possible, as modules with bifacialities of more than 0.99 have been fabricated [60]. At this point, a two-dimensional bilinear interpolation is used when 15°C $\leq T_M \leq$ 75°C and $100 W/m^2 \leq G_{corr} \leq 1100 W/m^2$, to determine the module efficiency. Otherwise, when the values of $G_{corr}$ and $T_M$ are outside the range of values given in the power table, a linear extrapolation is used. An example of the interpolation and extrapolation method is followed.

**Bilinear interpolation** ($G_1 \leq G_{corr} \leq G_2$ and $T_1 \leq T_M \leq T_2$): The efficiency of the module at a given temperature $T_M$ under $G_1$ and $G_2$ irradiance levels is obtained using the following equations:

$$\eta(G_1,T_M) = \eta(G_1,T_1) + \frac{T_M - T_1}{T_2 - T_1}(\eta(G_1,T_2) - \eta(G_1,T_1)) \tag{4.17}$$

$$\eta(G_2,T_M) = \eta(G_2,T_1) + \frac{T_M - T_1}{T_2 - T_1}(\eta(G_2,T_2) - \eta(G_2,T_1)) \tag{4.18}$$

In order to achieve the module efficiency for a different irradiance level ($G_1 \leq G_{corr} \leq G_2$), a bilinear interpolation using the result of the equation 4.17 and 4.18 should be applied as follows:

$$\eta(G_{corr},T_M) = \eta(G_1,T_M) + \frac{G_{corr} - G_1}{G_2 - G_1}(\eta(G_2,T_M) - \eta(G_1,T_M)) \tag{4.19}$$

**Linear extrapolation** (when $G_{corr}$ or $T_M$ is outside the range of the power table values): In this example, the parameters $G_{max}$ and $T_{max}$ correspond to the highest irradiance and module temperature given in the power table respectively.

If module temperature ($T_M$) is outside the range of the power table while the corrected irradiance ($G_{corr}$) is within the range of values given in the power table equations 4.20 to 4.22 are used.

$$\eta(G_{corr},T_{max}) = \eta(G_1,T_{max}) + \frac{G_{corr} - G_1}{G_2 - G_1}(\eta(G_2,T_{max}) - \eta(G_1,T_{max})) \tag{4.20}$$

$$\eta(G_{corr}, T_{max-1}) = \eta(G_1, T_{max-1}) + \frac{G_{corr} - G_1}{G_2 - G_1}(\eta(G_2, T_{max-1}) - \eta(G_1, T_{max-1})) \tag{4.21}$$

$$\eta(G_{corr}, T_M) = \eta(G_{corr}, T_{max-1}) + \frac{T_M - T_{max-1}}{T_{max} - T_{max-1}}(\eta(G_{corr}, T_{max}) - \eta(G_{corr}, T_{max-1})) \tag{4.22}$$

Finally, if both irradiance ($G_{corr}$) and module temperature ($T_M$) are outside the range of the power table, equations 4.23 to 4.25 are used.

$$\eta(G_{corr}, T_{max}) = \eta(G_{max-1}, T_{max}) + \frac{G_{corr} - G_{max-1}}{G_{max} - G_{max-1}}(\eta(G_{max}, T_{max}) - \eta(G_{max-1}, T_{max})) \tag{4.23}$$

$$\eta(G_{max}, T_M) = \eta(G_{max}, T_{max-1}) + \frac{T_M - T_{max-1}}{T_{max} - T_{max-1}}(\eta(G_{max}, T_{max}) - \eta(G_{max}, T_{max-1})) \tag{4.24}$$

$$\eta(G_{corr}, T_M) = \eta(G_{corr}, T_{max}) + \eta(G_{max}, T_M) - \eta(G_{max}, T_{max}) \tag{4.25}$$

Multiplying the resulted efficiency $\eta(G_{corr},T_M)$ for each hour of the year with the corresponding total irradiance on the module surface $G_{corr}$, the power output $P_M$ of the module can be obtained which can be easily converted to energy output for the given time period (1 hour) as follows:

$$E_{M_j} = P_{M_j}(G_{corr}, T_M) * 1hour \tag{4.26}$$

Finally, for the calculation of the annual energy yield, a sum is performed for all the hours of the selected climate

$$E = E_{M_{year}} = \sum_{j=1}^{j=8760} * E_{M_j} \tag{4.27}$$

where j is the hour of the year (one year consists of 8760 hours). In Table 4.3, the annual energy yield for monofacial and bifacial modules at the reference climates is shown, while in Figure 4.6, the monthly energy generation is displayed for the temperate coastal climate.

| Climate type | Energy yield [$kWh/m^2$] Monofacial modules | Bifacial modules |
|---|---|---|
| Tropical humid | 427.9 | 503.6 (+18.7%) |
| Subtropical arid (dessert) | 583.8 | 666.0 (+15.5%) |
| Subtropical coastal | 402.1 | 464.7 (+16.5%) |
| Temperate coastal | 268.5 | 312.9 (+17.2%) |
| High elevation (above 3000 m) | 591.5 | 677.7 (+15.8%) |
| Temperate continental | 346.2 | 397.1 (+15.6%) |

Table 4.3: Energy yield

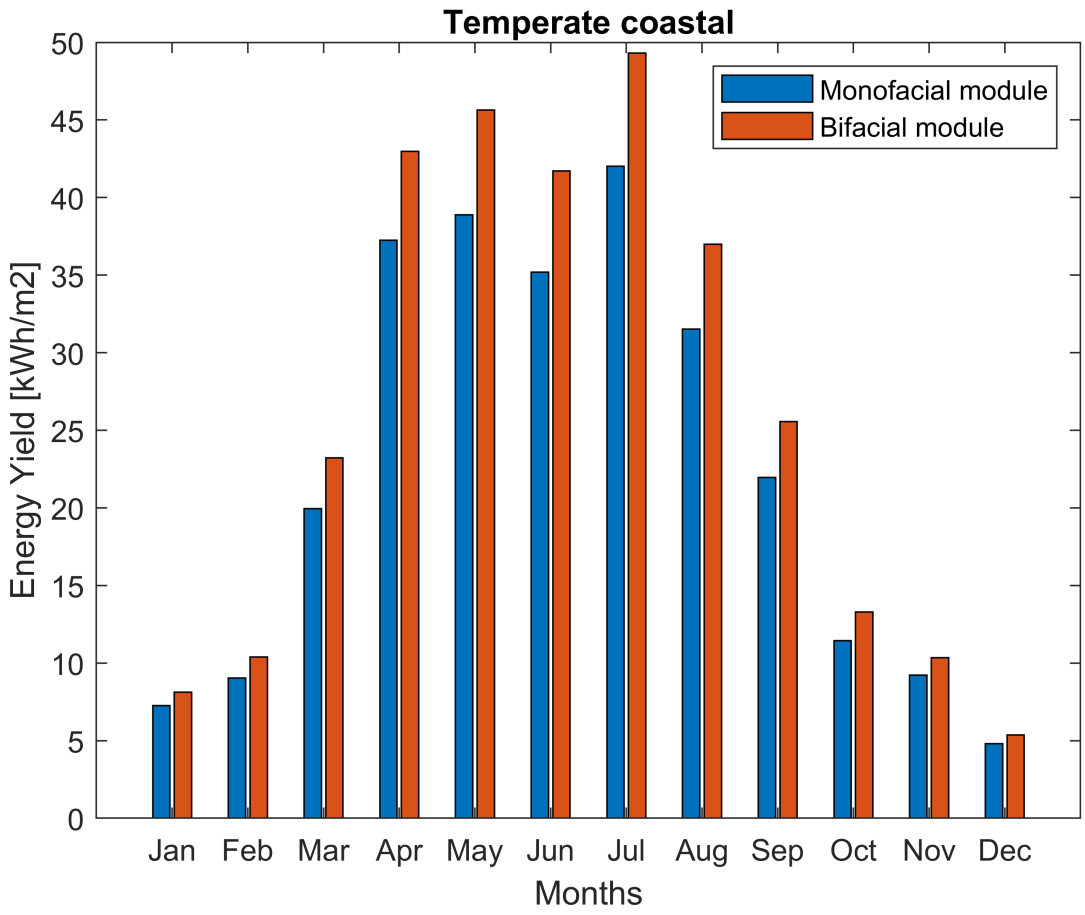


Figure 4.6: Monthly energy generation

It is important to highlight that, although the temperature of bifacial modules reach higher values than monofacial modules, higher energy is generated from bifacial modules. According to the results shown in Table 4.3, the effect of irradiance has greater impact on the energy generation than the effect of module temperature, and thus higher energy yield is produced when more irradiance is collected form the module.

Finally, using both energy yield and irradiance, the energy rating can be estimated as will be explained in the next section.

## 4.3. CSER calculation

For the calculation of CSER value, Equation 1.3 is used. However, this formula needs to be adjusted as it was developed for the computation of energy rating of monofacial and not for bifacial modules. Additionally, it should be taken into account that the STC are only developed for monofacial modules and therefore other conditions are required for bifacial modules.

Deline C. et al [55] evaluated multiple deployment scenarios for bifacial modules where the rear irradiance resource was obtained under the conditions assumed by IEC 60904-3 monofacial reference standard. More specifically, these conditions are axplicitly defined as AM1.5 sepctrum, with a single module deployed at 1m height over light soil ground cover (albedo=0.21), 1000W/$m^2$ irradiance on the front side of the module and 37° tilt angle. The value of rear irradiance ($G_{rear}$) on the test plane under these conditions found equal to 130-140W/$m^2$. Based on these simulations, multiple information were collected to finally propose and specify the bifacial standard test conditions (BSTC), which can be used as a reference irradiance for relative comparison between different bifacial PV modules. The BSTC propose 1000W/$m^2$ for the front-side irradiance ($G_{front}$) and 135W/$m^2$ for the rear-side irradiance ($G_{rear}$) which corresponds to the average rear-side irradiance under the reference spectrum of AM1.5G. Finally, the following formula was developed for the calculation of the equivalent irradiance ($G_E$) for bifacial PV devices [59]

$$G_E = G_{front} + BF \cdot G_{rear} \tag{4.28}$$

where, $G_{front}$ is the single-sided indoor flash irradiance under one-sun illumination and *BF* is the bifacial factor coefficient. A summary of the test conditions used to define BSTC is shown in Table 4.4.

| Parameter | Test conditions |
|---|---|
| Module Temperature | 25°C |
| Irradiance spectrum | AM1.5G |
| Front-side irradiance | 1000W/$m^2$ |
| Rear-side irradiance | 135W/$m^2$ |
| Equivalent irradiance | 1000W/$m^2$ + $BF$· 135W/$m^2$ |

Table 4.4: Bifacial Standard Test Conditions, [59]

Eventually, for the calculation of energy rating of bifacial modules ($CSER_{bif}$), the following equation can be used:

$$CSER_{Bif} = \frac{E_{year} \cdot G_{BSTC}}{P_{BSTC} \cdot H_{year}} \tag{4.29}$$

However, since no standard methodology exists for the calculation of CSER of bifacial modules, two approaches are used for its estimation in this work. In Figure 4.7, the energy rating under all climate conditions is shown where three colors can be distinguished. Black color, illustrates the CSER of monofacial modules as found in the standard ($CSER_{Mon_{std}}$), while the blue and red color represent the first ($CSER_{Bif_1}$) and second approach ($CSER_{Bif_2}$) used for the estimation of energy rating of bifacial modules respectively.

In the **first approach** used for the calculation of energy rating of bifacial PV modules ($CSER_{Bif_1}$) shown with blue color, the total energy yield and the total irradiance reaching the bifacial module are adjusted. More specifically, the total irradiance (front and rear) found in the irradiance model described in chapter 3 and the respective annual energy yield generated from both sides of the module are used as shown in the following formula.

$$CSER_{Bif_1} = \frac{E_{year_{total}} G_{STC}}{P_{STC} H_{year_{total}}} \tag{4.30}$$

This approach resulted in lower energy rating than mono-facial modules as can be seen in Figure 4.7. This can be attributed to the significant increase of total irradiation on the module surface $H_{year}$ compared to the increase of energy yield $E_{year}$. For instance, under temperate coastal climate conditions the $E_{year}$ increased by 44.4 $kWh/m2$ when bifacial modules were used instead of mono-facial, while $H_{year}$ increased by 175.8 $kWh/m2$ leading to lower energy rating. The lower value of CSER, implies that the productivity of mono-facial modules is higher than bifacial modules which is not true and therefore another approach was developed.

The **second approach** used to obtain energy rating of bifacial modules ($CSER_{Bif_2}$) is shown with red color. It takes into account the total energy yield of bifacial modules while the irradiance value is the same as for monofacial modules (front side irradiance). This means that for the calculation of the CSER of bifacial modules only the annual energy yield is adjusted compared to the monofacial modules.

$$CSER_{Bif_2} = \frac{E_{year_{total}} G_{STC}}{P_{STC} H_{year_{front}}} \tag{4.31}$$

As shown in Figure 4.7, the energy rating and as a result the productivity of bifacial modules using this approach is higher than that of mono-facial modules. Another advantage of this approach is that the energy rating can be easily calculated since only the front side irradiance is required in contrast to the first approach.

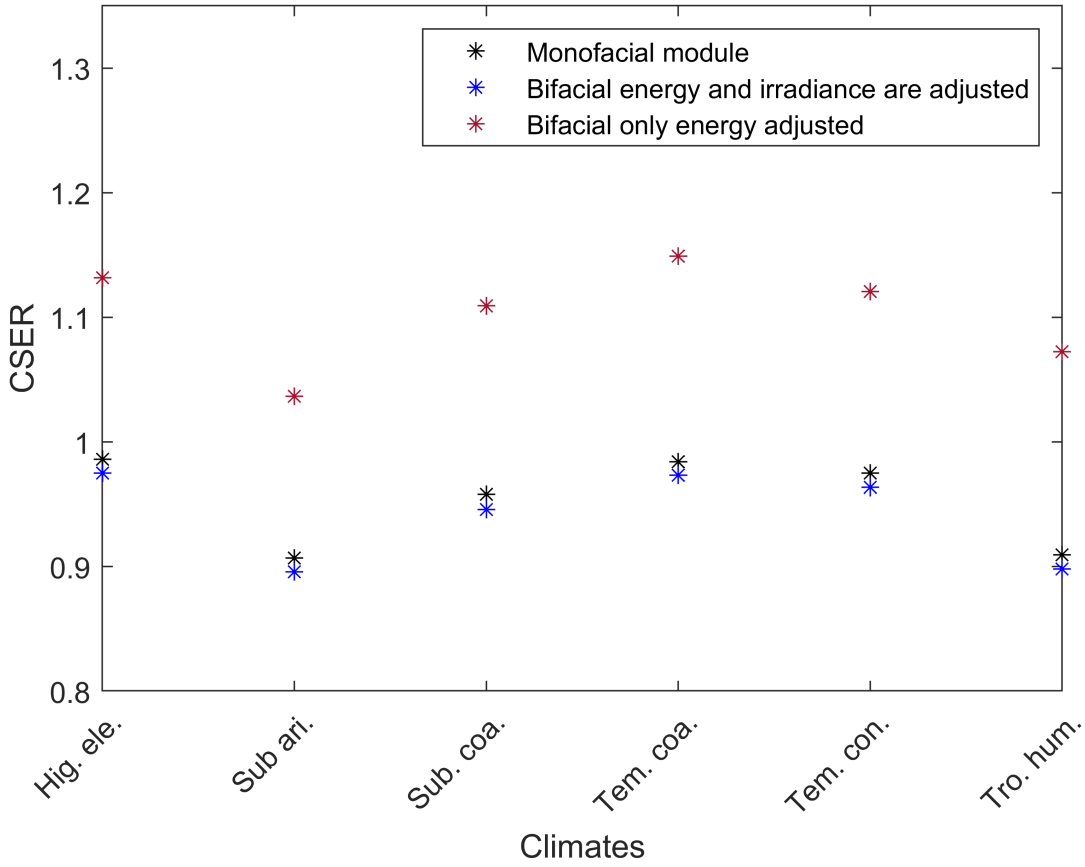


Figure 4.7: CSER of bifacial and monofacial modules

## 4.4. Comparison of CSER of monofacial and biafacial modules

In previous section, two approaches were described to obtain CSER of bifacial PV module and then compared with the CSER of mono-facial modules. In the first approach, the CSER of bifacial modules was found to be lower than that of monofacial modules ($CSER_{Bif_1} < CSER_{Mon_{std}}$), whereas in the second approach the opposite occurred ($CSER_{Bif_2} > CSER_{Mon_{std}}$). At the beginning of this section another technique based on the first approach is used to compare the energy rating values of monofacial and bifacial modules. Later on, different bifacial factors ($BFs$) will be introduced and implemented in both approaches.

According to the first approach, since the energy rating of bifacial modules found to be lower than that of monofacial modules, it was decided to change the way the $CSER_{Mon_{std}}$ is calculated. More specifically, it was assumed that a monofacial module behave in the same way as a bifacial module with bifaciality (*BF*) equal to zero. When bifaciality is equal to zero, it means that the effieciency of the rear side of the module is zero and therefore no power can be generated from that side or no irradiance can be absorbed. This is the same case as for monofacial modules where due to the deposition of an aluminum non-transparent foil at the rear side of the module no irradiance is absorbed and as a result no power is generated from that side. Therefore, the energy rating of monofacial modules is adjusted and calculated using Equation 4.32, where the total irradiance reaching both sides of the module is used.

$$CSER_{Mon_1} = \frac{E_{year_{front}} G_{STC}}{P_{STC} H_{year_{total}}} \tag{4.32}$$

In Figure 4.8, the resulted CSER value of the monofacial module using this technique is shown with black colour which it is obviously lower than the CSER value given in the standard. Note that for comparison purposes, this value of CSER for monofacial modules will be used from now on in the first approach and not the one given in the standard. Additionally, the CSER of bifacial modules using $BF = 0$ is illustrated with pink colour which is equal to the CSER of monofacial modules (black

colour). This is because when $BF = 0$, only the irradiance incident on the front side of the module can be absorbed as in the case of mono-facial modules. It is important to highlight that when BF equals zero, $G_{BSTC} = 1000W/m^2$ and $P_{BSTC} = 280W/m^2$ (same with STC). However, no bifacial modules with $BF = 0$ have been developed and therefore these values can only be used for the CSER of monofacial modules shown with black colour. Finally, the CSER of bifacial modules with bifaciality factor equal to unity is shown with blue color (as obtained in the previous section) which is now definitely higher than the CSER of monofacial modules (black color).

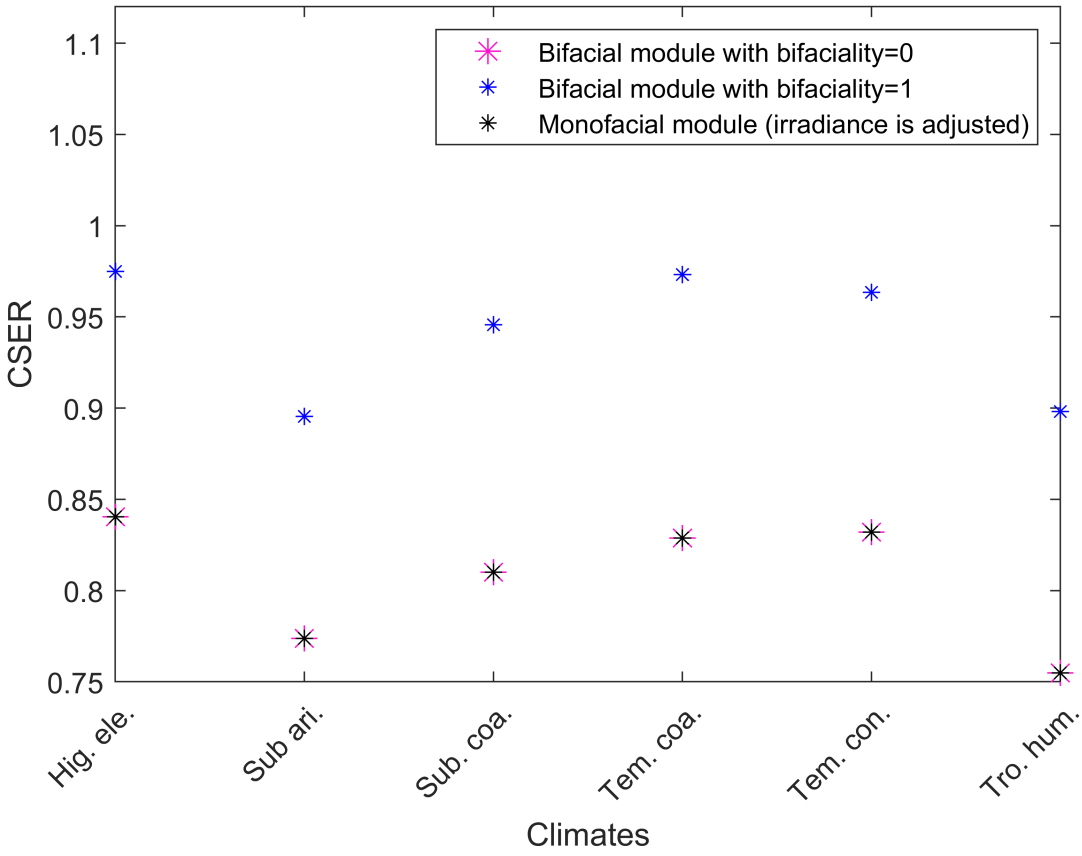


Figure 4.8: CSER for bifacial modules based on the first approach and monofacial modules when irradiance is adjusted

At this point, the effect of the bifacial factor ($BF$) on the energy rating is examined. In Figure 4.9, the energy rating using different *BFs* is illustrated for each climate condition where the orange, green and blue colour correspond to BF=0.5, 0.75, 1 respectively. As it was expected, when bifacial factor is low, less irradiance is absorbed, resulting in lower energy output and thus in lower CSER. It should be noted that when different BFs are used, the $G_{BSTC}$ and $P_{BSTC}$ values of equation 4.29 change as shown in table 4.5. Additionally, the annual energy output ($E_{year}$) used for the calculation of CSER (see Equation 4.29) was directly dependent with BF, while the total in-plane irradiance reaching both sides of the module ($H_{year}$) was independent form BF. In other words, to obtain $E_{year}$, the absorbed irradiance shown in equation Equation 4.33 was used while for the calculation of $H_{year}$ the irradiance on the rear side of the module as obtained from the irradiance model was simply added to the front side irradiance as given in the standard.

$$G_{corr} = G_{Fcorr} + BF * G_{Rcorr} \tag{4.33}$$

Finally, the power output and thus the energy yield $E_{year}$ were calculated using the procedure mentioned in subsection 4.2.3.

| | $G_{BSTC} = 1000 + BF \cdot 135[W/m^2]$ | $P_{BSTC}[W/m^2]$ |
|---|---|---|
| BF=0.5 | 1067 | 299 |
| BF=0.75 | 1101 | 308 |
| BF=1 | 1135 | 318 |

Table 4.5: Effect of bifacial factor coefficient

As can be observed in Figure 4.9, the CSER of monofacial module is the lowest. This implies that even both bifacial and monofacial modules receive the same amount of irradiance on both sides, the CSER of bifacial modules can reach higher values due to their ability to absorb additional irradiance from the rear side.

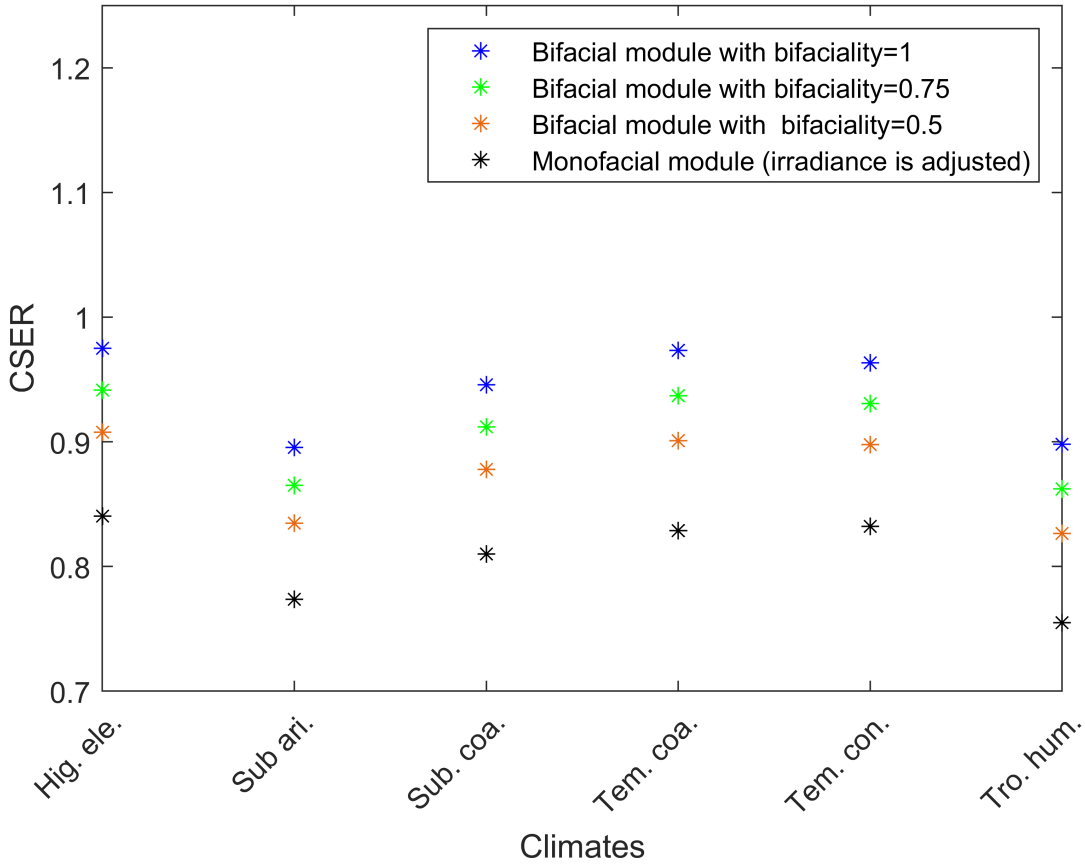


Figure 4.9: CSER for bifacial modules based on the first approach for different bifacialities

However, the question whether $BFs$ should be included in the calculation of $G_{BSTC}$ is still open. In Figure 4.10, the energy rating of bifacial modules ($CSER_{Bif_1}$) using a constant value of the indoor incoming light $G_{BSTC} = 1135\text{W}/m^2$ is shown. As can be seen, the effect of the different bifacialities doesn't have a huge impact on the energy rating (less than 1.3%) and therefore this method is not recommended.

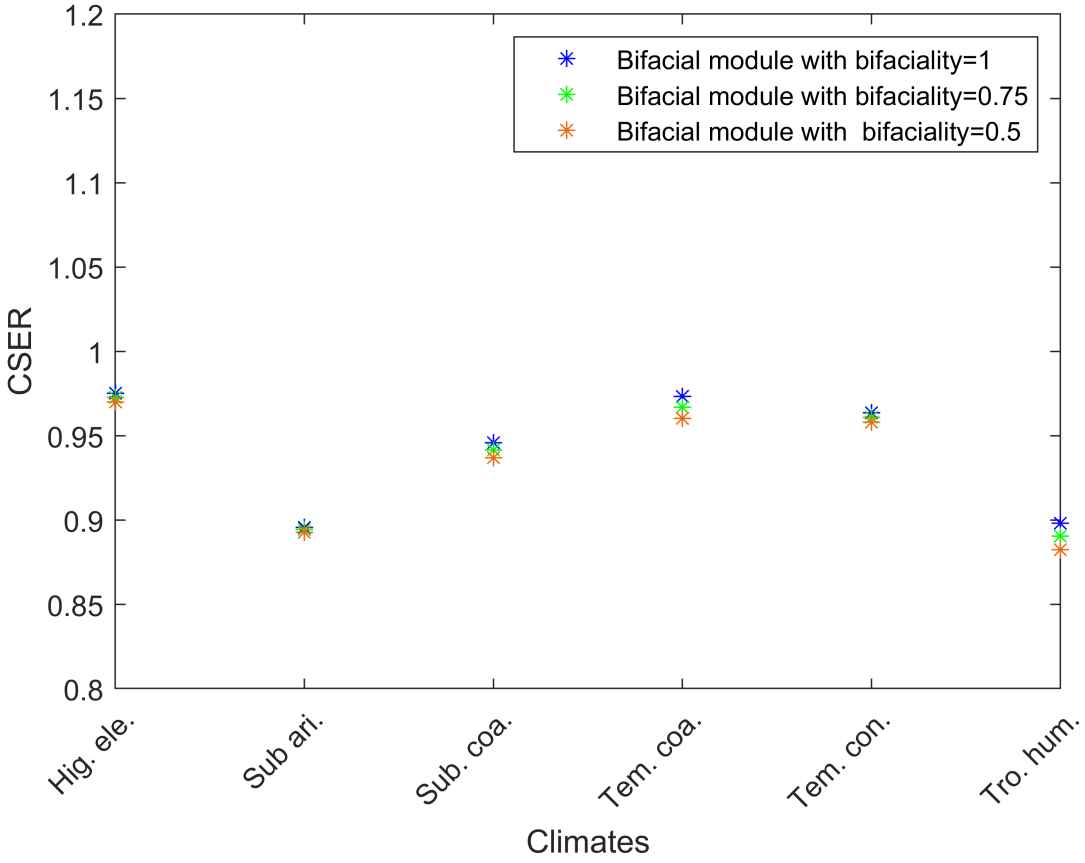


Figure 4.10: CSER based on the first approach when indoor irradiance is constant

In contrast to the first approach, the second approach mentioned in the previous subsection resulted in higher energy rating of bifacial modules compared to monofacial modules ($CSER_{Bif_2} > CSER_{Mon_{std}}$). This can be see in Figure 4.7 and 4.11, where the CSER of monofacial modules as given in the standard (shown with black colour) and the CSER of bifacial modules with BF=1 (shown with red colour) are illustrated. Additionally, in Figure 4.11, the CSER of bifacial modules ($CSER_{Bif_2}$) after the implementation of BF=0.75 and BF=0.5 is shown with green and orange colours respectively. As it was expected, the lower the BF, the lower the energy rating is. Finally, it is worth noting that similarly with the first approach, the energy rating of monofacial modules is equal to the energy rating of bifacial modules with BF=0.

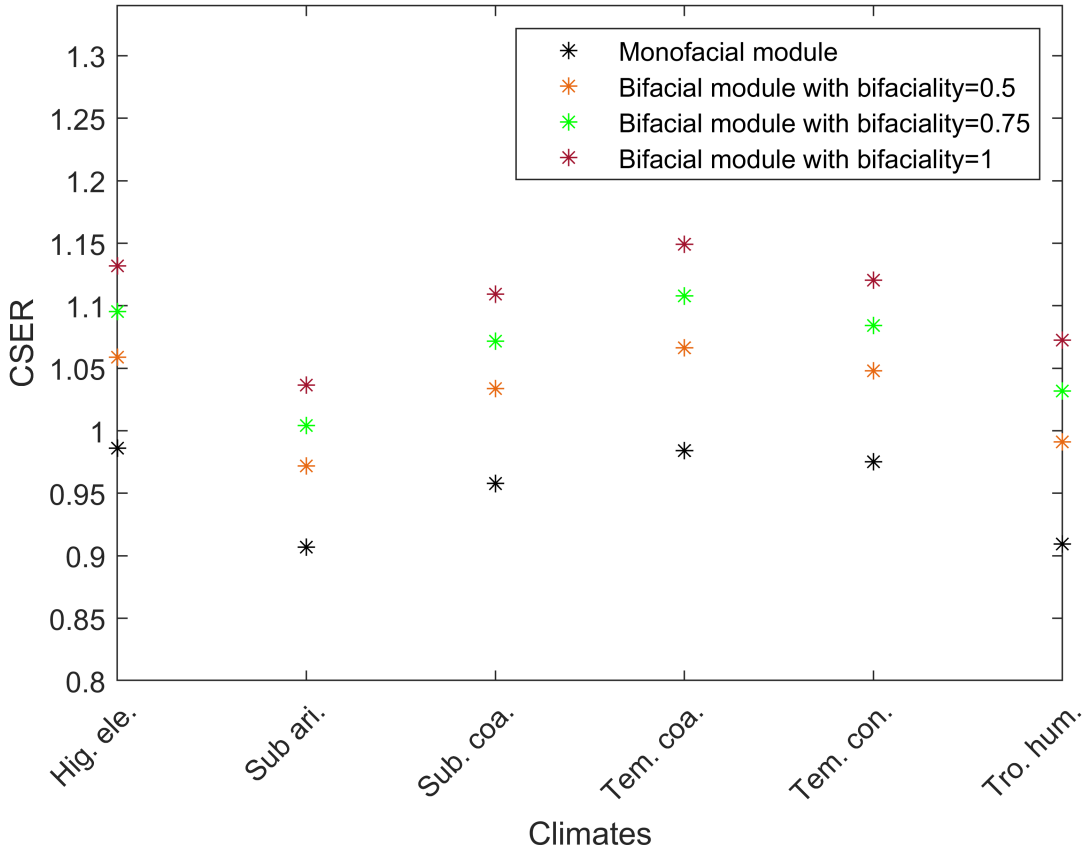


Figure 4.11: CSER for bifacial modules based on the second approach for different bifacialities

Finally, the case where the indoor incoming light ($G_{BSTC}$) used for the calculation of $CSER_{Bif_2}$ is constant to $1135 W/m^2$ is examined. The results can be seen in Figure 4.12 where as mentioned in the first approach, the impact of bifacial factor on the energy rating is relatively low and as a result this method is not recommended.

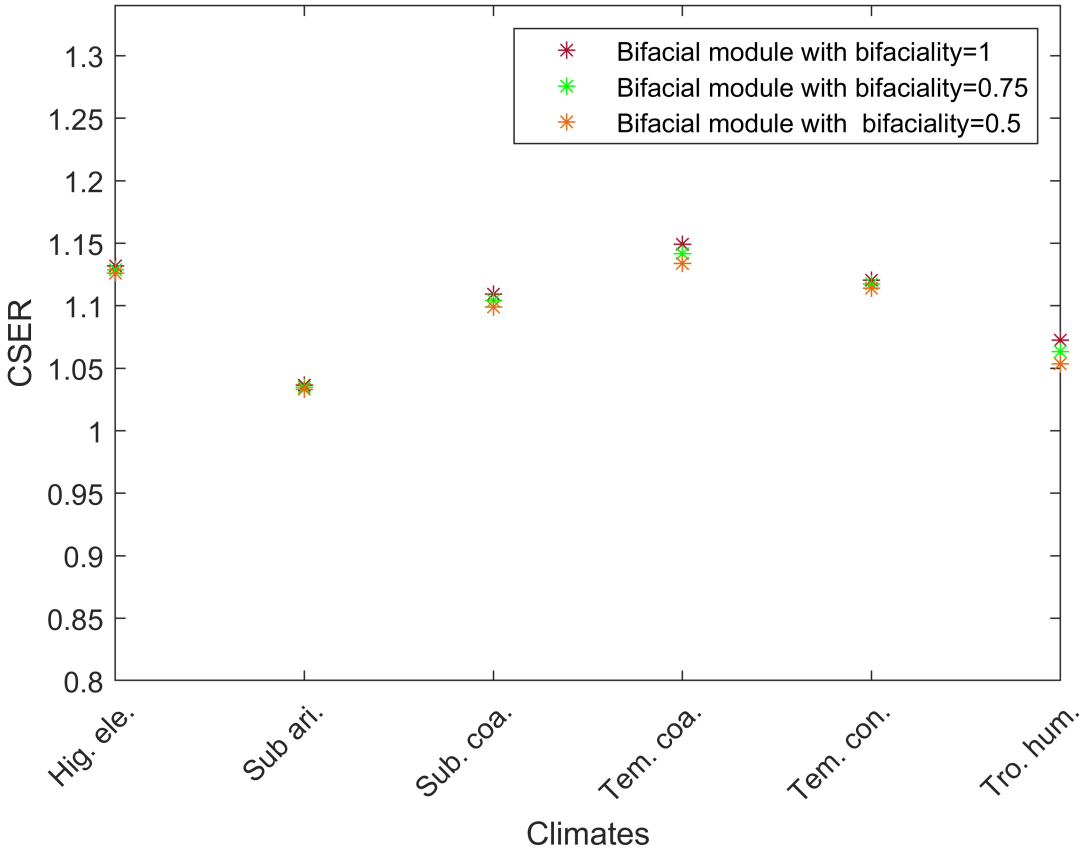


Figure 4.12: CSER based on the second approach when indoor irradiance is constant

Therefore, in this section two methods have been developed for the calculation of energy rating of bifacial modules ($CSER_{Bif_1}$ and $CSER_{Bif_2}$). In addition, the case where the $G_{BSTC}$ value is independent of BFs is analysed and it is decided that this method is not recommended since the impact of BF on the energy rating is very low. In the following table the methods used for the calculation of the energy rating for monofacial and bifacial modules are summarised.

| CSER | Equation | Difference between methods |
|---|---|---|
| $Mon_{std}$ | $\frac{E_{front}G_{STC}}{P_{STC}H_{front}}$ | Definition as given in the IEC-61853 standard |
| $Mon_1$ | $\frac{E_{front}G_{STC}}{P_{STC}H_{total}}$ | Total irradiance on both sides of the module is used |
| $Bif_1$ | $\frac{E_{total}G_{BSTC}}{P_{BSTC}H_{total}}$ | Energy yield and irradiance on both sides of the module are used |
| $Bif_2$ | $\frac{E_{total}G_{BSTC}}{P_{BSTC}H_{front}}$ | Energy yield of bifacial modules and the front side irradiance are used |

Table 4.6: CSER approaches

In Table 4.7, the difference between the energy rating of monofacial and bifacial modules for different bifacialities using the approaches shown in figures 4.9 and 4.11 is illustrated. As can be seen in the table, the difference in the first approach is similar with the difference of the second approach especially when low BF were used. Additionally, the relative difference in [%] between the first and the second approach is given in the table with red colour. As indicated, when BF=0.5 is used, the relative difference is relatively low (up to 1.3%) while for BF=1 the relative difference is higher (can reach values up to 2.7%). Therefore, it can be concluded that the two approaches are not directly proportional. This is because no relation is obtained for the energy rating of monofacial and bifacial modules since the relative difference between the two approaches is not the same.

| | High Elevation | Subtropical Arid | Subtropical Coastal | Temperate Coastal | Temperate Continental | Tropical Humid |
|---|---|---|---|---|---|---|
| | First approach [%] | | | | | |
| **BF=0.5** | 6.3 | 5.6 | 6.5 | 7.0 | 6.2 | 6.8 |
| **BF=0.75** | 9.4 | 8.4 | 9.7 | 10.5 | 9.4 | 10.2 |
| **BF=1** | 12.6 | 11.2 | 12.9 | 14.0 | 12.5 | 13.6 |
| | Second approach [%] | | | | | |
| **BF=0.5** | 7.3 (+1.0) | 6.5 (+0.9) | 7.6 (+1.1) | 8.2 (+1.2) | 7.3 (+1.1) | 8.1 (+1.3) |
| **BF=0.75** | 10.9 (+1.5) | 9.7 (+1.3) | 11.3 (+1.6) | 12.4 (+1.9) | 10.9 (+1.5) | 12.2 (+2.0) |
| **BF=1** | 14.6 (+2.0) | 13.0 (+1.8) | 15.1 (+2.2) | 16.5 (+2.5) | 14.5 (+2.0) | 16.3 (+2.7) |

Table 4.7: Relative difference between the CSER of bifacial and monofacial modules

### 4.4.1. Effect of losses on CSER

In this subsection the effect of different losses mechanisms on the energy rating of bifacial modules is analysed. More specifically, the change in the CSER obtained using the first approach, is calculated without taking into account the AOI correction, the spectrum correction and finally the module temperature. In Table 4.8 the effect of AOI, spectral variations and module temperature on the energy rating is shown, measured in %. According to the table, the effect of angular losses is higher than the spectrum effects due to the low tilt of the modules. Also the case where the modules operate under a constant temperature ($T_{STC}$=25ºC) is examined. For example, in tropical humid climates where ambient temperature is relatively high, the energy rating of the bifacial modules can be higher by 7.9% if the module temperature was kept constant at 25ºC using a cooling mechanism for instance. On the other hand, in temperate coastal climates the energy rating decreases if the module temperature is fixed at 25ºC. This is because in such climates the module temperature usually operates at lower temperatures generating higher energy yield (see Table 4.2). Therefore, the determination of module temperature at each hour of the year using the Faiman model but also the correction of irradince due AOI and spectrum effects are significantly important for the computation of CSER.

Finally, the change in the CSER for the aforementioned influencing factors is calculated and compared for different bifacialities. As shown in the table, the impact of these influencing factors to the CSER is greater for modules with higher bifacialities while this impact is minimized for modules with lower bifacialities.

| Climate | Bifacial Factor | Without AOI correction [%] | Without spectrum correction [%] | T= 25ºC [%] |
|---|---|---|---|---|
| Tropical humid | BF=1 | +4.2 | -2.9 | +7.9 |
| | BF=0.5 | +3.2 | -2.6 | +7.3 |
| | BF=0 | +2.1 | -2.4 | +6.7 |
| Subtropical arid | BF=1 | +3.4 | -0.6 | +7.0 |
| | BF=0.5 | +2.5 | -0.5 | +6.6 |
| | BF=0 | +1.7 | -0.5 | +6.2 |
| Subtropical coastal | BF=1 | +4.2 | -3.1 | +3.3 |
| | BF=0.5 | +3.2 | -2.8 | +3.1 |
| | BF=0 | +2.1 | -2.6 | +2.9 |
| Temperate coastal | BF=1 | +5.3 | -3.2 | -1.2 |
| | BF=0.5 | +4.1 | -3.0 | -1.1 |
| | BF=0 | +2.9 | -2.7 | -1.0 |
| High elevation | BF=1 | +3.8 | +1.8 | -3.5 |
| | BF=0.5 | +2.9 | +1.7 | -3.3 |
| | BF=0 | +2.0 | +1.6 | -3.1 |
| Temperate continental | BF=1 | +4.5 | -2.0 | -0.1 |
| | BF=0.5 | +3.5 | -1.9 | -0.1 |
| | BF=0 | +2.4 | -1.7 | -0.0 |

Table 4.8: Effect of AOI, spectral variations and module temperature on CSER of bifacial modules

## 4.5. Conclusions

The objective of this chapter is to extend the IEC61853 standard to bifacial modules. To calculate the energy rating of bifacial modules the irradiance on the rear side of the module obtained in the previous chapter is corrected for the AOI and spectrum effects. According to the results, the effect of angular losses is higher than the spectrum effects while the temperature of the module can significantly affect the results. The temperature of the module is obtained using the Faiman model and finally taking into consideration the corrected irradiance and module temperature the energy yield as well as the energy rating can be calculated. For the calculation of the energy rating of bifacial modules two approaches are proposed in this chapter. In the first approach, the total energy yield and the total irradiance incident on both sides of the module are used, resulting to an energy rating value lower than unity. To compare the energy rating of monofacial and bifacial modules obtained with this approach, the energy rating of monofacial modules needs to be recalculated using the total irradiance incident on both sides of the module. Since monofacial modules cannot generate energy from the rear side, the energy rating of bifacial modules is found to be higher than that of monofacial modules. In the second approach used for the calculation of the energy rating of bifacial modules, the total energy generated form both sides of the modules is used as in the first approach while only the front side irradiance is taken into account, leading to energy rating values higher than unity. The energy rating of bifacial modules can be compared with the the energy rating of monofacial modules as obtained in the standard. Note that in both approaches the energy rating of bifacial modules found to be up to 17% higher than that of monofacial depending on the bifaciality of the module and the climate conditions. Additionally, the difference in the CSER between climates suggests that the same modules can be more efficient in some climates compared to others. According to the results, in high elevation and temperate coastal climates PV modules found to have higher energy ratings than in other climates.

# 5

# Validation

This chapter is focused on the last objective of this work (see section 1.4) where the proposed model used for the calculation of the irradiance and energy yield of bifacial modules is validated against real-time measurements. To do that, existing recorded measurements of a system which was developed for the INNOZOWA project are used.

## 5.1. System overview

This section gives an overview of the system which is used to validate the proposed model. First, the INNOZOWA system is described, emphasizing its most relevant characteristics which are necessary for the proposed model. INNOZOWA is a dutch acronym which stands for 'INNovatieve Zon-pv op Water' which can be translated to 'Innovative Solar PV on Water'. The goal of the project was the following: "To accelerate the development of a solar PV system that can be utilized on bodies of inland water, which is competing and complementary for solar PV on land and has an added value for the goals of the water management", [61]. For this project three distinct subsystems were developed: the Ground based System, the Retractable System and the Tracker System. This system is located in Weurt, Eastern Netherlands (51.8514 °N, 5.7950 °E) shown with red point in Figure 5.1.


Figure 5.1: Location of the system, [62]

Figure 5.2: A bird's-eye view of the system, [61]

The Retractable and Tracker System are floating structures which the latter one has single-axis tracking capabilities. In addition, a Ground-based system was used to assess the differences and similarities between a land-based PV system and the two floating PV systems. However, in order to validate the irradiance model only the data from the ground based system are used. This is because, the current model is developed taking into account that bifacial modules are installed into the ground and have a fixed tilt. The Ground-based system consists of two mounting racks as shown in Figure 5.3 where each rack consists of four modules at a fixed tilt. In the front rack, monofacial PV modules were installed while on the back mounting rack bifacial modules were used.

Figure 5.3: Ground-based system, installed for the INNOZOWA pilot project, [61]

The technical specifications of the modules can be found in Table 5.1.

| | Parameter | LG330N1K-V5 | LG400N2T-J5 |
|---|---|---|---|
| Electrical properties | Maximum Power (Pmax) [Wp] | 330 | 400 |
| | Voltage (Vmpp) [V] | 34.1 | 42.2 |
| | Current (Impp) [A] | 9.69 | 9.49 |
| Mechanical properties | Type | Monofacial | Bifacial |
| | Number of cells | 6×10 | 6×12 |
| | Module dimensions (L×W ×H) | 1,686×1,016×40 mm | 2,024×1,024×40 mm |
| | Cell dimensions | 161.7×161.7mm | 161.7×161.7mm |
| Temperature coefficient | Pmax [%/ºC] | -0.36 | -0.36 |

Table 5.1: Technical specifications of the modules used in Ground-based system, [63], [64]

Using the mechanical properties of the modules and the picture of the system (Figure 5.3), the distance between the front and the back mounting rack is estimated and found approximately 2.9m. According to the findings of Tim Stark [61], monofacial and bifacial panel were installed at different angles. The measured tilt angle of monofacial panel and bifacial panels was found to be 12.7º and 7º respectively. Also, as shown in Figure 5.3, an orange reflector was installed beneath bifacial modules to reflect more light on the rear side of the bifacial module. A tabular overview of the ground based system is given in Table 5.2.

| Module Type | Tilt [º] | Azimuth [º] | Reflector | Number of modules |
|---|---|---|---|---|
| Monofacial | 12.7 | 180 | No | 4 |
| Bifacial | 7 | 180 | Yes | 4 |

Table 5.2: Overview of the ground based system

Furthermore, several sensors were installed at the specific location to monitor the ambient conditions. including a temperature sensor to measure the ambient temperature, a wind speed sensor and a horizontal irradiance sensor to measure GHI.

## 5.2. Input data

Since the irradiance model is developed according to the data given in the standard IEC-61853, the model had to be adjusted based on the available data of the specific system in Weurt. The data used

for the validation of the model for the time period between October 2019 and June 2020 are provided by Dr. Hesan Ziar, assistant professor at TU Delft. Data such us $T_{amb}$, *wind speed* and $GHI$ along with the respective time of the measurements are necessary for the validation of the irradiance model. However some data, which are required for the irradiance model are still missing and for that reason, additional calculations have been included in the model to obtain the desired data. These data are the following:

- Solar altitude ($\alpha_s$)
- Solar azimuth ($A_s$)
- DHI
- DNI

The solar altitude and solar azimuth for each hour of the selected period are obtained using the $PV\_LIB\ Toolbox$ developed at Sandia National Laboratories [65]. Inputs of this toolbox are the time and the latitude and longitude angles of the given location. It should be noted that the resulted $\alpha_s$ and $A_s$ are also calculated based on the equations provided in Appendix E of Solar Energy book to check the reliability of the toolbox and ensure the validity of the results [52]. The next step is to compare the simulated $\alpha_s$ and $A_s$ with real data. To do that, the weather data file from the PVMD toolbox is used which contains data for a system located in Weurt for a complete year 2005. More specifically, the simulated $\alpha_s$ and $A_s$ using the $PV\_LIBToolbox$ and the $\alpha_s$ and $A_s$ retrieved from the weather data are compared. In Figure 5.4, the simulated $\alpha_s$ and $A_s$ (blue colour) and the $\alpha_s$ and $A_s$ retrieved from the weather data file(orange colour) are shown for a random day of the year. As can be observed, the results shown with blue and orange colour are almost the same leading to the conclusion that the $PV\_LIB\ Toolbox$ can be used in the model for the prediction of $\alpha_s$ and $A_s$.

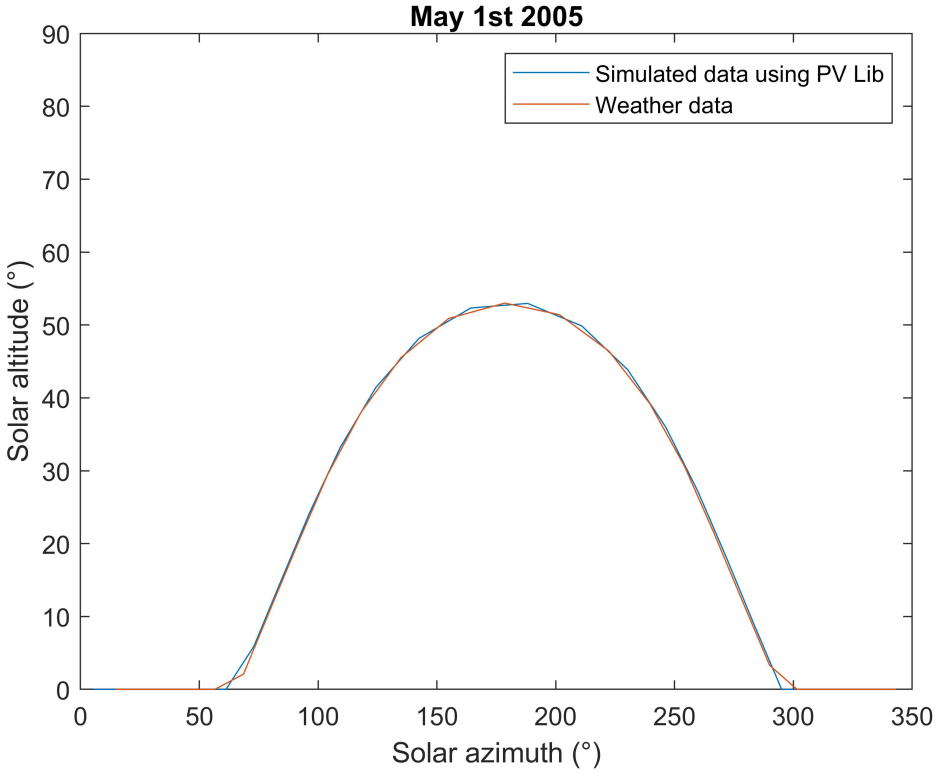


Figure 5.4: Solar altitude and solar azimuth on May 1st 2005

In order to generate the hourly DHI and DNI values, the Reindl-2 decomposition model is used. Decomposition models are generally used to estimate DHI from measured GHI based on the diffuse

fraction ($k_d$).

$$k_d = \frac{DHI}{GHI} \tag{5.1}$$

Several decomposition models such us the *Lee Model*, *Dutch-I* and *Dutch-II* models can also be used, but, according to the thesis of Abdalah Nour El Din the Reindl-2 model outperforms the other models [66]. This agrees with previous studies at TU Delft.

The Reindl-2 model was developed by D.T. Reindl in 1990 [67] which takes into account the sky clearness index ($k_t$) and the solar altitude ($\alpha_s$). The definition of the sky clearness index is given in Equation 5.2, where $G_{on}$ is the extraterrestrial irradiance on a plane normal to the sun obtained using Equation 2.19 used in Perez model.

$$k_t = \frac{GHI}{G_{on} cos(\theta_z)} \tag{5.2}$$

$$k_d = \begin{cases} 1.020 - 0.254k_t + 0.0123sin(\alpha_s), & k_t \leq 0.3 \\ 1.400 - 0.1749k_t + 0.177sin(\alpha_s), & 0.3 < k_t < 0.78 \\ 0.486k_t - 0.182sin(\alpha_s), & k_t \geq 0.78 \end{cases} \tag{5.3}$$

After the calculation of $k_d$ using Equation 5.3, the hourly DHI is calculated and finally the DNI is obtained using the definition of GHI (see Equation 5.4).

$$GHI = DHI + DNIsin(\alpha_s) \tag{5.4}$$

To check the validity of the results the weather data retrieved from PVMD toolbox are used again. In Figure 5.5, the annual DNI and DHI obtained from the weather data file and the simulated DNI and DHI values using the Reindl-2 model are shown with orange and blue color respectively.

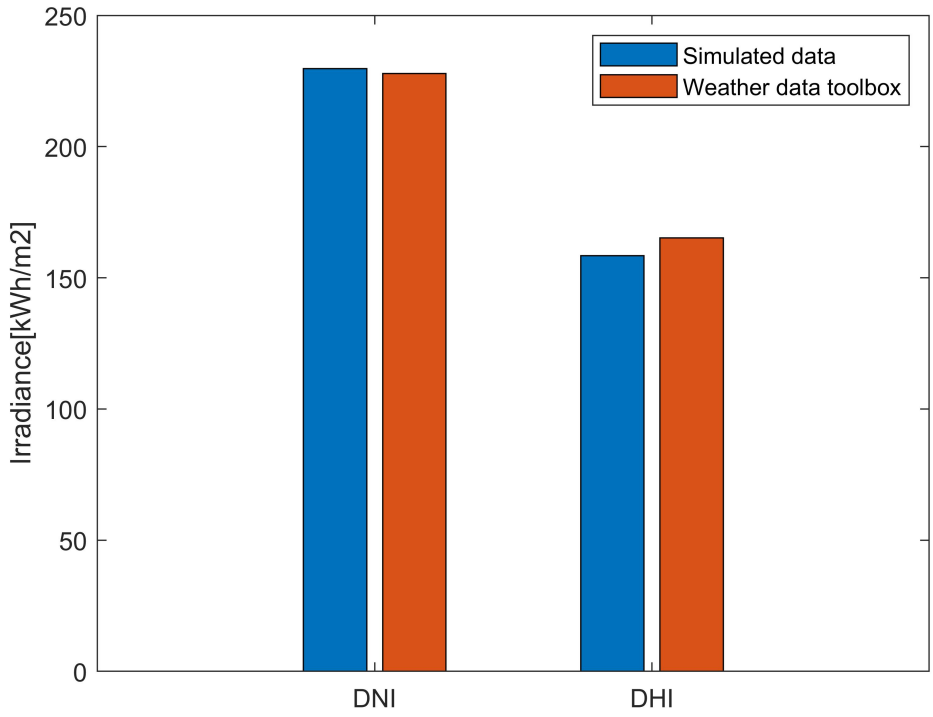


Figure 5.5: Annual DNI and DHI

The total simulated DNI is slightly lower than the measured data (weather data) with a difference of 0.79% while the simulated DHI is higher by 4.16% than the total DHI given in the weather data.

However, a small increase in the simulated DHI was already expected since the Reindl-2 model slightly overestimates the DHI values, especially for low-mid range values [66].

At this point, the models which are used to obtain the hourly $\alpha_s$, $A_s$, DNI and DHI values are defined. A summary of the data necessary to obtain the rear side irradiance on bifacial PV modules is listed below:

- Date (year/month/day/hour)
- Global Horizontal Irradiance (GHI) →Measured in the field
- Ambient temperaure ($T_{amb}$)→Measured in the field
- Wind speed →Measured in the field
- Solar altitude ($\alpha_s$) →$PV\_Lib$ *toolbox*
- Solar azimuth ($A_s$) →$PV\_Lib$ *toolbox*
- Diffuse Horizontal Irradiance (DHI) →Reindl-2 model
- Direct Normal Irradiance (DNI) →Obtained using Equation 5.4

In addition to these data, the albedo values of the reflector and the grass are required. Fortunately, the spectrally responsive albedo of the orange reflector and the grass were calculated in an earlier stage and their values are listed in Table 5.3.

| Material | Albedo |
|---|---|
| Grass | 0.298 |
| Reflector | 0.6849 |

Table 5.3: Spectral responsive albedo values, [61]

The Equation 3.27, mentioned in the previous chapter, was used for the calculation of the albedo values where an experiment was conducted on a piece of grass in Delft to obtain the effective albedo of grass, [61]. It is important to mention that in real conditions, the reflectivity of the grass change throughout the year. For example during winter, the grass is usually wet due to rainfalls leading to higher albedo value while in summer months the grass is completely dry and thus its albedo is lower. However, for simplicity of the simulation model, it is assumed that the reflectivity of the grass remains constant over time.

### 5.2.1. Average ground albedo value

For the calculation of the ground reflected irradiance the albedo value of the ground is used. However, in this case two different ground materials can be ”seen” by the rear side of the PV module, the grass and the orange reflector. This means that part of the solar light that reach the ground surface is reflected from the reflector while the rest is reflected from the grass. Since the shadowing effect is taken into account in the simulations as explained in the following subsection, it would have been very complex to include two different ground materials as well as the shading effect. This is because, part of the reflector and the grass can be shaded or not at any instant of time. Therefore, to reduce the complexity of the model it is decided to use an average value of the ground albedo which is calculated using view factors. Using the view factor of the reflector and the grass, an averaged albedo value can be obtained as follows:

$$Albedo_{ground} = Albedo_{reflector} * VF_{reflector} + Albedo_{grass} * VF_{grass} \tag{5.5}$$

Considering the geometrical parameters of both the module and the reflector, the view factor of the reflector is obtained using a 2D model as shown in Figure 5.6 (side view of the modules). The geometrical parameters of the module are given in Table 5.1 while the length of the reflector was measured in earlier study and found equal to 1.99m [61].

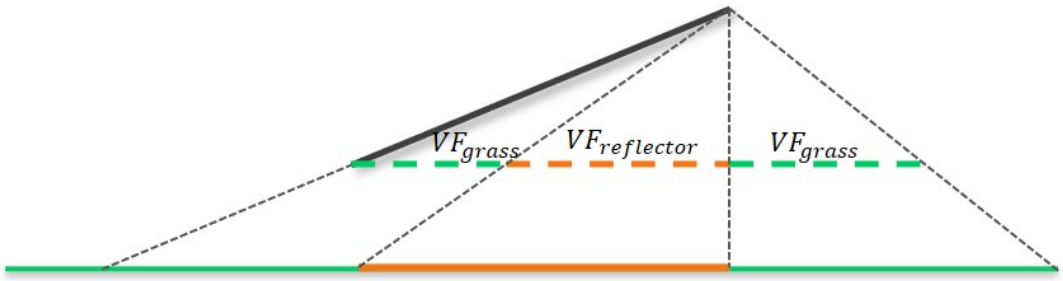


Figure 5.6: Schematic overview of the view factors used for the calculation of the average ground albedo

Finally, the view factor of the grass is calculated using the summation rule as shown in Equation 5.6.

$$VF_{grass} = 1 - VF_{reflector} - VF_{sky} \tag{5.6}$$

The resulted value of the ground albedo is obtained and found equal to 0.3541. Since the bifacial modules have a fixed tilt and the reflector is lain down on the ground, the same ground albedo value can be used in the calculations over the examined period.

### 5.2.2. Recalculation of view factor for the rear side

As mentioned at the beginning of this chapter, the environment where the bifacial modules are located in Weurt is different than the one used in the standard. In the standard, it was assumed that there are no other modules or obstacles around the system and as a result no shadow on the ground was observed except the shadow of the examined module. However, in the system located in Weurt another row of monofacial modules is located in front of the bifacial modules resulting in additional shadow of the ground which can significantly affect the ground reflected irradiance. To determine the additional shadow resulted from the front row of modules the mechanical properties of the monofacial modules need to be considered and using Equation 3.11 the shadow length of the monofacial modules is obtained. Finally, the view factor of the rear side of the bifacial module is adjusted to take into account the additional shadow. However, to solve this complication two different cases are analyzed.

First, it is examined whether the shadow of the monofacial modules reaches the front side of bifacial modules. This happens especially in winter months and during sunrises and sunsets where the sun is low. In that case, the ground beneath the module is fully shaded until the point where the shadow of the bifacial modules ends. As a result, the view factor for the shaded and not shaded areas ”seen” by the rear side of the module is obtained using the procedure mentioned in section 3.5. An illustration of this scenario is shown in Figure 5.7.

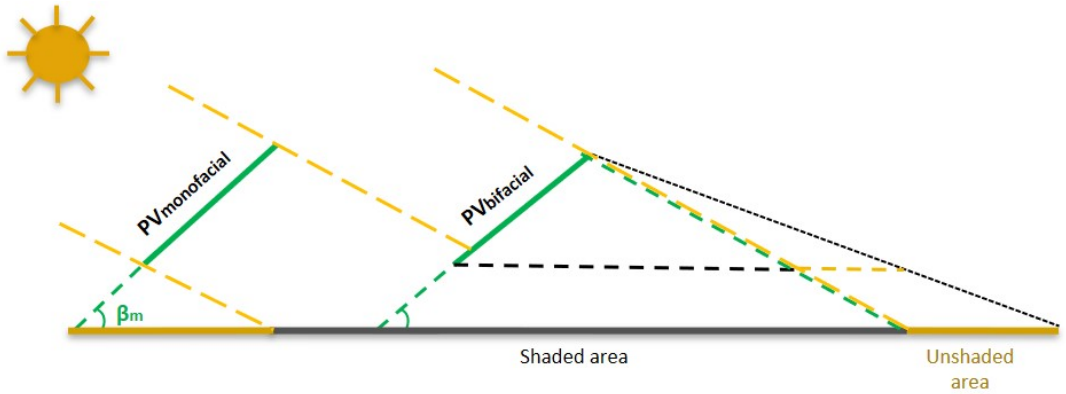


Figure 5.7: View factors for the first scenario

The second case is more complex. When the shadow of the monofacial module do not reach the surface of bifacial modules, it means that some part of the ground between the shadow of the monofacial

modules and the bifacial modules is not shaded. This is the case illustrated also in Figure 5.3. To obtain the total view factor for the shaded and unshaded regions the procedure mentioned in section 3.5 is followed where the view factor for each shaded or unshaded part of the ground is separately calculated. In order to get a better understanding of this scenario, the following scheme with the side view of the system is created.

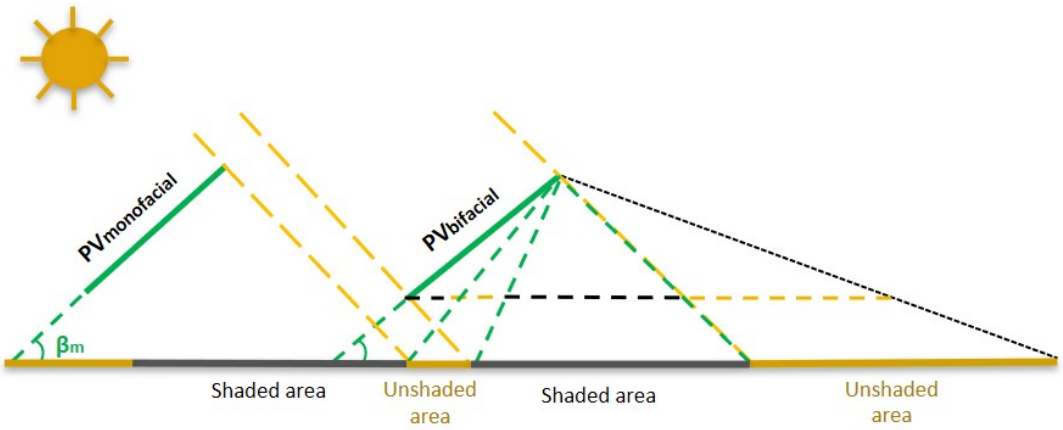


Figure 5.8: View factors for the second scenario

## 5.3. Validation results

The calculation of the aforementioned parameters using the on-site measurements (e.g GHI and wind speed), enabled the modelling of the irradiance incident on both sides of bifacial modules as well as the generated energy according to the procedure mentioned in chapter 3 and chapter 4. Since this section is to validate the correctness of the simulation model, the energy generated from the monofacial modules (front row) and bifacial modules (back row) is separately obtained. This is to ensure that the irradiance and energy generated from the monofacial modules agrees with the measured data and then analyze bifacial modules where the rear irradiance is taking place.

### 5.3.1. Irradiance

The simulated irradiance on the monofacial and bifacial modules for each month of the selected period (October 2019 until June 2020) is obtained as shown in Figure 5.9 and 5.10. As it was expected, more irradiance is being absorbed by the bifacial modules compared to monofacial modules. Note that this difference is not just due to the ability of bifacial modules to absorb solar light from the rear side but also due to the larger surface area and the different tilt angle of the bifacial modules compared to the monofacial modules. However, the in-plane irradiance on the modules was not measured in the field making it impossible to validate the simulated irradiance. Therefore, the energy yield is simulated and compared with the measured energy output of the modules as explained in the following subsection.

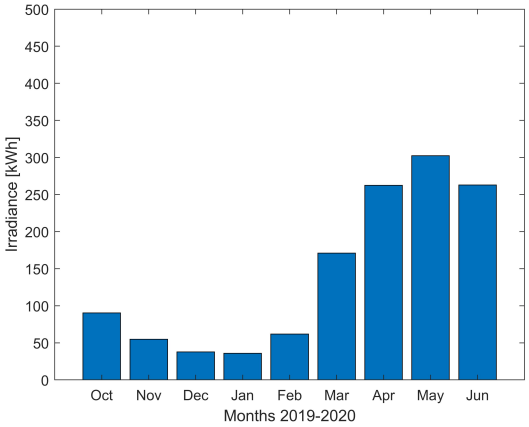


Figure 5.9: Total irradiance incidence on monofacial modules

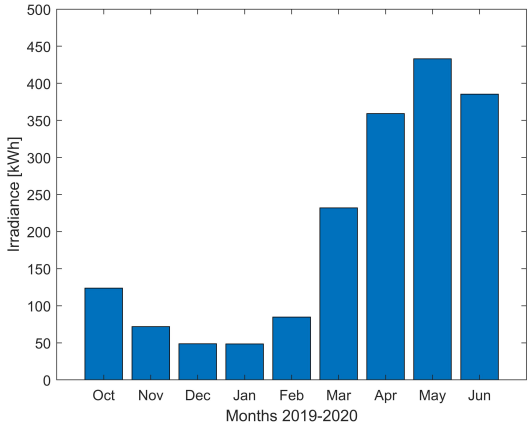


Figure 5.10: Total irradiance incidence on bifacial modules

### 5.3.2. Energy Yield

For the computation of the energy yield, the simulated irradiance is corrected for the AOI while the module temperature was obtained using the Faiman model as previously discussed. However,it should be noted that the irradiance is not corrected for the spectrum effects since no spectral information such us the spectral irradiance are available. Using both the corrected irradiance and the module temperature, the power output of the module is obtained using a power matrix. The power matrix of the monofacial and bifacial modules are shown in tables 5.4 and 5.5 respectively where the temperature coefficient of the modules and the maximum power in STC conditions mentioned in Table 5.1 are taken into account. The temperature coefficient indicates the rate at which a panel under-perform for any increase of the module temperature. Remember that at 25°C the maximum power under STC/BSTC is measured. As a result, for temperatures above 25°C the power output of the solar module decreases according to the temperature coefficient measured in $[\%/°C]$.

| | Temperature | | | |
|---|---|---|---|---|
| **G [W/m$^2$]** | **15°C** | **25°C** | **50°C** | **75°C** |
| **100** | 34.2 | 33.0 | NA | NA |
| **200** | 68.4 | 66.0 | NA | NA |
| **400** | 136.7 | 132.0 | 120.1 | NA |
| **600** | 205.1 | 198.0 | 180.2 | 162.4 |
| **800** | 273.5 | 264.00 | 240.24 | 216.5 |
| **1000** | 341.9 | 330.0 | 300.3 | 270.6 |
| **1100** | NA | 363.0 | 330.3 | 297.6 |

Table 5.4: Power matrix for the monofacial modules

| | Temperature | | | |
|---|---|---|---|---|
| **G [W/m$^2$]** | **15°C** | **25°C** | **50°C** | **75°C** |
| **100** | 41.4 | 40.0 | NA | NA |
| **200** | 82.8 | 80.0 | NA | NA |
| **400** | 165.8 | 160.0 | 145.6 | NA |
| **600** | 248.6 | 240.00 | 218.4 | 196.8 |
| **800** | 331.5 | 320.0 | 291.2 | 262.4 |
| **1000** | 414.4 | 400.0 | 364.0 | 328.0 |
| **1100** | NA | 440.00 | 400.40 | 360.80 |

Table 5.5: Power matrix for the bifacial modules

Additionally, it is assumed that the power output changes proportionally with the irradiance intensity which in reality this is not true. Looking at the I-V curve of a solar module shown inFigure 5.11, it can be observed that the current and voltage depend on the irradiance level. However, using the assumption that the relationship between power output and irradiance is linear, only the change in the current is taken into account while the value of the voltage remains constant. At this point, it should be noted that since the voltage changes less compared to the current values this assumption is a good approximation and can be used for the estimation of the power output of the module.

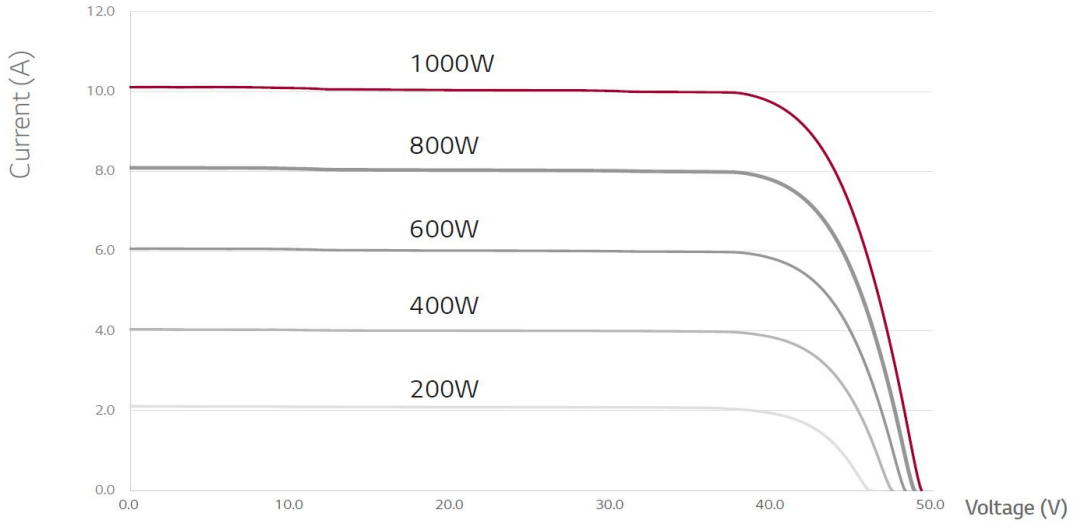


Figure 5.11: IV curve for different irradiance levels, [64]

After the calculation of the power output, the monthly energy yield is calculated and compared with the measured energy yield values, obtained using power optimizers. The SolarEdge P505 optimizer type was installed at each module [61]. In Figure 5.12, the average power output of the monofacial modules is shown with blue color while with orange color the simulated energy yield for a single module is illustrated. As can be observed, the simulated and measured energy yield values for each month of the period show a good match.

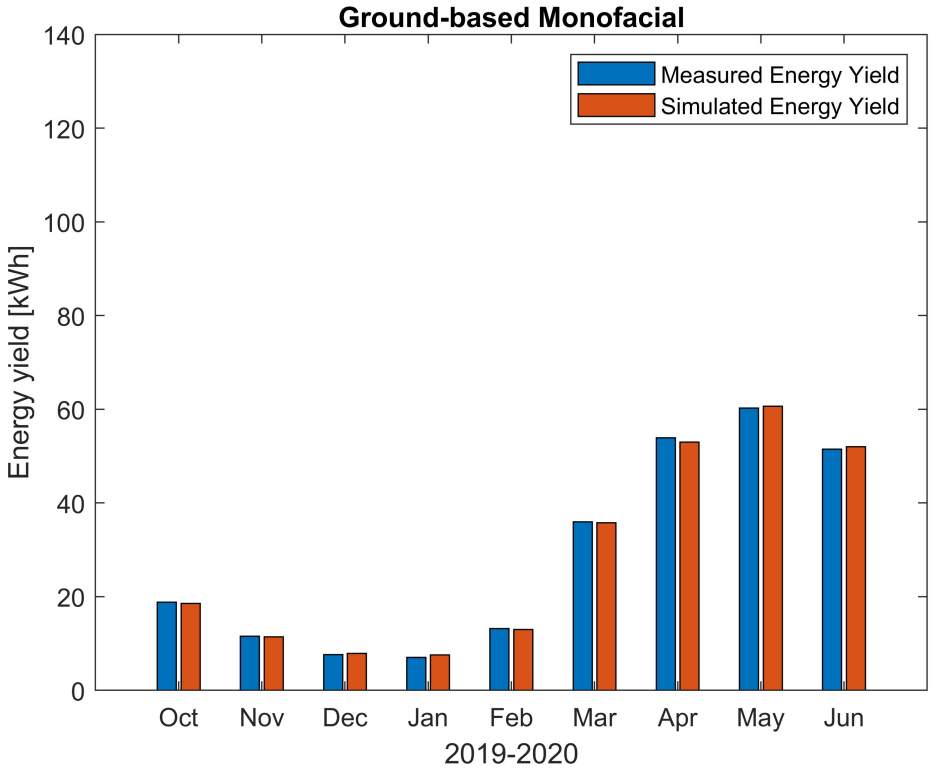


Figure 5.12: Measured and simulated energy yield of monofacial modules

In Table 5.6, the exact difference between the measured and the simulated energy yield is shown measured in [%]. In order to assess the quality of the modelled data and the model itself, a statistical

indicator namely " Root mean square deviation" ($RMSD$) is used. The RMSD quantifies the differences between modelled data points and the measured values and it is calculated using Equation 5.7. This values can never be negative and a value of zero would indicate a perfect fit between the modelled and measured data. Note that letter $m$ and $p$ in Equation 5.7 stand for measured and predicted (or simulated) data respectively. As shown in Table 5.6, the RMSD value between the difference of the measured and the simulated energy yield found to be just 3.05%, meaning that the simulation model is reliable, precise and can be used to validate the model used for monofacial modules.

$$RMSD = \sqrt{\frac{\sum_{i=1}^{\mathrm{N}} (m_i - p_i)^2}{N}} \tag{5.7}$$

| Month | Monofacial modules | Bifacial modules |
|---|---|---|
| October | -1.2% | -0.9% |
| November | -1.2% | +0.3% |
| December | +3.1% | +7.1% |
| January | +8.0% | +9.7% |
| February | -1.4% | -0.9% |
| March | -0.6% | -2.2% |
| April | -1.7% | -2.2% |
| May | +0.6% | +1.9% |
| June | +1.0% | +5.8% |
| **RMSD** | **3.0%** | **4.6%** |

Table 5.6: Monthly difference between measured and simulated energy yield

The measured and simulated energy yield per month for the bifacial system is shown in Figure 5.13. Similar to the monofacial system, an average value of the measured energy yield is used. As depicted in the figure, the measured and simulated energy yield are very close and the relative difference between the two is shown in Table 5.6. Additionally, to assess the performance of the module for the examined period of time, the RMSD value was obtained for the difference in the energy yield and found equal to 4.65%.

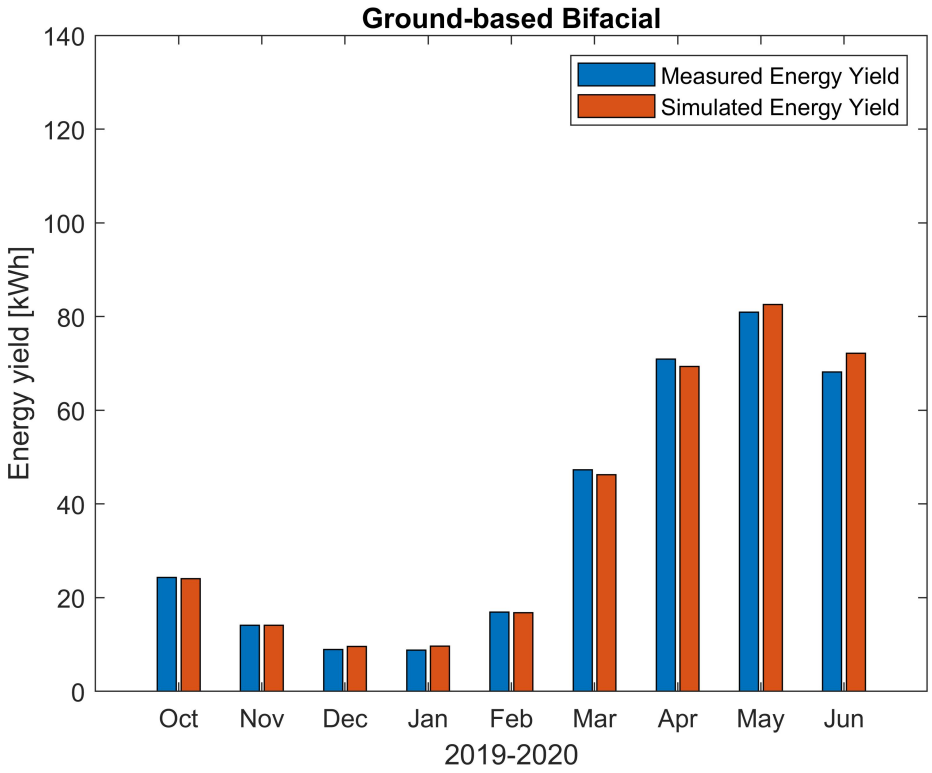


Figure 5.13: Measured and simulated energy yield of bifacial modules

## 5.4. Conclusions

In this chapter the proposed model used for the calculation of the energy yield of bifacial modules is validated. The validation of the model is performed using outdoor measurements of a bifacial system located in Weurt, Eastern Netherlands. In this system, an additional row of modules is installed in front of the bifacial modules and therefore the model is adjusted since free horizon area was initially assumed. An average value of the ground albedo is obtained (GA=0.35) using the view factor technique, taking into account the reflectivity of the orange color reflector installed underneath the bifacial modules and the surrounding grass. The in-plane irradiance on monofacial and bifacial modules is simulated and the energy yield is calculated and compared to the measured energy yield. The results show a good match between the simulated and measured energy yield for both monofacial and bifacial modules, for the period between October 2019 and June 2020. The total variation in the energy yield is also calculated using the RMSD and found equal to 3.05% for the monofacial modules and 4.65% for the bifacial modules. The validation results confirmed that the simulated irradiance and energy yield are very close to the real values measured in the field. Therefore, this model can be used to predict the irradiance and energy output of bifacial modules which are necessary for the calculation of the energy rating value.

# 6

# Conclusions and Recommendations

In this chapter the most important findings of this MSc thesis are summarised while at the end of the chapter some recommendations are proposed to be carried out in the future. At the beginning of this report the main research questions were introduced:

***1. How can the energy rating of bifacial PV modules be calculated?***
***2. Can the energy rating be used to assess the productivity of bifacial modules?***

To answer these questions, three objectives were formulated as described in section 1.4 which were answered throughout this thesis. In the following sections the answer for each objective is summarised.

## 6.1. Develop a model to calculate rear side irradiance on bifacial PV modules

In chapter 3, an irradiance model is developed to calculate the irradiance on the rear side of a bifacial module using the data acquired from IEC-61853 standard. The irradiance is separated into three components: direct, diffuse and ground reflected irradiance. For the calculation of direct irradiance component, the angle of incidence of the rear side of the module needs to be taken into account as shown in Equation 6.1.

$$B_r = DNI * cos(AOI_r) \tag{6.1}$$

To calculate the diffuse irradiance component, the Perez model which takes into account the clearness of the sky is used for both sides of the module. Finally, the calculation of the ground reflected irradiance is the most complex and therefore a deep research was conducted. In monofacial modules, the contribution of the ground reflected irradiance to the total irradiance is very low (e.g for low module tilts) and sometimes it can be neglected. However, this is not the case for bifacial modules since the ground reflected irradiance is the main source of the total irradiance incident on the rear side of the module. To calculate the ground reflected irradiance the view factor technique for a 2D geometry located in a free horizon area is used. Additionally, the shadow cast of the module is taken into account since it can significantly affect the irradiance reflected to the rear side of the module. For the estimation of the view factors, a distinction is made between the shaded and unshaded grounds. To do this, the view factors from the rear side of a single collector row to the shaded and unshaded grounds as defined by J. Appelbaum [54] are used. However, these view factor equations (defined by J. Appelbaum) were established for modules attached to the ground and since the modules used in this work are elevated from the ground surface the equations are adjusted accordingly. According to the results of the model, bifacial modules can absorb approximately 15-19% more irradiance compared to monofacial modules. Note that the ground reflected irradiance is the main source of the rear side irradiance for the case of bifacial modules as obtained in the model.

Finally, the effect of spectral albedo is examined. More specifically, using the spectral integrated and spectral responsive albedo for each hour of the year, the ground reflected irradiance on the rear side

of the module is obtained. According to the results, it is shown that the use of improper albedo values can lead to under/over prediction of the system irradiance by around 4% depending on the climate and ground material, leading to improper optimization of the PV system.

## 6.2. Extend mono-facial PV module energy rating to bifacial modules

As shown in the section 1.2, the standard test conditions (STC) where the efficiency of PV modules is measured can be far away from the real operating conditions. As a result, the efficiency of the PV modules provided in the manual data-sheet is not representative for such climates and for this reason energy ratings can be used to assess the productivity of a PV system. Currently, energy ratings have been developed only for monofacial modules and the aim of the proposed model is to calculate the energy rating of bifacial modules based on IEC-6183 standard. To do that, the irradiance on the rear side of the module is corrected for the AOI and spectrum effects and the temperature of the module is obtained. Using the corrected irradiance on the front and on the rear side of the module as well as the module temperature, the energy yield and the energy rating of the module are calculated. In this work, two approaches are developed for the calculation of energy rating of bifacial modules.

The first approach takes into account the total energy yield generated from both sides of the module as well as the total irradiance absorbed from the front and the rear side of the module resulting to an energy rating value lower than unity. To compare the energy rating of monofacial and bifacial modules using this approach, the energy rating of monofacial modules is obtained using a different method than the one described in the standard. More specifically, the CSER of monofacial modules is calculated using the total irradiance reaching both sides of the module as in the case of bifacial modules. However, bifacial modules have the ability to absorb irradiance from the rear side resulting to higher energy yield and thus higher energy rating than monofacial modules.

The second approach used for the calculation of the energy rating of bifacial modules takes into account the total energy generated form both sides of the modules while the only the front side irradiance is used, leading to energy rating values higher than unity. Since more energy is generated form bifacial modules the resulted energy rating found to be higher than that of monofacial modules. The CSER of bifacial modules using this approach can easily be obtained since only the front side irradiance is required and also can be used for the comparison of monofacial and bifacial modules emphasising on the energy output.

In both approaches, the energy rating of bifacial modules found to be 12-17% higher than the energy rating of monofacial modules depending on the climate conditions. Afterwards, the effect of bifaciality is investigated where it is observed that the higher the bifacial factor of a module is, the higher the energy rating. This is due to higher efficiency of the rear side of the module compared to front side of the module. Additionally, in subsection 4.4.1, the effect of different losses mechanisms on the energy rating values is analysed and found that the effect of angular losses is higher than the spectrum effects due to the low tilt of the modules (up to 5% and 3% respectively). It is also shown that the module temperature can significantly affect the CSER of a module (by almost 8%) depending on the climate conditions. Therefore, the determination of the module temperature under operating conditions but also the correction of irradince due AOI and spectrum effects are very important to precisely calculate the value of CSER.

## 6.3. Validation of the model using real data

In chapter 5 of this report, the validation of the model is performed using outdoor measurements of a bifacial system located in Weurt, Eastern Netherlands. The energy yield is obtained using power optimizers installed at each module for the time period between October 2019 and June 2020. Note that in this system, an additional part of the ground is shaded since another row of modules is installed in front of the bifacial modules. Therefore, the model is slightly adjusted to include this shadow effect in the calculation of the ground reflected irradiance since free horizon area was initially assumed. For the calculation of the ground reflected irradiance, a constant albedo value of 0.3541 is used which is obtained using the view factor technique. This is an average value of the ground albedo taking into

account the reflectivity of the orange color reflector installed underneath the bifacial modules and the surrounding grass.

Then, the irradiance incident on both sides of the module is simulated and the energy yield is calculated and compared to the measured energy yield of bifacial modules. The results show a good match between the simulated and measured energy yield for each month of the selected period and the total simulated energy yield found to be slightly overestimated with RMSD of 4.65%. Thus, it can be concluded that the proposed model can be used for the calculation of the energy yield and thus the energy rating of bifacial modules.

## 6.4. Recommendations

In this section, the recommendations for possible improvement of the model in the future are given below:

- The rear irradiance model can be further improved with the implementation of the transmission of light through the module. Additionally, the irradiance on the rear side of each cell can be modelled taking into account the height of the cells from the ground surface. In that case, the irradiance at the rear side of the module will not be uniform leading to more precise results.
- The shadow of the mounting structure and other equipment (e.g junction box) are not considered in the model. Therefore, a shading factor can be introduced to the rear irradiance model to account for these effects.
- The temperature model can be compared with other temperature models such us the fluid dynamic model [52] to see how the temperature prediction changes.
- To validate the model, another method can be used for the calculation of the power matrix for a set of defined conditions.
- A separate model based on the optical properties of the module can be developed to calculate the spectral responsivity of the rear side of the module as well as the temperature coefficients used in the Faiman model. Currently, the same parameters used in the IEC61853 standard for monofacial modules are implemented.
- Currently, the model was validated to only one location using a bifacial system in Weurt, Eastern Netherlands. To further improve the reliability of the model, it should be validated for other locations with different climate conditions. This will make the proposed model more reliable and trustworthy.

# A

# Direct irradiance correction

For the calculation of the rear side irradiance an assumption was used for one of the reference climates. Using the data for the temperate continental climate given by the IEC61853-4, the direct irradiance component for each hour of the year was obtained with the help of the rear irradiance model as explained in chapter 3. However, one of the resulted values of the hourly direct irradiance was considerably greater than normal leading to inaccurate results. More specifically, the hourly direct in-plane irradiance reached the value of more than 5kW/$m^2$ which does not make sense. Below, a detailed analysis for the calculation of the direct irradiance component is shown.

$$DNI = B_h / cos(\theta_z) \tag{A.1}$$

where the direct horizontal irradiance $B_h$ given by the standard and was equal to 20.37 W/$m^2$. The sun zenith angle was calculated and found equal to 89.97° leading to the following value of the DNI.

$$DNI = 20.37 / cos(89.97) = 38903.84 W/m^2 \tag{A.2}$$

After the DNI was obtained, the direct in-plane irradiance $B$ was calculated as follows:

$$B_r = DNI * cos(AOI_r) = 38903.84 * cos(82.50) = 5077.97 W/m^2 \tag{A.3}$$

Obviously, the value of $B_r$ is extremely high and therefore it was decided to remove this value from the calculation of the direct irradiance component on the rear side of the module while the values of the diffuse and ground reflected irradiance will remain untouched.

This assumption is based on the fact that the irradiance level should be very low at this time since the sun is almost under horizon (late sunset, $\alpha_s$=0.0243°). Another reason, is that direct irradiance has the least contribution on the rear side irradiance and therefore, setting $B = 1$ for the specific hour, the final result is expected to negligibly change.

# B

# Monthly in-plane irradiance

In the following figures the monthly in-plane irradiance on monofacial and bifacial modules for each climate given in the standard is illustrated. As it was expected, bifacial modules absorb more irradiance than monofacial moduleas under all climate conditions.

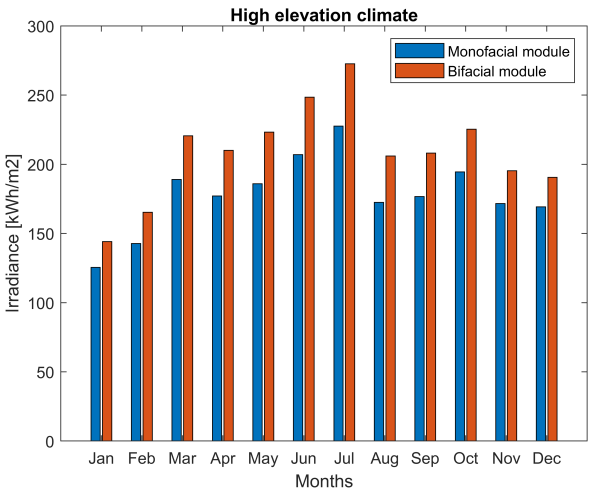


Figure B.1

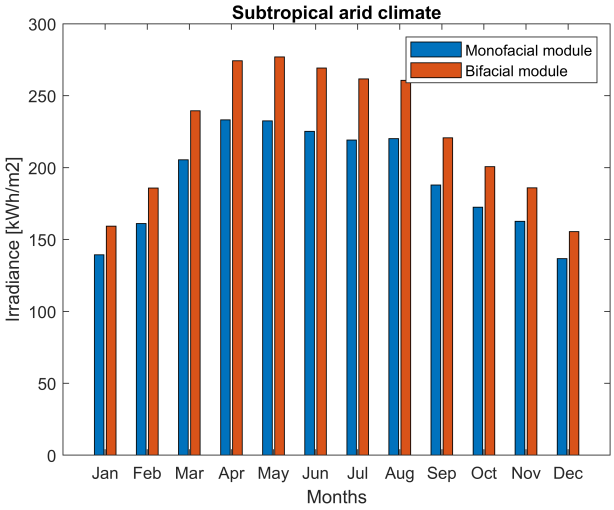


Figure B.2

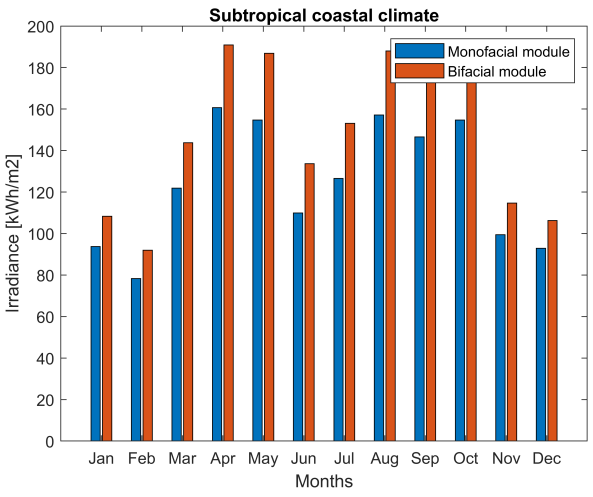


Figure B.3

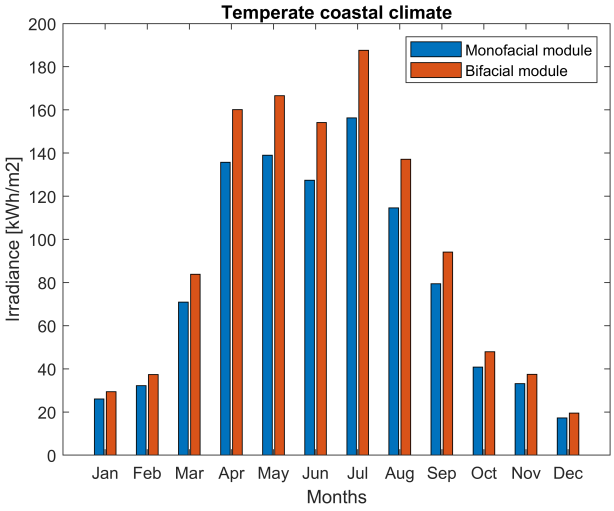


Figure B.4

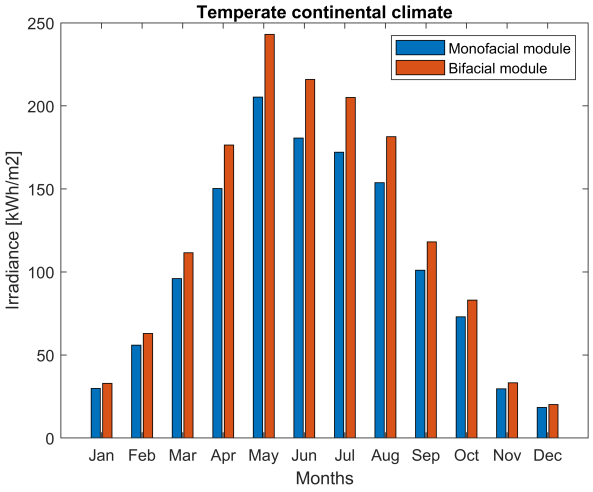


Figure B.5

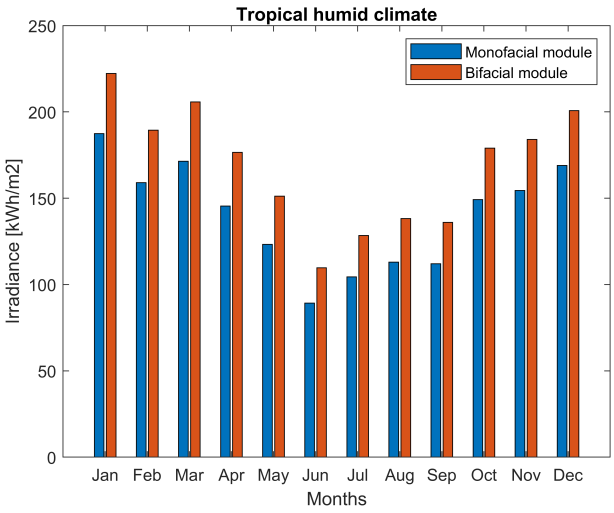


Figure B.6

# Bibliography


[1] NASA. *The Causes of Climate Change*. https://climate.nasa.gov/causes/, Date accessed:2020-25-11. 2020.

[2] IEA. *Solar PV power generation in the Sustainable Development Scenario, 2000-2030*. https://www.iea.org/data-and-statistics/charts/solar-pv-power-generation-in-the-sustainable-development-scenario-2000-2030, Date accessed:2020-25-11. 2020.

[3] Christopher E. Valdivia et al. “Bifacial Photovoltaic Module Energy Yield Calculation and Analysis”. In: (2017).

[4] R. Kopecek and J. Libal. “Towards large-scale deployment of bifacial photovoltaics”. In: *Nature Energy* (2018).

[5] R. Guerrero-Lemus et al. “Bifacial solarphotovoltaics – A technology review”. In: (2016).

[6] A. Cuevas, A. Luque, and J. M. Ruiz. “Bifacial trancells for luminiscent solar concentration”. In: *Instituto de Energia Solar. Universidad Politecnica Madrid. Spain* (1979).

[7] Jose E. Castillo-Aguilella and Paul S. Hauser. “Multi-Variable Bifacial Photovoltaic Module Test Results and Best-Fit Annual Bifacial Energy Yield Model”. In: (2016).

[8] Chris Deline et al. “Evaluation and Field Assessment of Bifacial Photovoltaic Module Power Rating Methodologies”. In: (2016).

[9] Radovan Kopecek and Joris Libal. “Bifacial Photovoltaics 2021: Status, Opportunities and Challenges”. In: *Energies* (2021).

[10] Usha Mandadapu, Victor Vedanayakam, and K. Thyagarajan. “Effect of temperature and irradiance on the electrical performance of a PV module.” In: *International Journal of Advanced Research* 5 (Mar. 2017), pp. 2018–2027.

[11] IEC 61853-3. “Photovoltaic (PV) module performance testing and energy rating - Part 3: Energy rating of PV modules”. In: (2018).

[12] IEC 61853-4. “Photovoltaic (PV) module performance testing and energy rating - Part 4: Standard reference climatic profiles”. In: (2018).

[13] Thomas Huld et al. “Photovoltaic energy rating data sets for Europe”. In: *Solar Energy* (2016).

[14] IEC 61853-1. “Photovoltaic (PV) module performance testing and energy rating - Part 1: Irradiance and temperature performance measurements and power rating”. In: (2011).

[15] IEC 61853-2. “Photovoltaic (PV) module performance testing and energy rating - Part 2: Spectral responsivity, incidence angle and module operating temperature measurements”. In: (2016).

[16] D.P.Gribnau. *Physically based irradiance model for photovoltaic applications*. http://repository.tudelft.nl/, Date accessed:2021-20-01. 2020.

[17] Matthieu Chiodetti et al. “PV bifacial yield simulation with a variable albedo model”. In: (2016).

[18] Clifford W. Hansen et al. “A Detailed Model of Rear-Side Irradiance for Bifacial PV Modules”. In: (2017).

[19] T. Muneer et al. “Finite-element view-factor computations for radiant energy exchanges”. In: *Journal of Renewable and Sustainable Energy* (2015).

[20] Hartmut Nussbaumer et al. “Accuracy of simulated data for bifacial systems with varying tilt angles and share of diffuse radiation”. In: *Solar Energy* (2020).

[21] Gregory J. Ward. “The RADIANCE Lighting Simulation and Rendering System”. In: (1994), pp. 459–472.

[22] Richard C. Jordan Benjamin Y.H. Liu. “The interrelationship and characteristic distribution of direct, diffuse and total solar radiation”. In: (1960), pp. 1–19.

[23] J. E. Hay, J. A. Davies. “Calculations of the solar radiation incident on an inclined surface”. In: *In Proceedings First Canadian Solar Radiation Data Workshop* (1980), pp. 59–72.

[24] PV Performance Modelling Collaborative. *Hay and Davies Sky Diffuse Model*. https://pvpmc.sandia.gov/modeling-steps/1-weather-design-inputs/plane-of-array-poa-irradiance/calculating-poa-irradiance/poa-sky-diffuse/hay-sky-diffuse-model/, Date accessed:2020-20-12. 2020.

[25] Dorota Chwieduk. “Chapter 2 - Availability of Solar Radiationon the Earth”. In: *Solar Energy in Buildings* (2014), pp. 21–62.

[26] PV Performance Modelling Collaborative. *Reindl Sky Diffuse Model*. https://pvpmc.sandia.gov/modeling-steps/1-weather-design-inputs/plane-of-array-poa-irradiance/calculating-poa-irradiance/poa-sky-diffuse/reindl-sky-diffuse-model/, Date accessed:2020-20-12. 2020.

[27] Ralph C.Temps and K.L.Coulson. “Solar radiation incident upon slopes of different orientations”. In: (1977).

[28] PV Performance Modelling Collaborative. *Perez Sky Diffuse Model*. https://pvpmc.sandia.gov/modeling-steps/1-weather-design-inputs/plane-of-array-poa-irradiance/calculating-poa-irradiance/poa-sky-diffuse/perez-sky-diffuse-model/, Date accessed:2020-20-12. 2020.

[29] Richard Perez et al. “A new simplified version of the Perez diffuse irradiance model for tilted surfaces”. In: *Pergamon Journals Ltd.* (1987).

[30] Christian A. Gueymard. “A reevaluation of the solar constant based on a 42-year total solar irradiance time series and a reconciliation of spaceborne observations”. In: *Elsevier* (2018), pp. 2–9.

[31] Xingshu Sun et al. “Optimization and performance of bifacial solar modules: A global perspective”. In: *Applied Energy* (2018), pp. 1601–1610.

[32] Bill Marion et al. “A Practical Irradiance Model for Bifacial PV Modules”. In: (2017).

[33] Sandia National Laboratories. *ASHRAE IAM Model*. https://pvpmc.sandia.gov/modeling-steps/1-weather-design-inputs/shading-soiling-and-reflection-losses/incident-angle-reflection-losses/ashre-model/, Date accessed:2021-12-06.

[34] W. De Soto, S.A. Klein, and W.A. Beckman. “Improvement and validation of a model for photovoltaic array performance”. In: *Solar Energy* 1 (2006), pp. 78–88.

[35] N. Martin and J.M. Ruiz. “Calculation of the PV modules angular losses under field conditions by means of an analytical model”. In: (2000).

[36] N. Martin and J.M. Ruiz. “Corrigendum to ”Calculation of the PV modules angular losses under field conditions by means of an analytical model””. In: (2001).

[37] Jinsuk Kang et al. “Practical comparison between view factor method and ray-tracing method for bifacial PV system yield prediction”. In: (2019).

[38] PVsyst. *Bifacial Systems*. https://www.pvsyst.com/help/bifacial_systems.htm,Date accessed:2021-06-01. 2020.

[39] Silvana Ayala Pelaez et al. “Comparison of Bifacial Solar Irradiance Model Predictions With Field Validation”. In: *IEEE Journal of Photovoltaics* 9.1 (2019), pp. 82–88.

[40] Djaber Berrian, J. Libal, and Stefan Glunz. “MoBiDiG: simulations and LCOE”. In: (Oct. 2017).

[41] Dimitrij Chudinzow et al. “Simulating the energy yield of a bifacial photovoltaic power plant”. In: *Solar Energy* 183 (2019), pp. 812–822.

[42] IEC904-1. “International Standard Geneva”. In: (1987).

[43] IEC 60904-3. “Photovoltaic devices - Part 3: Measurement principles for terrestrial photovoltaic (PV) solar devices with reference spectral irradiance data”. In: (2019).

[44] David Faiman. “Assessing the Outdoor Operating Temperature of Photovoltaic Modules”. In: *Progress in Photovoltaics: Research and Applications* 16 (June 2008), pp. 307–315.

[45] Daniela Dirnberger, Björn Müller, and Christian Reise. “PV module energy rating: Opportunities and limitations”. In: *Progress in Photovoltaics Research and Applications* (May 2015).

[46] IEC 60904-7. “Computation of the spectral mismatch correction for measurements of photovoltaic devices”. In: (2019).

[47] SOLARGIS. *Weather data and software for solar power investments*. https://solargis.com/, Date accessed:2021-04-06.

[48] Wolfgang Heydenreich, Björn Müller, and Christian Reise. “Describing the World with three Parameters: A new Approach to PV Module Power Modelling”. In: (Sept. 2008), pp. 2786–2789.

[49] D. Jordan and S. Kurtz. “Photovoltaic Degradation Rates—an Analytical Review”. In: *Progress in Photovoltaics: Research and Applications* (Jan. 2013).

[50] Markus Schweiger et al. “Understanding the Energy Yield of Photovoltaic Modules in Different Climates by Linear Performance Loss Analysis”. In: *IET Renewable Power Generation* (Jan. 2017).

[51] John A. Duffie and William A. Beckman. *Solar Engineering of Thermal Processes, Fourth Edition*. 2013. ISBN: 978-0-470-87366-3.

[52] Arno Smets et al. *Solar Energy: The physics and engineering of photovoltaic conversion, technologies and systems*. English. UIT Cambridge Limited, 2016. ISBN: 978-1-906860-32-5.

[53] Christian A. Gueymard. “Direct and indirect uncertainties in the prediction of tilted irradiance for solar engineering applications”. In: *Solar Energy* (2009), pp. 432–444.

[54] Joseph Appelbaum. “The role of view factors in solar photovoltaic fields”. In: *Renewable and Sustainable Energy Reviews* 81 (Jan. 2018), pp. 161–171.

[55] Chris Deline et al. “Assessment of Bifacial Photovoltaic Module Power Rating Methodologies—Inside and Out”. In: *IEEE Journal of Photovoltaics* (Jan. 2017), pp. 1–6.

[56] Rob Andrews and Joshua Pearce. “The Effect of Spectral Albedo on Amorphous Silicon and Crystalline Silicon Solar Photovoltaic Device Performance”. In: *Solar Energy* (Mar. 2013), pp. 233–241.

[57] M.P. Brennan et al. “Effects of Spectral Albedo on Solar Photovoltaic Devices”. In: *Solar Energy Materials and Solar Cells* (May 2014), pp. 111–116.

[58] NASA. *ECOSTRESS Spectral Library - Version 1.0*. https://speclib.jpl.nasa.gov/, Date accessed:2021-07-04. Feb. 2018.

[59] Christos Monokroussos et al. “Rear-side spectral irradiance at 1 sun and application to bifacial module power rating”. In: *Progress in Photovoltaics: Research and Applications* (Mar. 2020).

[60] Malte Ruben Vogt et al. “Impact of using spectrally resolved ground albedo data for performance simulations of bifacial modules (EUPVSEC 2018)”. In: (Oct. 2018).

[61] Tim Stark. *Modeling and monitoring of a floating photovoltaic pilot system*. http://repository.tudelft.nl/,Date accessed:2021-05-02. 2020.

[62] Google. *Google Maps Weurt*. https://www.google.com/maps, Date accessed:2021-10-05.

[63] LG. *LG NeON 2Black*. https://www.lgenergy.com.au/uploads/download_files/71aa1dd78a6f41bd0b9281110047ae343741f67f.pdf, Date accessed:2021-15-05.

[64] LG. *LG NeON 2Bifacial*. https://www.lg.com/es/download/resources/CT32016002/CT32016002_2463.pdf, Date accessed:2020-12-05. 2020.

[65] Sandia National Laboratories. *PV LIB Toolbox*. https://pvpmc.sandia.gov/applications/pv_lib-toolbox/, Date accessed:2021-20-05.

[66] Abdallah Nour El Din. *Improved electrical model and experimental validation of the PVMD toolbox*. http://repository.tudelft.nl/, Date accessed:2021-02-05. 2020.

[67] D.T. Reindl, W.A. Beckman, and J.A. Duffie. “Evaluation of hourly tilted surface radiation models”. In: *Solar Energy* 45.1 (1990), pp. 9–17.